AEDC-TR-70-123 C 1

A SUMMARY REPORT OF THE CRYOSORPTION PUMPING OF HYDROGEN BY CARBON DIOXIDE FROST

K. E. Tempelmeyer

ARO, Inc.

June 1970

AEROSPACE ENVIRONMENTAL FACILITY
ARNOLD ENGINEERING DEVELOPMENT CENTER
AIR FORCE SYSTEMS COMMAND
ARNOLD AIR FORCE STATION, TENNESSEE

NOTICES

When U. S. Government drawings specifications, or other datn are used for any purpose other than a definitely related Government procurement operation, the Government thereby incurs no responsibility nor any obligation whatsoever, and the fact that the Government may have formulated, furnished, or in any way supplied the said drawings, specifications, or other data, is not to be regarded by implication or otherwise, or in any manner licensing the holder or any other person or corporation, or conveying any rights or permission to manufacture, use, or sell any patented invention that may in any way be related thereto.

Qualified users may obtain copies of this report from the Defense Documentation Center.

References to named commercial products in this report are not to be considered in any sense as an endorsement of the product by the United States Air Force or the Government.

A SUMMARY REPORT OF THE CRYOSORPTION PUMPING OF HYDROGEN BY CARBON DIOXIDE FROST

K. E. Tempelmeyer
ARO, Inc.

FOREWORD

The research presented in this report was sponsored by the Arnold Engineering Development Center (AEDC), Air Force Systems Command (AFSC), Arnold Air Force Station, Tennessee, under Program Element 64719F.

The results reported herein were obtained by ARO, Inc. (a subsidiary of Sverdrup & Parcel and Associates, Inc.), contract operator of AEDC, AFSC, under Contract F40600-69-C-0001. The research was conducted from April 1969 through September 1969, under ARO Project No. SW3003, and the manuscript was submitted for publication on March 27, 1970.

The work described herein was used in partial fulfillment of Ph. D. dissertation requirements for The University of Tennessee Space Institute. The author would like to acknowledge many helpful suggestions, ideas, and comments, which contributed significantly to the progress of this work, from his colleagues.

The assistance provided by Dr. R. L. Young, Deputy Director for Educational Programs at the University of Tennessee Space Institute, and by Mr. Ronald Dawbarn, ARO, Inc., deserves particular mention.

This technical report has been reviewed and approved.

Michael G. Buja
First Lieutenant, USAF
Research Division
Directorate of Plans
and Technology

Harry L. Maynard
Colonel, USAF
Director of Plans
and Technology

ABSTRACT

The sorption of hydrogen by cryodeposited frosts of CO_2, SO_2 and CH_3Cl at temperatures between 12° and 22°K has been investigated both analytically and experimentally. Equilibrium sorption isotherms and the dynamic pumping characteristics of the sorbent, sorbate combination were systematically measured for chamber pressures between 10^{-7} and 10^{-4} torr. Frost cryosorbents which were formed in a manner to make them more disordered or amorphous exhibited greater equilibrium sorption capacities for hydrogen. Carbon dioxide sorbents were formed which were able to sorb one hydrogen molecule for every two predeposited CO_2 molecules. Warming the frost evidently alters its structure and thereby decreases its sorption capacity. It was found that equilibrium sorption isotherms of frost cryosorbents could be predicted by the semiempirical Dubinin-Radushkevich Equation. Calculated isotherms are presented for a wide range of frost temperatures and chamber pressures. The pumping speed of a frost cryosorbent decreases with increasing amount of gas sorbed. A general model of the sorption dynamics was formulated and approximate closed-form solutions were obtained: (1) in the limit of rather compact frosts whose sorption behavior would be limited by the ability of the molecules to penetrate and diffuse into the frost, and (2) in the limit of very porous frosts in which the adsorption rate on the frost surface governs the pumping. Theoretical calculations for these limiting cases agreed with the observed pumping characteristics of the more compact and more porous frosts. Comparisons between theory and experiment indicated that the diffusion constant for H_2 in a variety of cryodeposits varies from 10^{-8} to 10^{-15} cm^2/sec.

TABLE OF CONTENTS

LIST OF TABLES

LIST OF FIGURES

FIGURE PAGE

FIGURE PAGE

FIGURE PAGE

FIGURE PAGE

FIGURE PAGE

NOMENCLATURE

A	Area
A^o	Constant in Equation 27 equal to ϕk^2
A_1, A_2	Constants
B_1, B_2	Constants
C_1, C_2	Constants
a	Solubility constant in Henry's law
a_o	Lattice constant
b	Adsorption coefficient in Langmuir's equation, defined by Equation 17
C	Dimensionless sorption capacity, ratio of the number of molecules sorbed to the number of molecules predeposited in the frost sorbent
C^o	Sorption capacity constant of Equation 27
C_m	Maximum sorption capacity
c	Sticking probability
D	Diffusion constant
E_a	Energy of adsorption
E_B	Surface barrier energy
E_D	Diffusion energy
E_d	Sorption energy
E_L	Energy of vaporization
G	Mass transfer constant
J	Molecular flux, molecules/cm^2-sec
J_o	Initial pumped flux

K	Leak conductance
k	Boltzmann's constant
k_o	Desorption coefficient
ℓ	Frost thickness
$\bar{\ell}$	Mean thickness
ℓ^*	Effective thickness of adsorbed gas layer
M	Molecular weight
m	Mass of a molecule
N	Number of molecules
N_D	Diffusion Biot number
N_F	Fourier modulus
N_o	Number of adsorbed molecules on the frost surface
$\dot{N}$	Molecular strike or flow rate
n	Number of layers (BET theory)
n	Number density of sorbed particles
n'	Transformed number density, $n' = n - n_o$
$\dot{n}$	Molecular strike rate per unit area
n^*	Calculated mean number density of sorbed molecules
n_o	Equilibrium number density at surface
n,m	Summation indices
P	Pressure
P^*	Pressure gage output
P_o	Vapor pressure of the bulk liquid
Q	Quantity of gas in torr-liter
$\dot{Q}$	Throughput, torr-liter/sec
r	Radial distance

S	Pumping speed
S_o	Initial pumping speed
s	Unit pumping speed
s_o	Initial unit pumping speed
T	Temperature
T_R	Return temperature of helium cryogen
T_S	Supply temperature of helium cryogen
$T(t)$	A function only of time
t	Time
t_r	Residence time
V	Volume
V_L	Liquid volume occupied by sorbed gas
V_o	Sorbent volume available for sorbate
$V(r)$	Potential energy as a function of r
$X(x)$	A function only of x
x	Coordinate

Greek Letters

α	Gage sensitivity factor
α_o	Condensation coefficient
β	Boltzmann factor in BET theory defined by Equation 20
ϵ	Energy of gas-surface interaction
$\lambda^{(n)}$	Characteristic value
μ	Refractive index
ρ	Density
σ	Lennard-Jones well depth distance

τ Period of vibration of adsorbed molecule

ϕ Parameter in Equation 26 describing sorbent porosity

ψ Functions defined by Equations A-23 and A-24

Subscripts

a Gas addition system or adsorbed

add Added

c Chamber

calc Calculated

d Desorbed

e Effective

f Frost

f_m Maximum temperature experienced by frost

form Formation

g Gas

i Initial of incident

L Liquid

max Maximum

meas Measured

out Outgassing

p Pure substance or pumped

r Reflected

s Sorbent in gas state

sat Saturation

sorb Conditions at time of sorption

T	Total
u	Ultimate
v	Voids
warmed	Intervening condition when frost was warmed
1	Region 1, thin surface layer
2	Region 2, bulk of frost

CHAPTER I

INTRODUCTION

Cryopumping [1 and 2][1] has come into widespread use over the past decade because the entire interior walls of a space simulation chamber may be lined with cryogenically cooled panels and extremely high pumping capacities may be achieved. Unfortunately, this pumping technique is not usually economically feasible for the removal of hydrogen, neon and helium because of the very low condensation temperatures of these gases at low pressures. Neon does not generally present a problem because of its rarity, however, hydrogen and helium are present in most vacuum systems and often limit the ultimate pressure which may be achieved. Moreover, these gases are widely used in aerospace technology and frequently it is necessary to remove large amounts of them from large space simulation chambers. The problem of removing large amounts of hydrogen is of particular concern because of the increasing need to evaluate the operation of small space propulsion units in ground-based space chambers [3]. A number of such tests have been conducted at the Arnold Engineering Development Center (AEDC).

---

[1]Numbers in brackets refer to similarly numbered references in the bibliography.

The maximum altitude which may be simulated during these tests is governed by the amount of hydrogen introduced into the chamber from the rocket engine and has been generally limited to about 200,000 to 250,000 ft.

Hydrogen may be pumped by various methods [4]; diffusion pumps, turbo-pumps, ion pumps and others. Each offers certain advantages, but each also has a limited pumping speed and/or capacity for these gases. The use of diffusion pumps is limited by the amount of chamber wall space available for mounting the pumps. The use of molecular turbo-pumps and various types of ion pumps, for example, are all limited by their low pumping speeds.

In addition, various types of sorption[2] pumps have been employed in which either physical or chemical adsorption[2] and chemical reactions at a surface are utilized. For example, titanium films are widely used to chemically adsorb hydrogen (see [5] for example). This method was initially planned for the removal of H_2 in a pumping system at AEDC, but the titanium film was saturated by other gases (mainly nitrogen), and as a result was ineffective for pumping H_2.

---

[2]The definitions of various terms unique to this mode of pumping are contained in Chapter II.

Cryodeposited frosts formed by condensing certain gases (such as CO_2, A, O_2, N_2) on surfaces at temperatures between 10 and 20°K have been shown to provide an effective means of pumping hydrogen by cryosorption.[2] Moreover, these frosts will also effectively pump helium if the cryosurface temperature is maintained at 4.2°K and below. Various investigators have studied and reported the cryosorption pumping properties of cryodeposits. This previous work has indicated that frost cryosorption pumping offers a number of advantages over the use of metal getters for pumping H_2 and the use of cold molecular sieves for pumping H_2 and He:

1. They have higher pumping speeds per unit area and sorption capacity for unit volume than do metal films or molecular sieves.
2. They are readily cooled and kept cold in contrast to molecular sieves material.
3. They can be simply reactivated by depositing a fresh frost layer over one that has been previously saturated.
4. Providing a fresh frost layer does not introduce as large a heat load on the system as occurs when a new titanium film is deposited.
5. They are not as subject to contamination by other gases as are titanium films.

Only a few studies of the cryosorption properties of cryodeposits have been carried out to date. Although the pumping effectiveness of various cryofrosts for both H_2 and He have been reported, the exact pumping mechanism and the factors which influence it are essentially unknown. A detailed research program was carried out to determine both analytically and experimentally the basic nature of the frost cryosorption pumping process, and to explore ways to improve the effectiveness of frost cryosorption pumping. This report is a complete summary of this program. Particular aspects of this work have been previously reported in [6, 7 and 8]. In addition, all of the known previous work on this pumping method is contained in [9 through 18].

CHAPTER II

A SURVEY OF PREVIOUS FROST CRYOSORPTION STUDIES

Inasmuch as the terminology employed to describe cryosorption phenomena is not used consistently in the literature and because the similarity of terms can often give rise to confusion, it is appropriate at the onset to provide a number of definitions[3]:

Adsorption describes a phenomenon in which the molecules striking a surface adhere to it and remain for a finite time. Surfaces may be covered with monolayers or multiple layers of molecules due to adsorption.

Absorption will be used to describe the migration of adsorbed molecules away from their adsorption sites and into the interior of the material. Absorption may occur by interstitial diffusion through a crystal structure or by surface diffusion into pores, cracks, grain boundaries, and so forth which lead into the interior of the material. Molecules which are adsorbed onto a surface might then be absorbed into the material.

Physical Sorption denotes an adsorption mechanism in which the van der Waals attractive forces existing

[3]These definitions are used consistently throughout this work, and are most commonly used in the open literature.

between all substances are responsible for binding the molecule to the surface.

Chemisorption describes an adsorption mechanism in which the forces binding the molecule to the surface are chemical in nature. Chemisorption is believed to occur in two steps. First, molecules are physically adsorbed on the surface, then they enter into a chemical reaction with the surface and are bound to it chemically as a new compound.

Sorption is often used as a general term to describe adsorption and/or absorption processes where the adsorption may be either physical or chemical. This term is frequently used to represent a combined adsorption-absorption phenomenon as well as to describe some sort of adsorption/absorption phenomenon which is not well defined.

The Sorbate is the gas being sorbed by a Sorbent. For example, in this investigation H_2 is the sorbate while the cryodeposited frost is the sorbent.

The term Condensation Temperature is used herein to describe the temperature at which a large quantity of gas would be condensed and cryopumped at a pressure of about 10^{-7} torr. However, the condensation temperature changes only slightly with orders of magnitude changes in the pressure. Generally, it is about 5°K lower than is specified by the vapor-pressure curve [2], or about 80°K for CO_2, 26°K for argon, 23°K for N_2, and 5°K for H_2.

Cryopumping is achieved by condensing a gas onto a cryogenically-cooled surface whose temperature is below the condensation temperature. It is, in effect, a special form of adsorption in which the surface acts as an energy sink and greatly decreases the probability of desorption.

Cryosorption is used to describe a sorption process in which the sorbent is cooled by a cryogenic fluid but to temperatures above the normal condensation temperature of the gas being pumped.

Cryotrapping describes a phenomenon in which a non-condensible gas is swept onto a cryosurface by a condensing gas and buried and trapped there by the condensed gas.

The Adsorption Energy, sometimes called the heat of adsorption, is the amount of energy interchanged when a gas is adsorbed on a surface. Physical sorption is characterized by an adsorption energy of a few kilocalories/mole while chemisorption involves energies of 10 to 100 kilocalories/mole.

The Desorption Energy is similarly defined as the amount of energy an adsorbed molecule must acquire before it is energetic enough to leave the surface.

I. PREVIOUS EXPERIMENTAL STUDIES

As long ago as 1933, Keesom and Schmitt in Holland [19] noticed that gaseous helium would stick to a glass container cooled to liquid helium temperatures, perhaps due

to physical adsorption. In the intervening years many investigators have reported that the partial pressures of H_2 and He were lower than expected in vacuum chambers containing cryosurfaces cooled to about 20°K.

1. Cryosorption of Hydrogen

In 1961 Brackman and Fite [20] may have supplied the explanation of these anomalies. While studying the reflection properties of atomic and molecular hydrogen from cold surfaces using a molecular beam, they found that cryosurfaces at temperatures below 20°K which were partially covered with water ice were capable of condensing H_2. After a brief study they stated: ". . . it seems appropriate to suggest that the experimental results indicate either true adsorption of H_2 to frozen-water surfaces or trapping of H_2 by simultaneously condensing water vapor or perhaps both."

These investigators presented no data but also reported that water frost at temperatures between 7° and 14°K appeared to pump helium while oxygen was pumped by water frost in the 60°K to 90°K temperature range. As a result they proposed the use of ice pumping as "the world's least expensive method of producing a vacuum." However, Brackman and Fite did not offer any analysis of this pumping phenomenon.

A short time later, Hunt, Taylor and Omohundro reported the results of a more extensive investigation of

this phenomenon [9, 10]. These researchers employed a conventional vacuum chamber which contained a small cylindrical cryosurface cooled with gaseous helium. After the chamber was evacuated to 10^{-7} torr and valved off from its diffusion pump, the cryosurface was cooled to 11°K. A particular gas was then admitted to the chamber forming a thin frost deposit on the 11°K cryosurface. Generally, about 1 to 20 torr-liters of gas were admitted over a 1 to 1-1/2 hour period which resulted in an estimated mean cryodeposit thickness of 0.02 to 0.05 microns formed at a very slow rate. However, due to their system geometry the frost could not have been deposited uniformly over the cryosurface. After the gas addition was completed, hydrogen at 300°K was introduced through a palladium leak.

These investigators report high adsorption rates and sticking probabilities of room temperature hydrogen on cryodeposit films of A, N_2, O_2, H_2O, N_2O and CO_2. All of their test results are summarized here in Figure 1 which shows the pumping speed of the frost as a function of its capacity to pump H_2[4]. It is observed that the various frosts pump H_2 at various pumping speeds until they approached saturation and then the pumping speed diminishes very rapidly. They concluded that adsorption was responsible for the pumping action and that pumping ceased once

[4]The capacity is defined here as the number of molecules sorbed divided by the number of molecules predeposited in the frost sorbent.

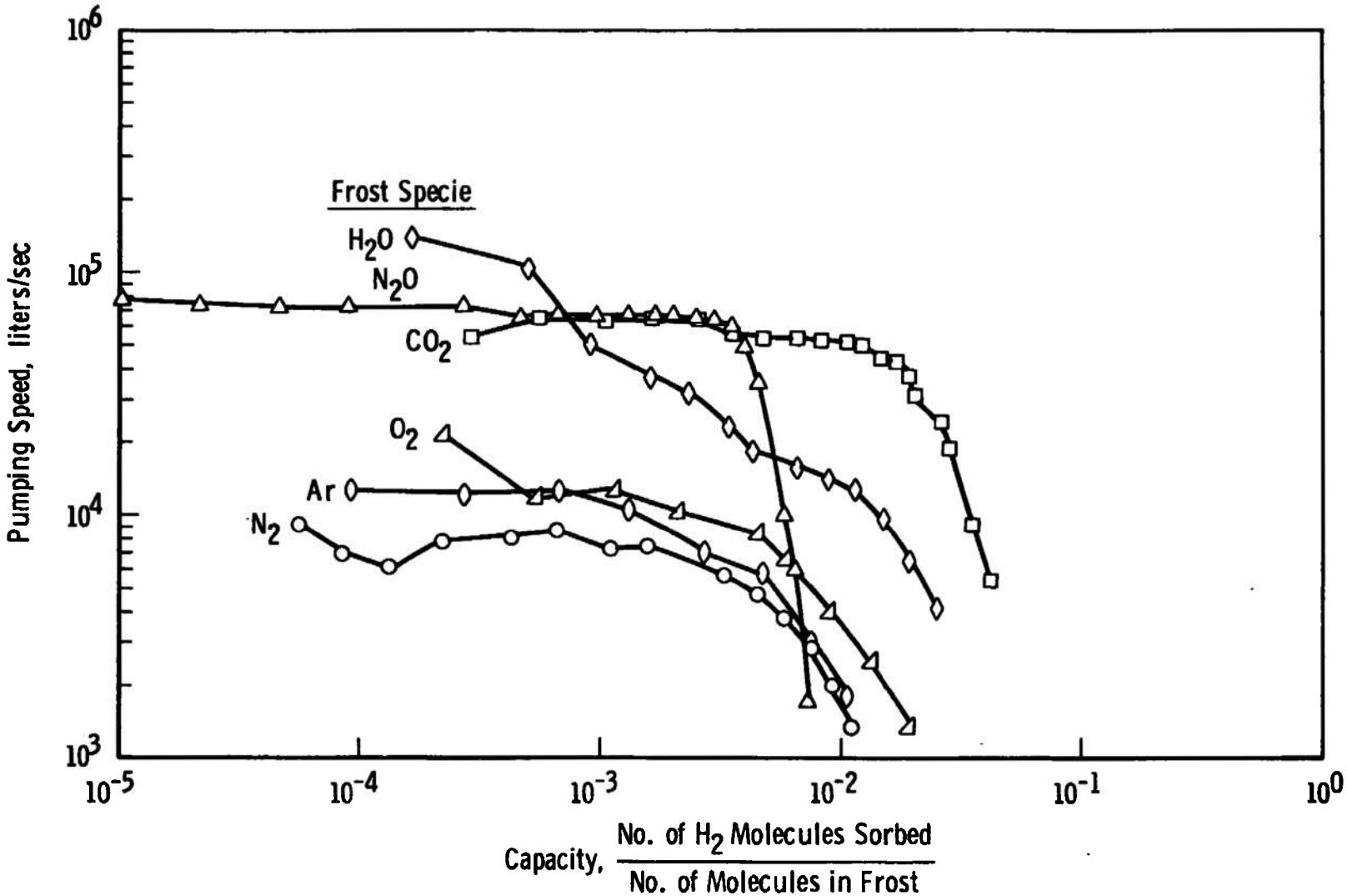

Figure 1. Dynamic Frost Cryosorption Measurements of Hunt, Taylor and Omohundro for 300°K Hydrogen on Various Frosts at 11°K.

the monolayer of H_2 was formed on the frost. Also, they estimated the adsorption energies were a few hundred calories per mole. In addition, it was found that the H_2 could be readily desorbed by increasing the frost temperature to 20°K and when the frost was cooled again it would pump almost as well as it did initially. Although this group concluded that "adsorption cryopumping," of hydrogen, as they called it, was feasible, they apparently did not pursue it further.

The investigation of cryodeposited frost films as sorbents for hydrogen apparently lay dormant for the next four or five years. During this time the interest and emphasis shifted to cryosorption in which molecular sieves were used to sorb H_2 [21 through 24, for example]. The results of a few studies of hydrogen cryotrapping also began to appear in the literature [25, 26][5]. Then in 1965 the use of H_2O and CO_2 frosts for the cryosorption of H_2 was accidentally rediscovered by Southerlan [11] and independently discovered again in 1966 in Russia by Busol and Yuferov [12].

Southerlan [11] was investigating the cryosorption characteristics of molecular sieves on a large scale in a

---

[5]Some investigators, apparently unaware of Hunt's work, have reported cryotrapping of helium and hydrogen. In retrospect, they may have been witnessing a cryosorption process rather than trapping.

seven-foot space simulation chamber at the Arnold Engineering Development Center (AEDC). During these tests he intentionally attempted to contaminate a molecular sieve panel at 20°K with water vapor, but found that the water frost had a higher H_2 pumping speed than the sieve material at the same temperature. As a result he carried out a few additional cryosorption tests with water and CO_2 frosts on a cryopanel at 20.4°K and about 16°K, respectively. It is significant to note that the CO_2 frost deposited at 16°K was warmed to about 28°K and subsequently cooled to 16°K before the sorption test began. Southerlan's data are difficult to compare with those of other investigators because several factors were allowed to vary during the course of a sorption test. However, he concluded that the capacity of CO_2 frost at 16°K to sorb 77°K hydrogen was considerably lower than the capacity of 20.4°K water frost to sorb 300°K hydrogen, which is somewhat surprising, particularly in the light of subsequent tests by Dawbarn [13].

Dawbarn continued investigation of cryosorption of H_2 with CO_2 frost at AEDC in a smaller research chamber. His experimental apparatus and procedure were similar to those used by Hunt, et al. [10]. However, Dawbarn used a gaseous helium cooled spherical cryosurface situated such that a uniform frost thickness could be obtained and he deposited frosts of approximate thicknesses of either 0.05 or 1 micron at the same temperature at which the subsequent

sorption pumping was carried out. The influence of the temperature of the frost and, to some extent, the temperature of the hydrogen were the prime variables studied in this investigation. It was found that the pumping speed (Figure 2) and capacity of the frost to sorb H_2 significantly increased with decreasing frost temperature; and, at a frost temperature of 25°K no measurable pumping occurred. The maximum sorption capacities which were achieved during these tests at a chamber pressure of 5×10^{-7} torr are summarized as follows:

Temperature of CO_2 Cryodeposit °K	Capacity: Number of H_2 molecules Sorbed / Number of CO_2 molecules in Frost
20	0.005
16	0.020
12	0.125

These studies also indicated in a limited way that the amount of hydrogen which could be pumped was proportional to the frost volume, and the pumping mechanism was more complicated than just surface adsorption as suggested by Hunt, et al. In addition, it was found that nitrogen readily contaminated the CO_2 frost causing a significant decrease of the pumping speed.

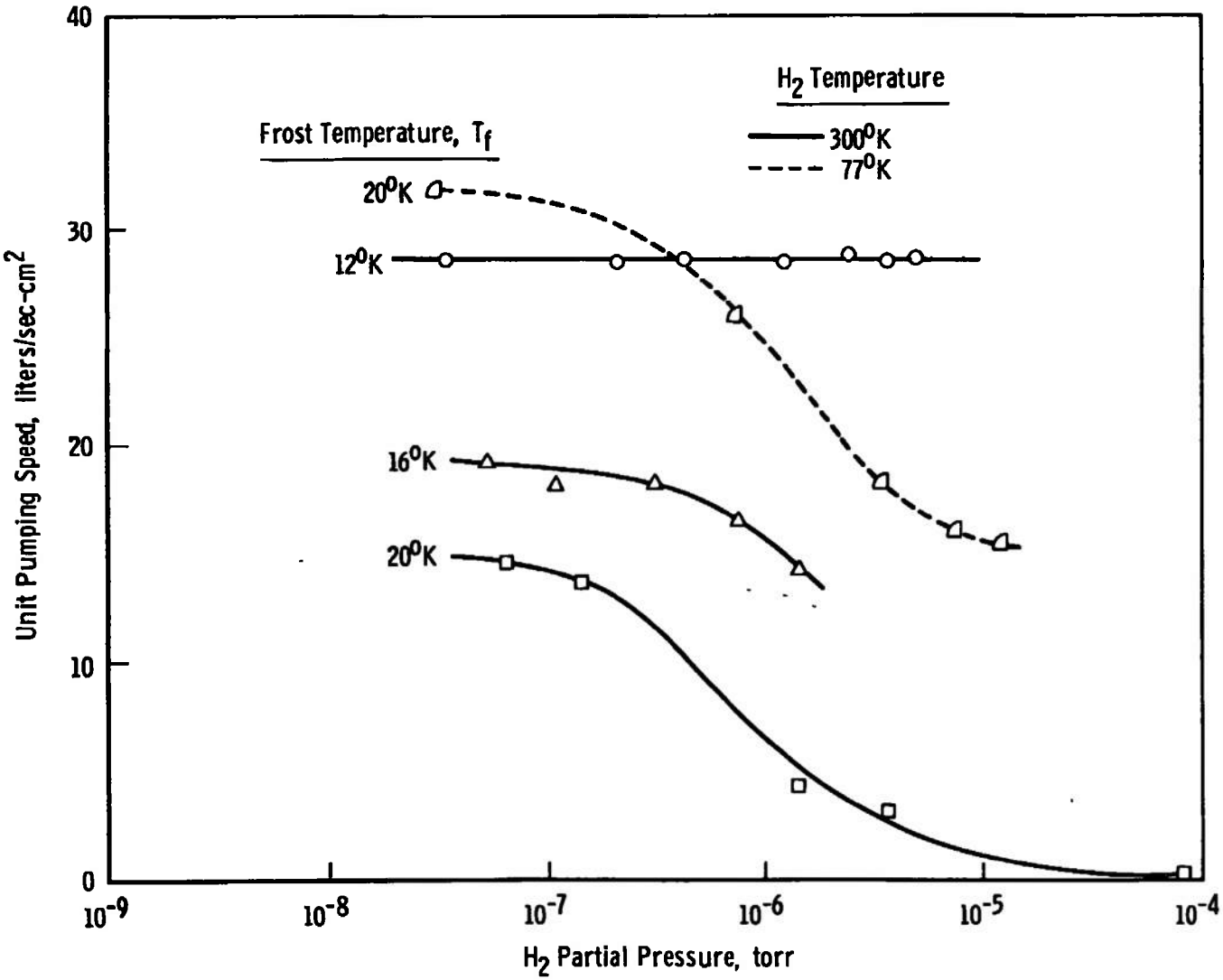

Figure 2. Cryosorption Pumping Speed Measurements of Hydrogen by CO_2 Frost at Various Temperatures.

Dawbarn suggested a more complicated mechanism for the sorption of H_2 by cryodeposits; but he did not attempt to formulate a mathematical model. His ideas were based largely on the data given in Figure 2.

Dawbarn states that the sorption process might be considered in two parts:

(1) Impingement of H_2 molecules at the surface of the cryodeposit results in surface capture. For a fixed quantity of H_2 added to the system, one would thus expect an equilibrium to be established where for a specific concentration of H_2 molecules within this surface, the re-evaporation rate would match the condensation rate. At this point the pumping would stop. However, coupled with this process there is:

(2) A diffusion of H_2 molecules within the cryodeposit matrix from the region of high concentration at the surface. The rate constant for this diffusion is evidently strongly dependent upon the cryodeposit temperature.

In parallel with Dawbarn's studies, Busol and Yuferov were investigating cryosorption of H_2 with a variety of frosts (CO_2, H_2O, N_2, Ar, alcohol, benzene and acetone) in Russia [12, 14]. Their experimental apparatus was very similar to Dawbarn's but they formed the cryodeposits in a different way. The frost layer was always

formed at about 20°K after filling the sphere with LH_2; then the temperature of the sphere and frost were reduced to 16°K or 14°K by lowering the pressure of the boiling hydrogen, and hence supercooling it. These investigators measured pumping speeds for CO_2 frost which were consistent with the trends of data published by Hunt, et al. [10] and Dawbarn [13] and shown in Figures 1 and 2, pages 10 and 14.

The main and new contribution of Busol and Yuferov to the knowledge of cryosorption properties of frost was their measurement of the equilibrium isosteres and isotherms[6] for H_2 sorption by CO_2 and other frosts. For experimental convenience, these investigators measured the sorption isosteres which are given in Figure 3. These data were cross-plotted to produce the isotherms shown in Figure 4. It should be noted that these isotherms represent frosts at various temperatures but formed at a temperature of 20°K. The significance of the isotherms or isosteres is that they specify the maximum sorption capacity that can be expected from a sorbent at given chamber pressures and frost temperature. Also, for equilibrium

---

[6]The amount of gas, V_a, at a given temperature adsorbed or sorbed by a substance under equilibrium conditions may be empirically expressed by a function: $V_a = f(P,T)$. One may experimentally measure the amount of gas sorbed at various chamber pressures by a constant temperature sorbent and hence define an isotherm as, $V_a = f(P)$ for $T_{sorbent}$ = constant. Alternatively, one may define an isostere as $P = f(T)$ for V_a = constant. Plots of these functions are widely used to generalize gas adsorption data [27, 28, and 29].

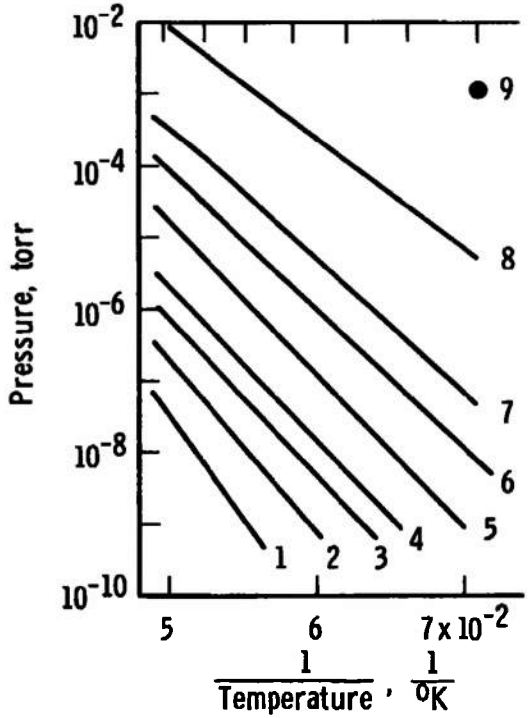

H_2 Capacity in CO_2 Frost, percent

1. 0.4	7. 5.8
2. 0.8	8. 11.3
3. 1.2	9. 18.3
4. 1.6	
5. 2.6	
6. 4.1	

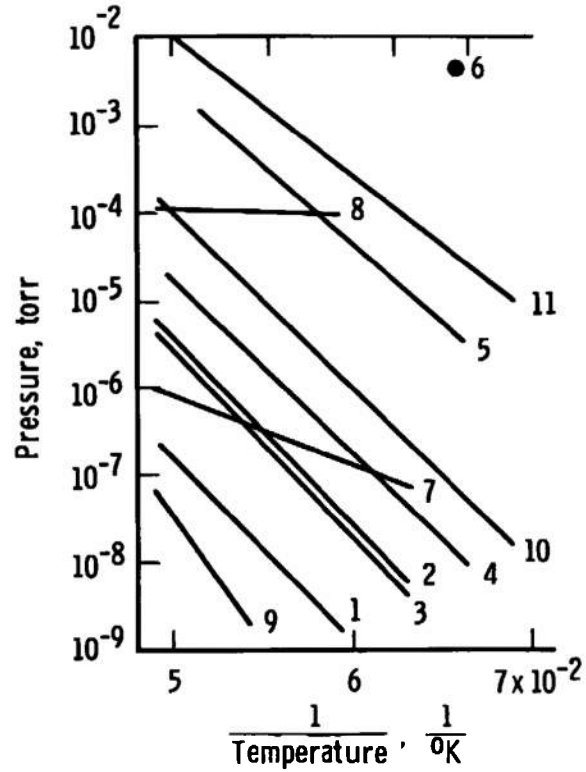

Sorbate-Sorbent Combinations

1. 0.32-percent H_2 in H_2O	7. 0.4-percent H_2 in N_2
2. 0.64-percent H_2 in H_2O	8. 0.4-percent H_2 in Ar
3. 0.5-percent Ne in CO_2	9. 0.4-percent H_2 in CO_2
4. 1.0-percent Ne in CO_2	10. 4.1-percent H_2 in CO_2
5. 4.1-percent Ne in CO_2	11. 11.3-percent H_2 in CO_2
6. 11.8-percent Ne in CO_2	

Figure 3. Sorption Isosteres Measured for Various Sorbent-Sorbate Combinations by Yuferov and Busol.

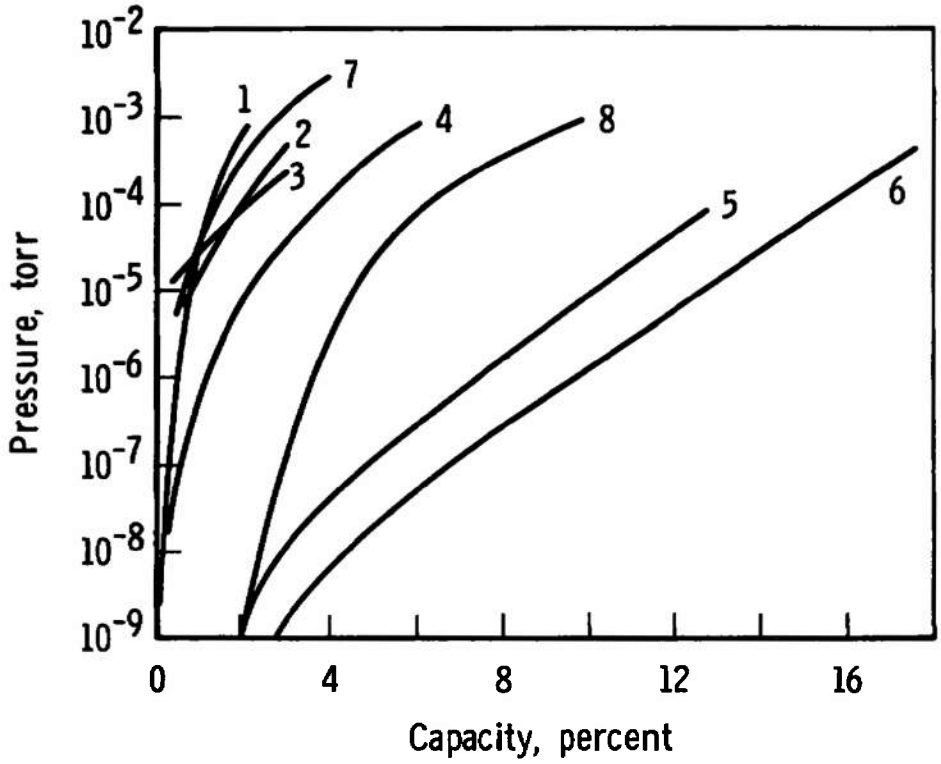

Curve	Sorbate	Sorbent	Sorbent Temperature, ^{o}K
1	H_2	H_2O	20.4
2	H_2	Alcohol	20.4
3	H_2	Acetone	20.4
4	H_2	CO_2	20.4
5	H_2	CO_2	16
6	H_2	CO_2	14
7	Ne	CO_2	20.4
8	Ne	CO_2	16

Figure 4. Sorption Isotherms Measured by Yuferov and Busol for 300°K H_2 and Ne on Various Frost Cryosorbents.

systems the isostere data (Figure 3) may be used with the Clapeyron-Clausius equation to determine the heats of sorption. Busol and Yuferov reported that the heat of sorption of H_2 on CO_2 frost varies from 800 to 1400 cal/mole. Because the measured heat of sorption is far less than typical heats of chemisorption, Busol and Yuferov concluded that physical sorption must occur.

They also found that capacity of the frost depended upon its volume in agreement with Dawbarn and that the hydrogen penetrated rapidly into the CO_2 frost. They reported that N_2 and argon exhibited very poor sorption capacity for H_2. As a result they speculated that the frost had many finely divided pores of atomic dimension and that more complex polyatomic molecules have greater sorption capacity. At one point they suggest that, "only carbon-containing substances have an effective pumping action" [12]. Carbon dioxide frost possessed the best capacity of all the cryodeposits they examined and the maximum capacities they report (see Figure 4) for CO_2 at 14°K are significantly greater than those reported by Hunt, et al. (Figure 1, page 10). They also observed that the presence of N_2 reduced the pumping speed and capacity of CO_2 frost, as had Dawbarn.

In addition to measuring sorption isotherms and showing that frost sorption is a physical sorption process, Busol and Yuferov were the first investigators to point out

the importance of the frost structure and speculate about the role it played. They did not propose a complete sorption mechanism but concluded that CO_2 frost possessed a "more open" structure.

The only other reported study of the cryosorption of H_2 by cryodeposits is a brief paper by Müller [15] which presents some isotherm data for H_2 sorption on CO_2 frost. Müller measured a heat of adsorption of about 900 cal/mol which agrees very well with the values obtained by Busol and Yuferov. He also notes that solid nitrogen, argon and methane sorbents were ineffective for sorption of H_2, neon or helium. Unfortunately, he gave no details concerning his frost formation procedure.

Finally, it should be noted that Hemstreet, et al. [26] (as well as other investigators) simultaneously added H_2 with a relatively large amount of another gas (N_2, CF_4, CH_4, $CClF_3$, $CHClF_3$, CCL_2F_2, and CO_2) in a chamber which contained a 20°K cryosurface. They detected various degrees of H_2 pumping and attributed it to trapping by the condensible gas. They stated that CO_2 was the best "trapping media." These investigators refer to cryotrapping as the process of burying and physically trapping noncondensible gases in the solid structure of the condensed gases formed during conventional cryopumping. It is believed by this author, however, that the phenomenon they observed was the frost cryosorption phenomenon described here. The

amount of H_2 that Hemstreet, et al. could continuously pump while simultaneously adding CO_2 is reasonably consistent with Busol and Yuferov's isotherm data. In any case, these investigators were the first to show that the sorbent may be formed continuously and need not be pre-deposited.

2. Cryosorption of Helium

Few investigations of the cryosorption of helium by various kinds of cryodeposits have also been reported. Brackman and Fite [20] stated that H_2O frost at 7° to 14°K would pump helium but presented no data. Haygood and Dawbarn [16, 17] appear to be the first investigators to systematically study cryosorption of helium on cryodeposited frosts. Their initial studies [16] were carried out with a spherical cryosurface cooled with liquid helium to 4.2°K. The experimental apparatus was essentially the same as previously used by Dawbarn [13] to study the cryosorption of hydrogen. Later tests [17] were carried out using a more practical concave hemispherical pumping surface. The chamber walls were cooled with LN_2 in all tests resulting in 77°K helium striking the frost. They measured the helium sorption isotherms for CO_2, A, N_2 and O_2 frosts (Figure 5). Although CO_2 had the largest capacity to sorb helium these investigators advocate the use of argon as a sorbent for practical reasons, and obtained argon isotherms at lower temperatures by subcooling the liquid helium in the pump (Figure 6).

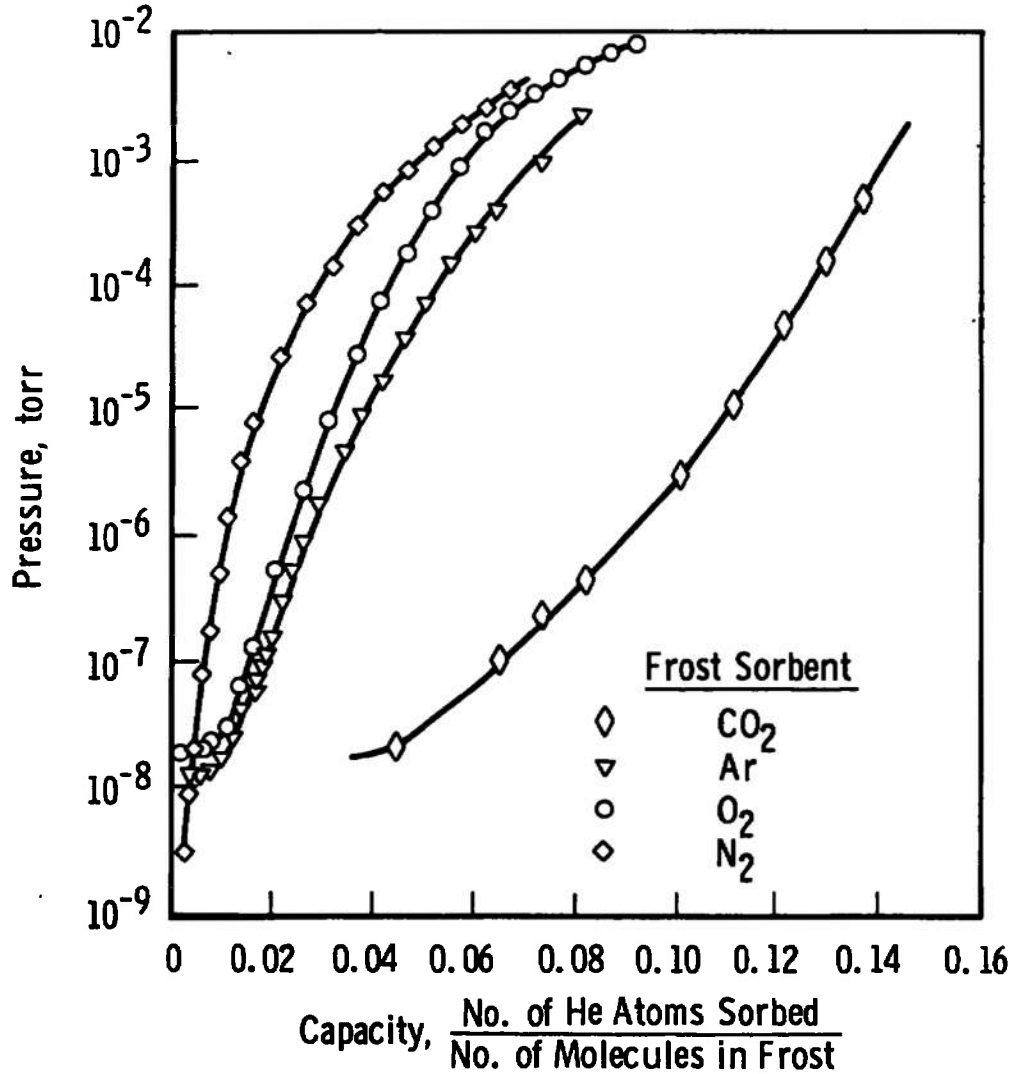

Figure 5. Sorption Isotherms Measured by Dawbarn and Haygood for 77°K He on Various Frosts of 4.2°K.

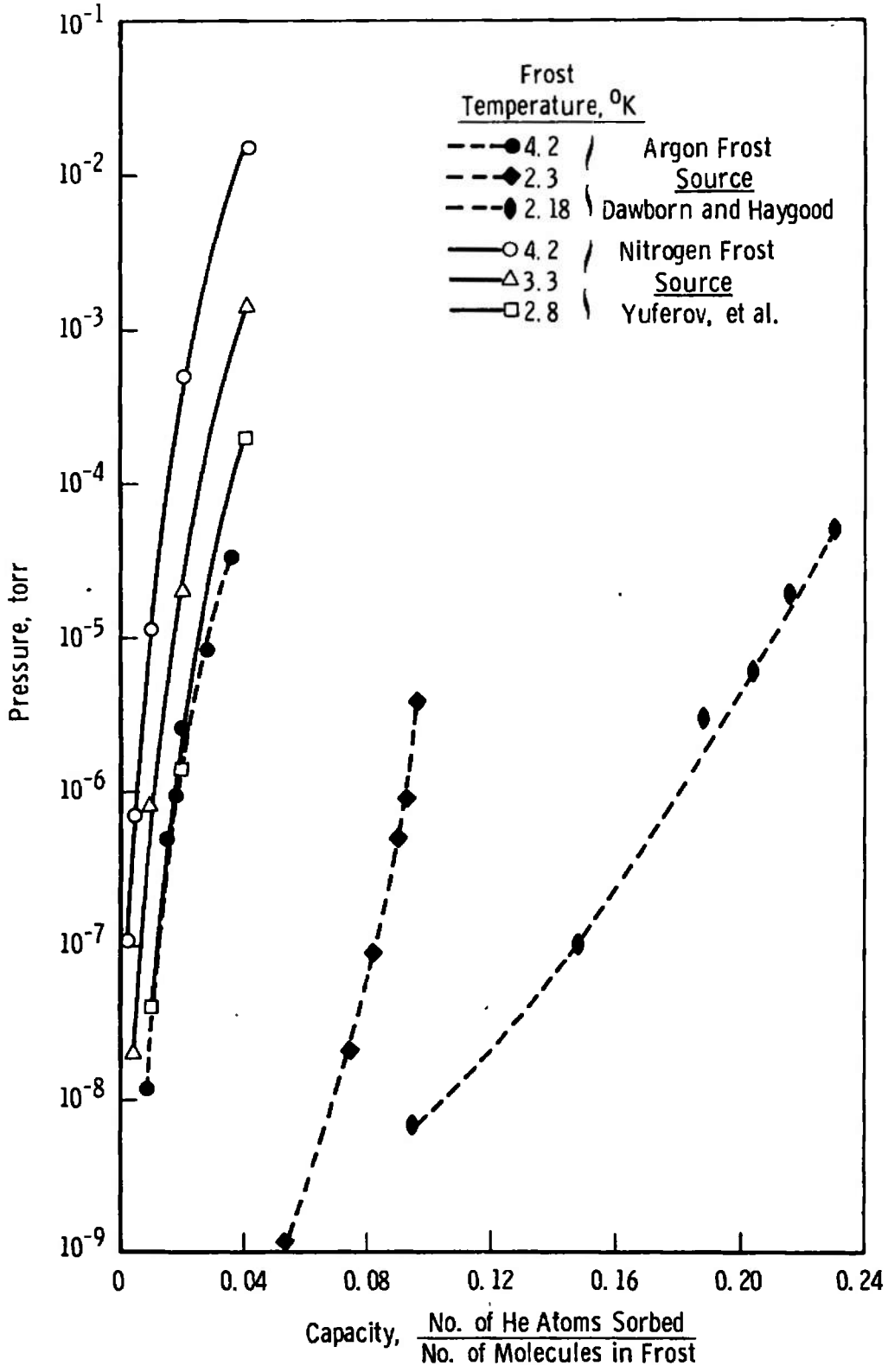

Figure 6. Comparison of Isotherms for Sorption of Helium on Argon and Nitrogen Frosts at Various Temperatures.

Haygood and Dawbarn also reported that 4.2°K argon frost could pump 77°K helium at a speed of about 12 and 16 liters/sec-cm^2. Decreasing the frost temperature did not significantly alter the pumping speed, but it did increase the capacity. They also noted that the capacity of very thin frost layers was not directly related to the frost volume in contrast to what had been observed previously during the sorption of hydrogen. Further, they found that the presence of H_2 would seriously reduce the pumping speed of helium [17] much in the same manner that N_2 reduced the pumping speed of CO_2 frost for hydrogen. They concluded that H_2 acted as a barrier slowing the diffusion of He into the argon cryodeposit.

Yuferov, et al., carried out similar studies of the sorption of helium on frosts of H_2, N_2, Ar and CH_4 at about the same time period [18]. They stated, "nitrogen possessed the optimum absorbing power among the gases investigated," and only presented isotherms for the sorption of helium by N_2 layers. This result conflicts with the data published by Haygood and Dawbarn (Figure 5) which indicated that argon frost is superior to N_2 frost. Isotherms measured by Yuferov, et al. are also shown in Figure 6 and illustrate this variance. The Russian data indicate the heat of adsorbing He by N_2 frost is about 100 cal/mole. Yuferov, et al. also reported sticking probabilities of He on N_2 frost of about 0.1 while

Haygood and Dawbarn reported values as high as 0.6 when argon frost was employed as the sorbent. Both of these investigations demonstrated that the pumping speeds decreased as the helium concentration in the frost increased.

Although there are specific differences between these two investigations, and only a few results are available, the sorption phenomena appear to be quite similar to those described in the preceding section for H_2. No additional results of helium cryosorption with frosts could be found in the literature.

3. Cryosorption of Neon

Yuferov and Busol [14] have also measured isotherms for the sorption of neon on CO_2 frost at 15° and 20°K. These results are shown here in Figure 4, page 18. In both cases the frost was deposited at a cryosurface temperature of 20°K. They reported the heat of sorption was about 1000 cal/mole, and the pumping speed of the CO_2 frost decreased as the amount of sorbed neon increased. Müller [15] also presents an isotherm for neon on 20.4°K CO_2 and measured a sorption energy of 1020 cal/mole.

II. PREVIOUS ANALYTICAL STUDIES

Dawbarn has proposed a possible pumping mechanism for the sorption pumping of cryodeposits which involves: (1) adsorption of H_2 or He molecules onto the frost "surface" and, (2) then diffusion of molecules from this

"adsorbed layer" into the cryodeposit. Pumping would continue until the cryodeposit became saturated with the absorbed gas. Also, Busol and Yuferov concluded that the frost structure must play an important role. Except for these two suggestions none of the investigators, who have reported the results of cryosorption tests with frosts, attempted to formulate an analytical model of the process. There exists, however, a body of information concerning sorption kinetics and adsorption isotherms which can serve as a basis for analysis of the sorption characteristics of cryodeposits.

A theory for the adsorption dyanmics of a porous media was first proposed by McBain in 1909 [30]. He suggested that the sorption of H_2 on charcoal occurred in two steps: (1) almost instantaneous adsorption onto the surface and, (2) a diffusion process in which the H_2 went into solid solution with the charcoal. Thus, in concept, the pumping mechanism suggested by Dawbarn is identical to that analyzed by McBain. To treat the second step McBain solved:

Ficks 1st Law

$$J = -D \frac{\partial n}{\partial x} \tag{1}$$

and Ficks 2nd Law

$$\frac{\partial n}{\partial t} = D \frac{\partial^2 n}{dx^2} \tag{2}$$

for the conditions of:

$$n = n_o \quad \text{at} \quad x = 0 \quad \text{and} \quad x = \ell$$

$$\text{and } n = 0 \text{ at } t = 0$$

A thin frost sorbent would require different boundary conditions. Several solutions to equations of the form of Equations 1 and 2 have been published and works by Barrer [31], Jost [32], and Arpaci [33] catalog many of these. More recently, analyses of the cryosorption dynamics of cooled charcoal or cooled molecular sieves have been carried out by solving Equations 1 and 2 (see [21] for example). Such an analysis could be applied to analytically investigate the cryosorption dynamics of frosts.

It is clear that solutions to Equations 1 and 2 will involve the diffusion constant for the sorbate molecules in cryodeposits. Unfortunately, this information is apparently not available. Moreover, a query of the National Bureau of Standards has indicated that they are not aware of any measurements of the diffusion constants in cryodeposits. Interstitial diffusion into a regularly orientated cryodeposit crystal structure may occur or adsorbed molecules may diffuse in a two-dimensional sense over surfaces and into pores, crevices or crystal defects. Ash, Barrer and Pope report diffusion constants of about 10^{-4} cm^2/sec for the diffusion of N_2 or argon in porous charcoal at about 77°K [34]. Other investigators have

indicated that the self-diffusion constant of argon in solid argon at 80°K [35] and H_2O in ice at about 250°K [36] is about 10^{-10} to 10^{-12} cm^2/sec. In the temperature range between 11° and 20°K, Cremer [37] has previously estimated that the self-diffusion constant for H_2O in ice varies from 10^{-17} to 10^{-13} cm^2/sec. Considering the cryodeposit temperatures employed in cryosorption pumping, and that the diffusion constant decreases exponentially with decreasing temperature of the frost, only gross estimates of the diffusion constants for H_2 in cryodeposits at temperatures below 20°K are possible. They may have values anywhere from 10^{-8} to 10^{-18} cm^2/sec.

III. SUMMARY

Taken in total, all of the investigations of cryosorption of H_2, He and Ne by cryodeposits are consistent in that they show that frosts can be an effective sorption pumping medium. Because of the large number of variables involved, and the differences in the experiments themselves, it is difficult to make meaningful comparisons between investigations. However, when the differences in the factors which have been shown to influence the pumping speed and/or capacity of the frost (i.e., frost temperature, frost specie, sorbate gas temperature) are taken into account, there are still significant inexplicable differences between the various investigations.

As an example, data from four investigations of the sorption of 300°K H_2 by CO_2 frost are summarized in Figure 7. The pumping speeds vary[7] between about 20 and 30 liters/sec-cm^2, but the maximum capacities of the frost vary by almost an order of magnitude. The variation of capacity measured by the various investigators cannot be attributed solely to the different frost temperatures. Also, it has been shown both with the sorption of H_2 and He that the pumping speed and sorption capacity can be significantly reduced if certain other gases are present in the chamber. Clearly, other factors which are as yet undefined must be influencing the cryosorption effectiveness of frosts.

The sorption process is governed by van der Waals attractive forces, but the pumping process is more complicated than simple surface adsorption. As yet no analysis of the fundamental pumping mechanism has been carried out which might define and illustrate the influence of various factors which govern this sorption pumping process.

With this as a starting point, an experimental test program was undertaken to attempt to resolve many of the differences in the existing data, as well as to provide information which might lead to a better understanding of the entire process. Because it was felt that the frost

---

[7]These differences are due in part to the different ways in which the pumping speed is defined and calculated.

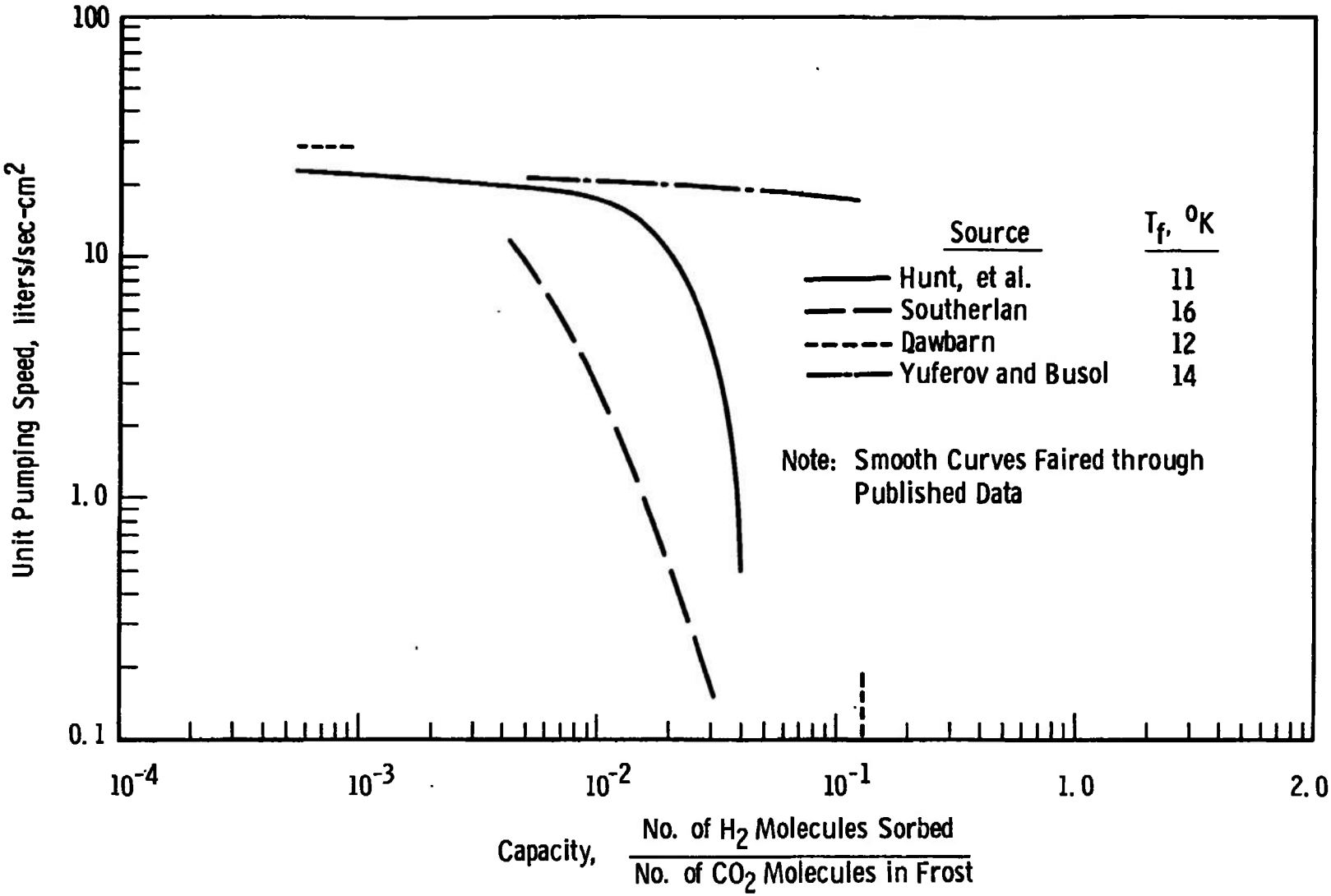

Figure 7. Comparison of Dynamic Sorption Pumping Curves from Various Investigations for 300°K Hydrogen on CO_2 Frost.

structure was the key to putting the entire pumping process into perspective, formation of the frost sorbents was more carefully controlled and documented than had been done by previous investigators. In addition, analysis of the sorption dynamics and equilibrium sorption phenomena was initiated.

CHAPTER III

EXPERIMENTAL APPARATUS AND CALIBRATIONS

I. CHAMBER AND PUMPING SYSTEM

The 36 inch high by 30 inch diameter stainless steel vacuum chamber used for cyrosorption of hydrogen is schematically shown in Figure 8. Its pumping system consisted of a mechanical roughing pump and a 6 inch oil diffusion pump which was equipped with a liquid nitrogen cooled baffle, and had a pumping speed of 1500 liters/sec. A 6 inch high-vacuum, air-operated gate valve was used to isolate the chamber from the pumping system. Access to the chamber is achieved by means of a removable top which employs an O-ring seal. The chamber base pressure without bakeout was between 5×10^{-7} and 1×10^{-7} torr.

A 25 inch high by 24 inch diameter stainless steel shroud was installed in the chamber. It was constructed from overlapping slats (see Figure 8) in a manner to allow free passage of the molecules, but was optically tight. The shroud was maintained at room temperature for all of the hydrogen sorption tests. The cryosorption pump was centrally located inside the shroud, and together with the shroud was attached to the removable chamber top. After correcting for the space occupied by the shroud, sorption

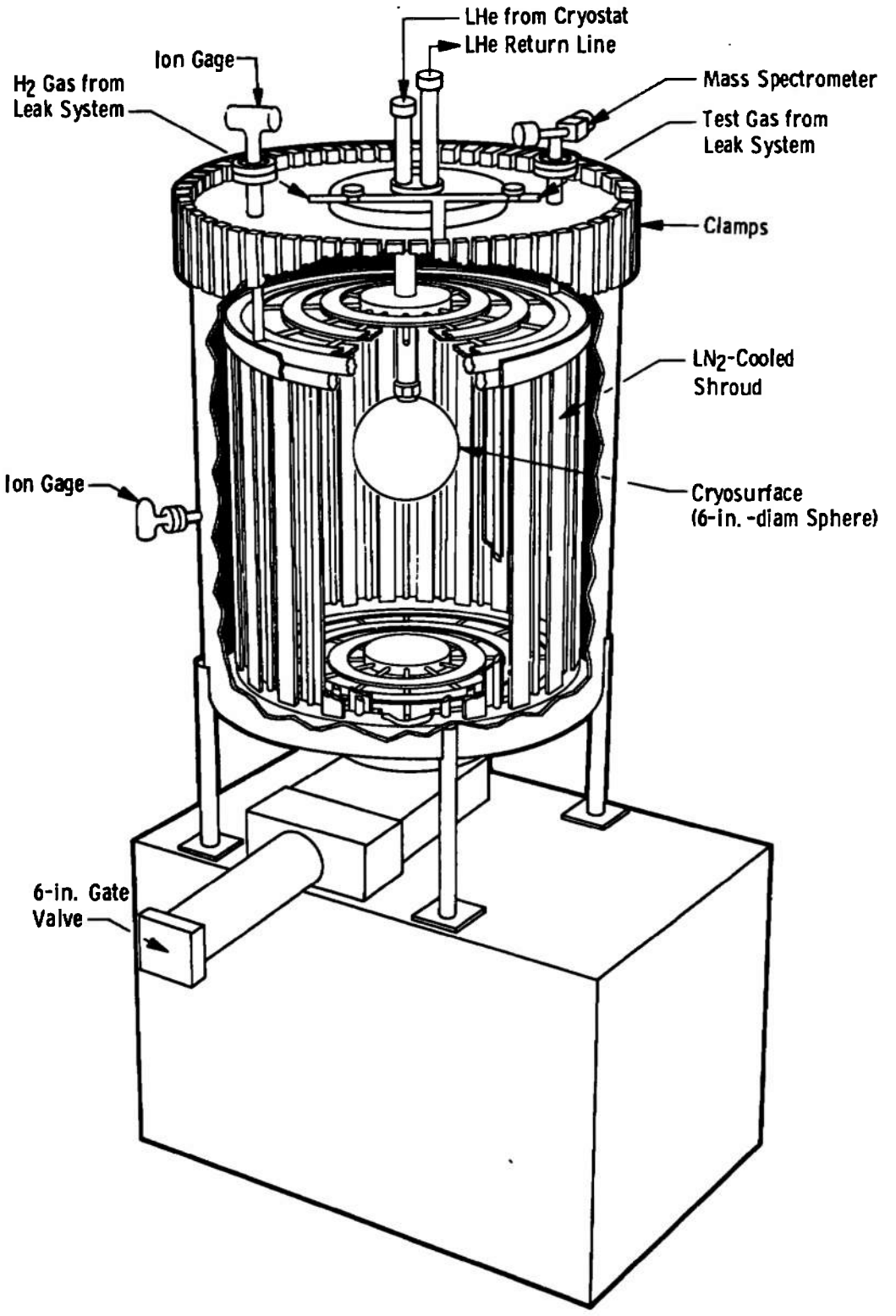

Figure 8. Schematic of Chamber Used for Hydrogen Cryosorption Tests.

pump and other items the chamber had a free volume of 300 liters.

II. CRYOSORPTION PUMP

The cryosurface upon which the frost sorbent was deposited was a simple 6 inch diameter stainless steel sphere with an available pumping area of 970 cm^2 as shown in Figure 9. It was attached to a vacuum jacketed concentric gaseous helium supply and return line which was installed in the removable lid. This concentric line was in turn plumbed directly to a helium refrigerator via vacuum jacketed transfer lines. The refrigerator was a modified Collins cryostat which had about 180 watts of refrigeration capacity and supplied gaseous helium in the temperature range from 12 to 70°K.

III. GAS ADDITION SYSTEM

Hydrogen, as well as the various gases pre-deposited to form the sorbents were obtained from commercially available high-pressure bottles. These gases were introduced into the top of the chamber in the region between the shroud and chamber wall by means of two gas addition systems. Generally, one system was used to add the sorbent gas and the other to add hydrogen. Both systems are schematically shown in Figure 10.

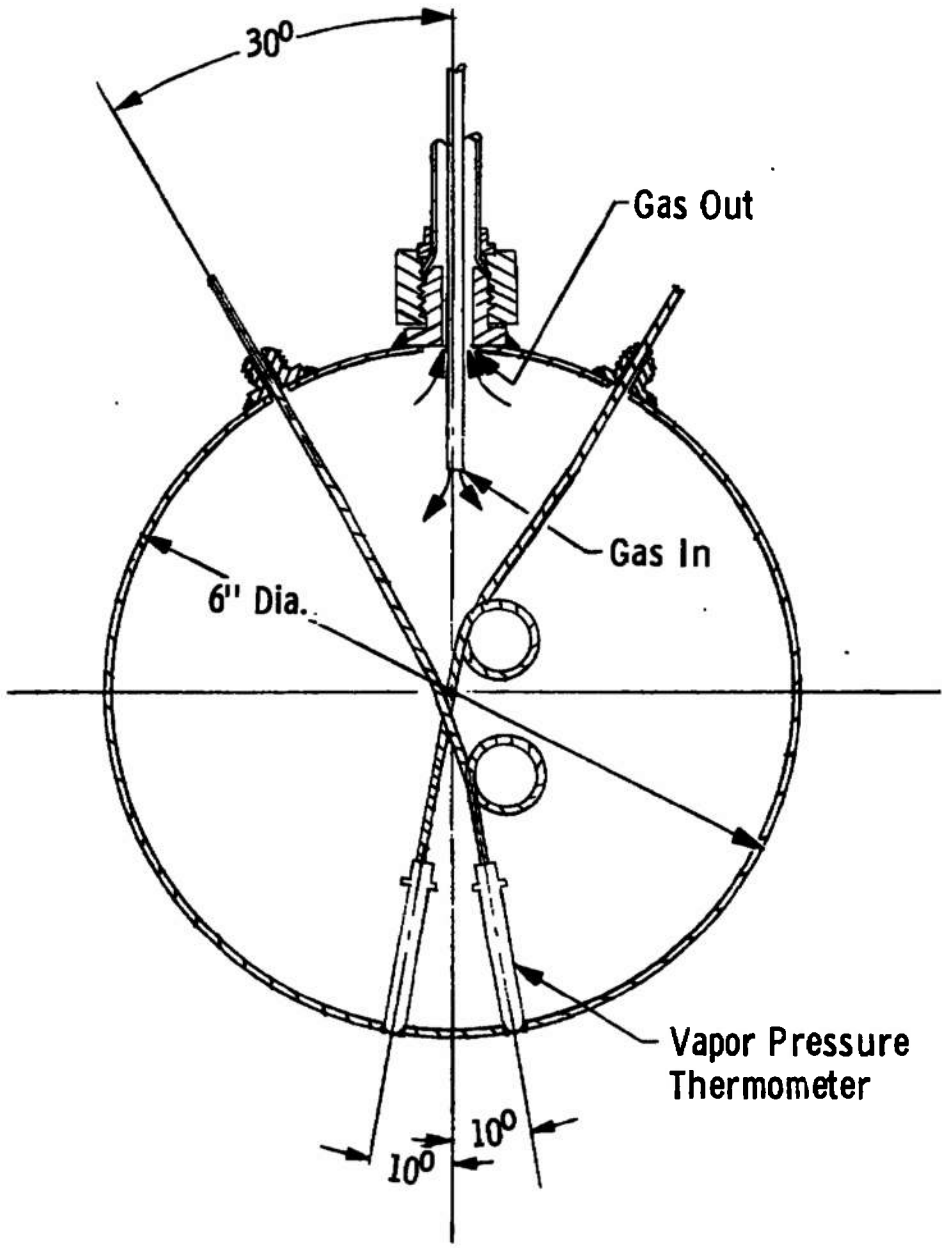

Figure 9. Test Cryosurface.

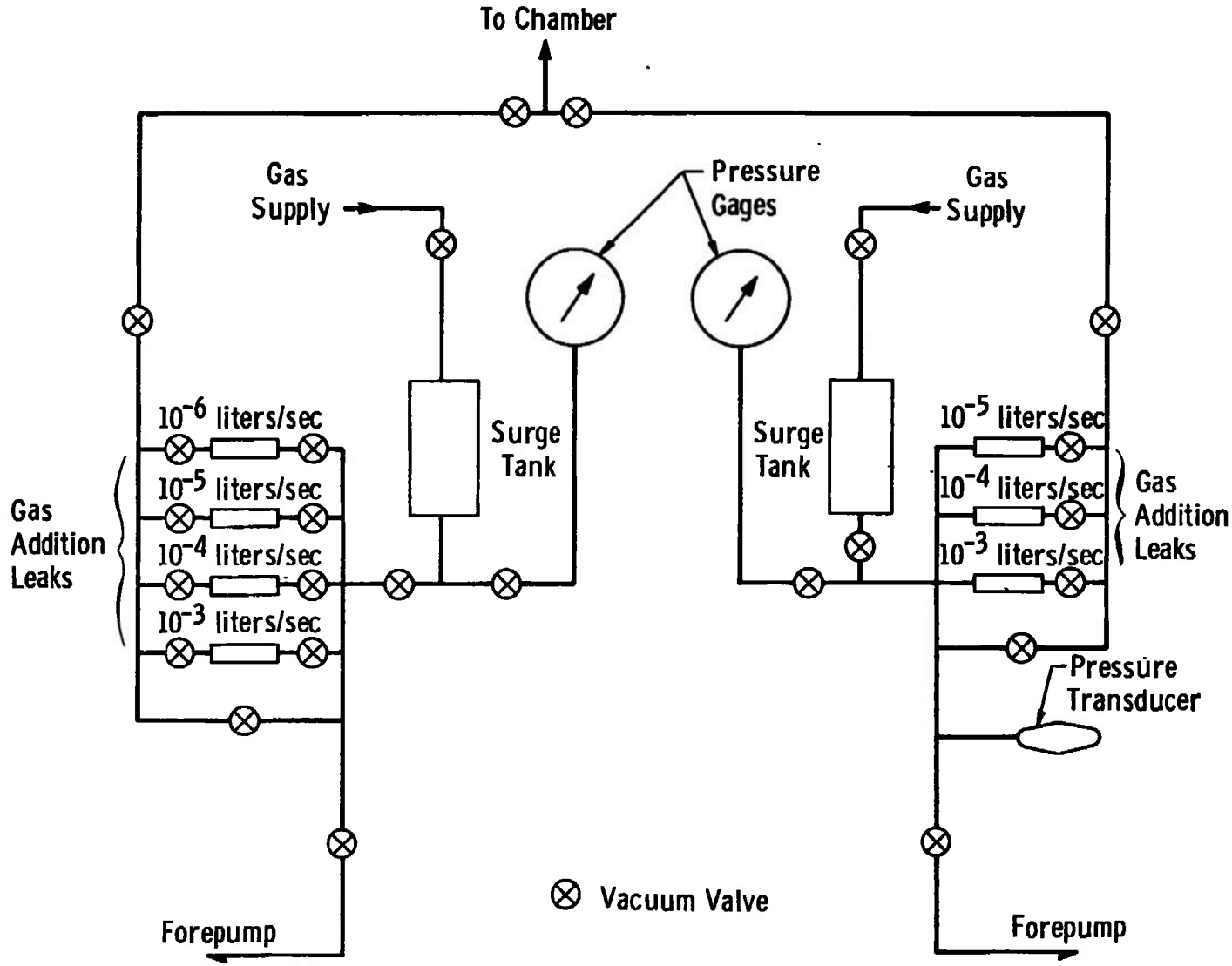

Figure 10. Schematic of the Gas Addition System.

It was not possible to measure directly either the sorbent thickness or its uniformity. However, since the gas molecules would have to have many collisions with the chamber walls and baffles, before they could pass through the optically tight shroud, it is believed that the molecules struck the pumping surface randomly from every direction. As a check, however, both the sorbent gas and H_2 were introduced sequentially into the chamber at the same point, for some of the tests. If the particle ballistics were such that more sorbent was deposited in one place than another, then the H_2 would also strike at a higher rate in these same regions. However, the test results appear unaffected by the gas addition location. After the sorbent had been added on the pumping surface at temperatures below 20°K and before the H_2 addition was started, the base pressure decreased to about 1×10^{-8} to 4×10^{-8} torr.

IV. INSTRUMENTATION

An ion gage and a magnetic-deflection type mass spectrometer were used to measure the pressures in the chamber (see Figure 8, page 33). Tubulation inside the chamber was: (1) employed to prevent the gages from directly sensing the pumping surface, and (2) oriented so that the gages would sense about the same flux of particles as the pumping surface. The time constant of

the tubulation has been calculated to be 3.8×10^{-6} sec for 300°K H_2 [13]. For higher pressure tests the ion gage was replaced with an Alphatron. Ion gage and mass spectrometer outputs were recorded on strip charts with time as a variable. The pressure on the high-pressure side of the porous plug leaks in the gas addition system was monitored with a conventional bellows-type gage, and recorded by means of a transducer and a strip chart recorder.

A hydrogen vapor-pressure thermometer was used to determine the temperature of the gaseous helium cooled surfaces at temperatures between 10 and 25°K. At higher temperatures a helium gas thermometer was employed. The bulbs of both of these devices were located inside of the sorption pump and heliarc welded into holes in the pumping surface (Figure 9, page 35). Iron oxide was used in the bulb of the H_2 vapor thermometer as a catalyst to promote conversion to parahydrogen.

V. GAS ADDITION LEAK CALIBRATION

If two volumes at pressure levels of P_a and P_c are connected by a small leak with a conductance K, then the resulting throughput[8], may be expressed by,

[8]The throughput in vacuum parlance is defined as the product of the volumetric flow rate and the fore-pressure.

$$\dot{Q} = - V_a \frac{dP_a}{dt} = K (P_a - P_c)$$

When $P_c << P_a$ this equation may be easily integrated, yielding

$$- \ln P_a = \frac{Kt}{V_a} + \ln C_1$$

For some initial value of $P_a = P_i$ at $t = 0$, this equation may be solved for the conductance of the leak, resulting in

$$K = - \frac{V_a}{t} \ln \frac{P_a}{P_i} \tag{3}$$

By utilizing Equation 3 each leak was calibrated for each of the gases used by recording the forepressure decay in the gas addition system as gas flowed through the leak into the evacuated chamber. The volume of the gas addition system upstream of the porous plug leak, V_a, had previously been measured by filling the system with alcohol and measuring its volume [13]. The calibrations were carried out several times during the course of the tests. The variation of the leak conductances during these calibrations was within ±5 percent. Some typical calibration curves and typical values of the leak conductances are given in Figure 11.

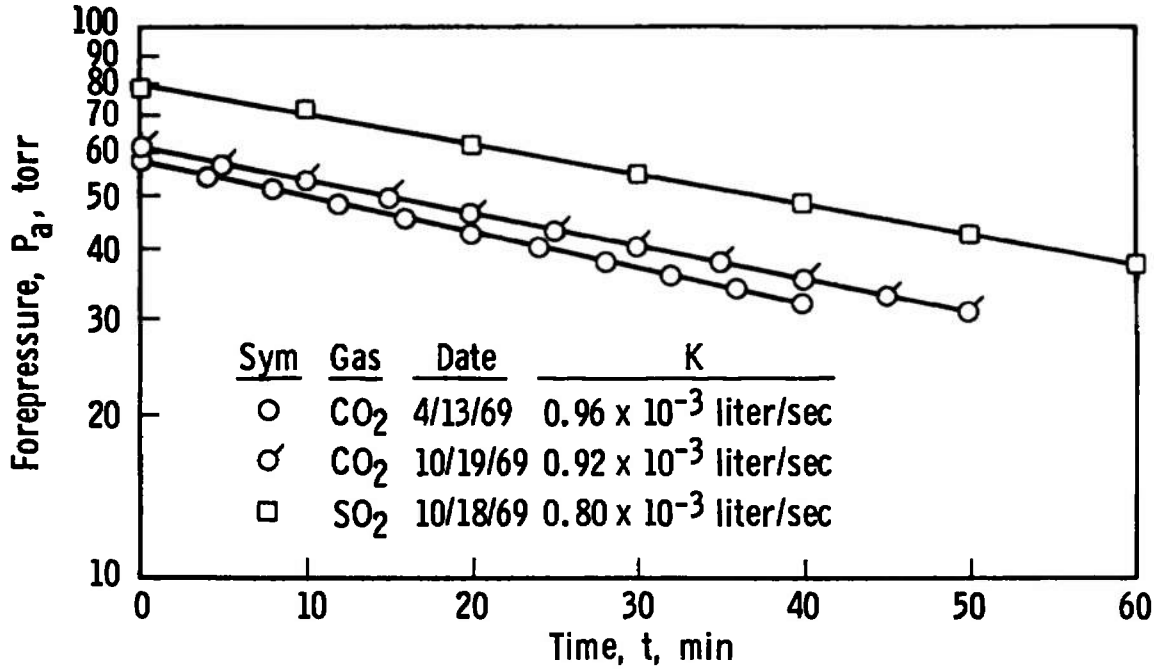

(a) Sorbent Gases

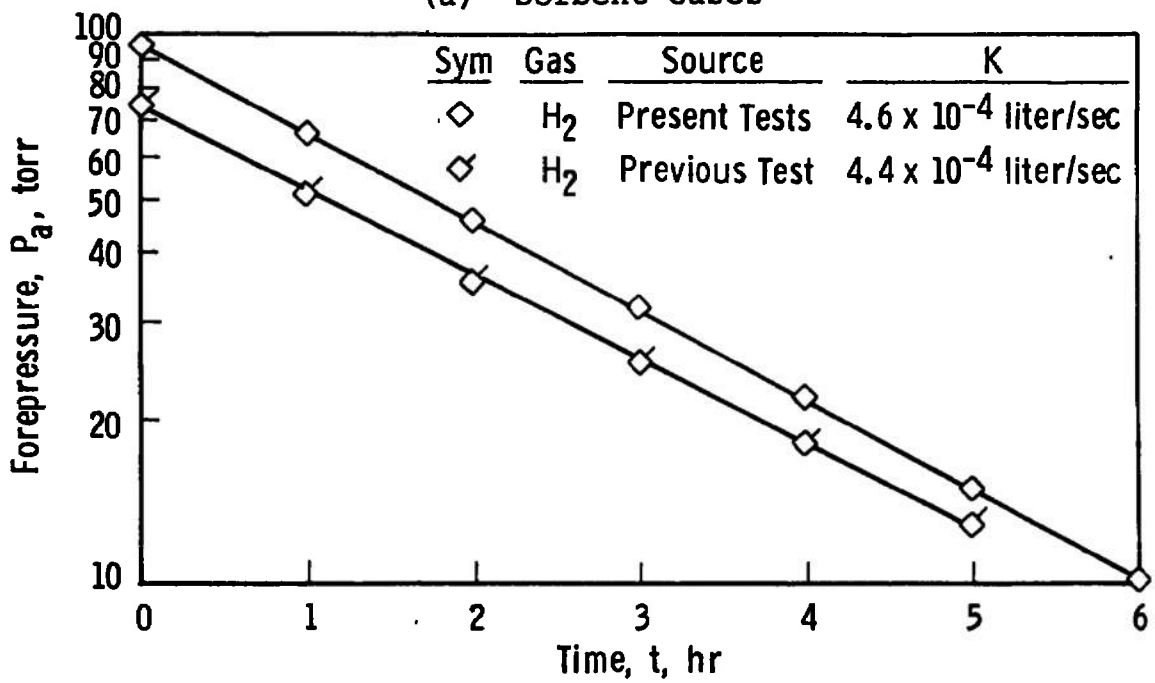

(b) H_2 Sorbate Gas

Figure 11. Typical Gas Addition System Leak Calibration Data.

VI. ION GAGE AND MASS SPECTROMETER CALIBRATION

The sensitivity, α, of an ion gage or mass spectrometer is defined by

$$P = \alpha P^*$$

where P^* is the gage reading. All pressure gages were calibrated in place to determine their sensitivity for hydrogen. The calibration technique is described below.

As gas is introduced into a vacuum chamber which is isolated from its pumping system, the chamber pressure increases due to the addition, as well as due to chamber outgassing and leakage. For a constant volume chamber the rate of pressure increase may be written as

$$\frac{dP}{dt} = \frac{\dot{Q}_{add} + \dot{Q}_{out}}{V_c}$$

where $\dot{Q}_{add}$ is the throughput being added to the chamber and $\dot{Q}_{out}$ is an equivalent throughput due to outgassing, leakage, etc. The amount of gas added through a calibrated leak is given by,

$$\dot{Q}_{add} = P_a K$$

The outgassing and inleakage gas load may be expressed by,

$$\dot{Q}_{out} = V_c \left[\frac{dP}{dt}\right]_{out}$$

where $\left.\frac{dP}{dt}\right|_{out}$ is the rate of pressure increase in an isolated chamber due to outgassing and leakage along. These equations can be combined to obtain the following expression for the pressure gage sensitivity; assuming that α is independent of time for short times.

$$\alpha = \frac{P_a K}{V_c\left[\frac{dP^*}{dt} - \left.\frac{dP^*}{dt}\right]_{out}\right)} \tag{4}$$

Equation 4 illustrates that $\frac{dP^*}{dt}$ versus P_a plots should yield straight lines the slope of which are proportional to the gage sensitivity, and can be used to determine the ion gage and mass spectrometer sensitivities in the following manner.

After the chamber was pumped to its ultimate pressure level by means of the diffusion pump it was then valved-off from the pumping system. As the pressure in the chamber rose due to outgassing and leakage the ion gage and mass spectrometer readings were recorded continuously on a strip chart to obtain $\left.\frac{dP^*}{dt}\right|_{out}$. Then, the chamber was again evacuated and the valve closed. Next, hydrogen was bled into the chamber through a previously calibrated sintered steel leak at a given forepressure, P_a, and the ion gage and mass spectrometer readings recorded continuously to obtain $\frac{dP^*}{dt}$. This procedure was repeated for several forepressures. Typical calibration

curves are given in Figure 12. It was found that the ion gage sensitivity exhibited a characteristic long-term decrease apparently due to contamination effects (see [4], page 95). Consequently, all of the pressure instrumentation was calibrated prior to each series of tests. The gage sensitivities did not change sufficiently rapidly to require calibration before each individual test run.

VII. VAPOR AND GAS THERMOMETER CALIBRATIONS

A hydrogen vapor pressure thermometer was employed to measure temperatures from 10 to 25°K. The hydrogen vapor pressure was measured with a 0 - 100 psia gage having a low internal volume and used to obtain temperatures from the parahydrogen vapor pressure curve shown in part a of Figure 13. The thermometer had previously been calibrated at 20.4°K by submerging the bulb in liquid hydrogen at atmospheric pressure. The supply and return temperatures of the cold helium supplied to pumping surfaces were also measured with factory calibrated gaseous helium thermometers installed in the cryostat. As shown in part b of Figure 13, temperatures measured with the H_2 vapor thermometer were within 2°K of the arithmetic mean temperature in the refrigerated helium in the supply and return lines. It is assumed that the surface temperature of the frost is closely approximated by the temperature indicated by the vapor or gas bulb thermometers (Figure 9, page 35). Temperatures

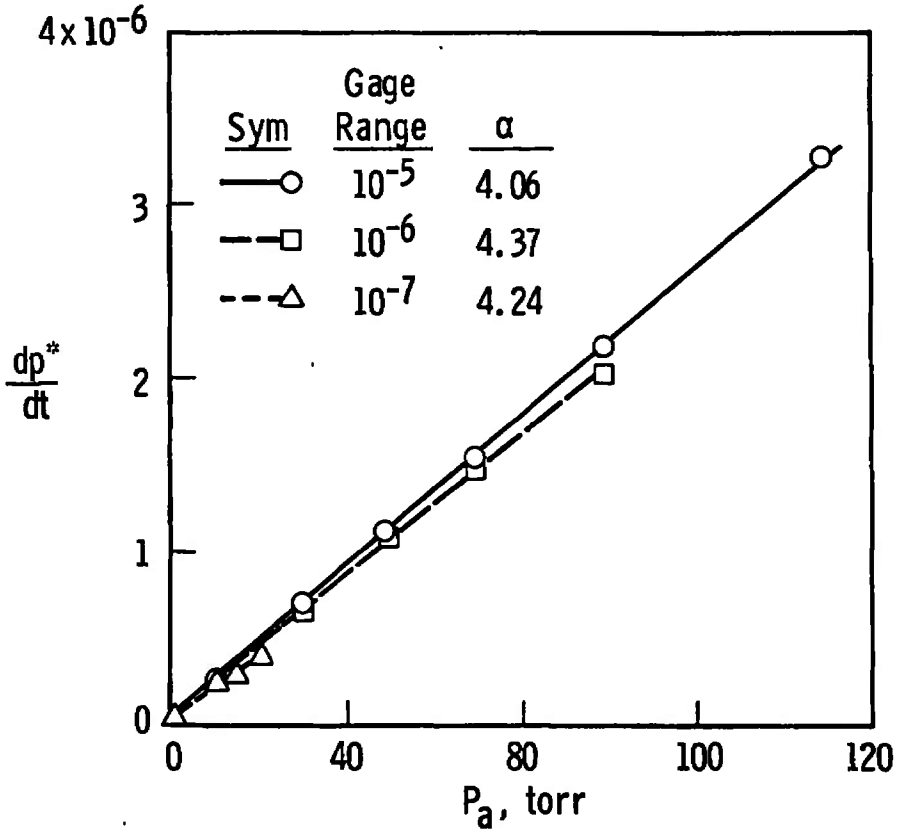

(a) Veeco Ion Gage

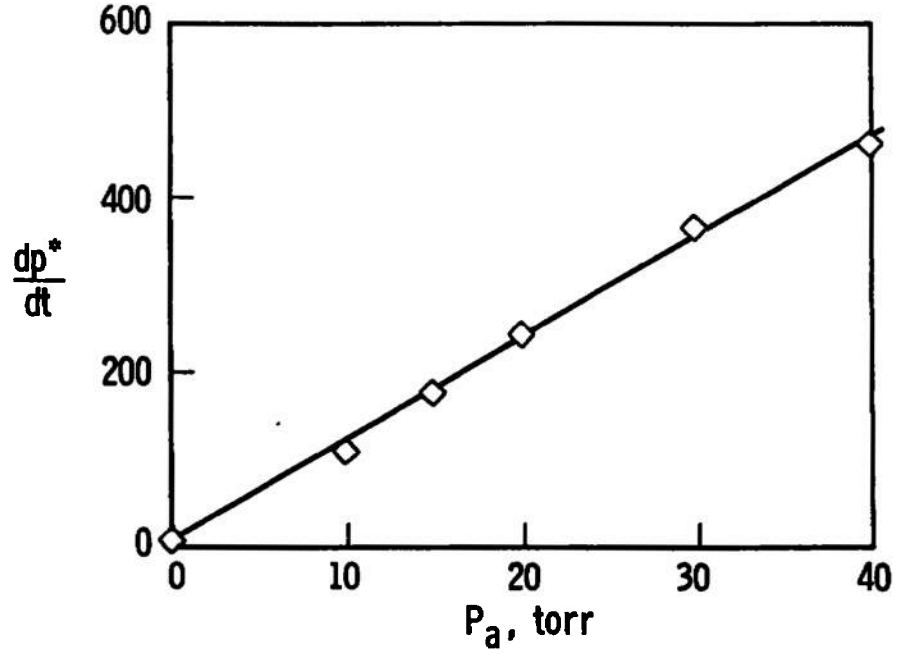

(b) Veeco Mass Spectrometer

Figure 12. Typical Pressure Gage Sensitivity Calibration Data.

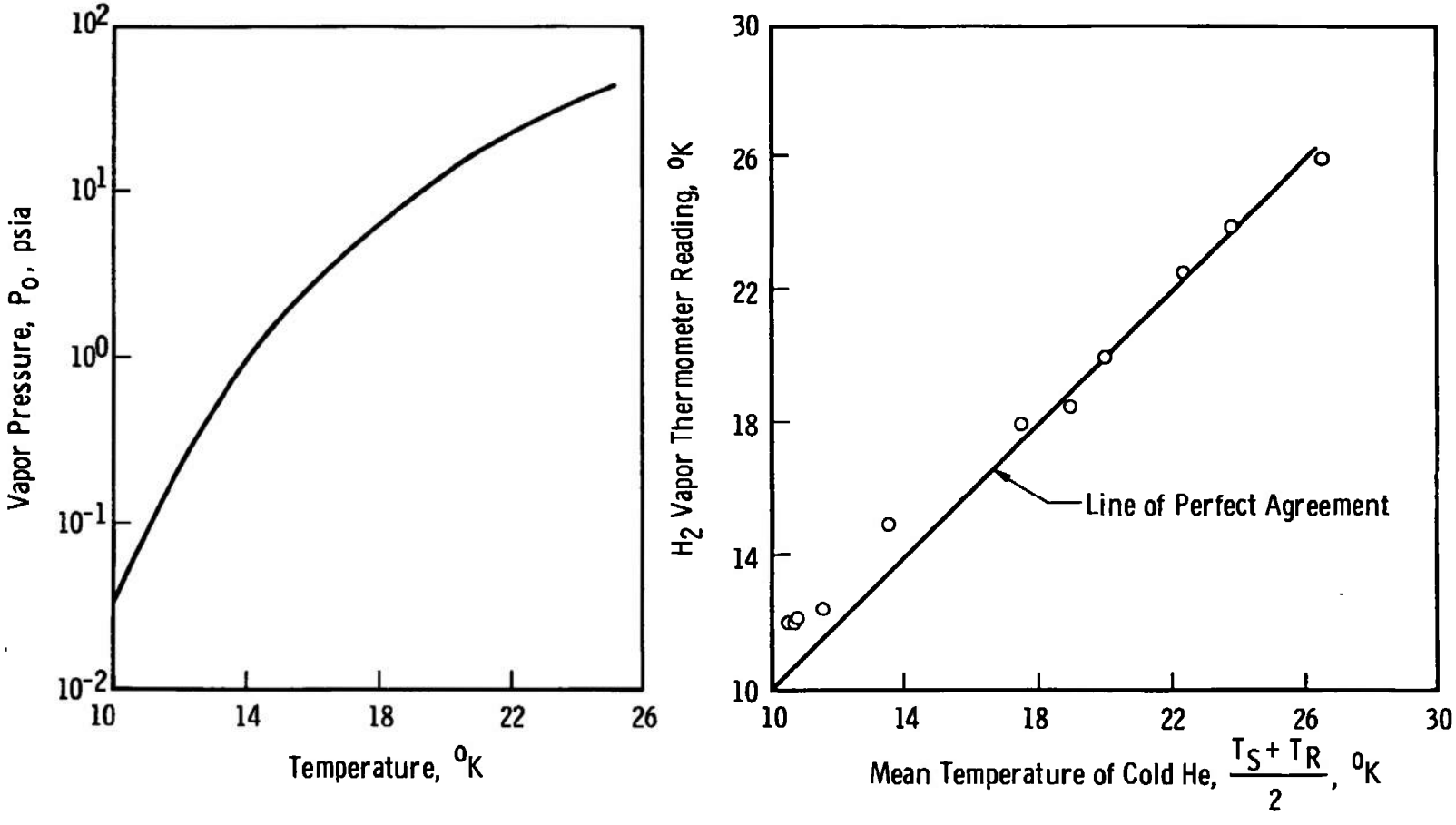

(a) H_2 Vapor Pressure Curve

(b) Comparison of Measured Temperatures

Figure 13. Hydrogen Vapor Pressure Thermometer Results.

obtained with the hydrogen vapor thermometer are believed to be accurate to ±0.5°K in the range between 12 and 25°K.

For tests during which the sorbent was warmed above 25°K, a helium gas themometer was used. It was calibrated against the H_2 vapor pressure thermometer in the range from 12 to 25°K. This calibration curve (Figure 14) was extrapolated to higher temperatures as guided by the mean temperature in the gaseous helium supply and return lines. Temperatures between 25°K and 40°K are believed to be accurate to within ±5°K.

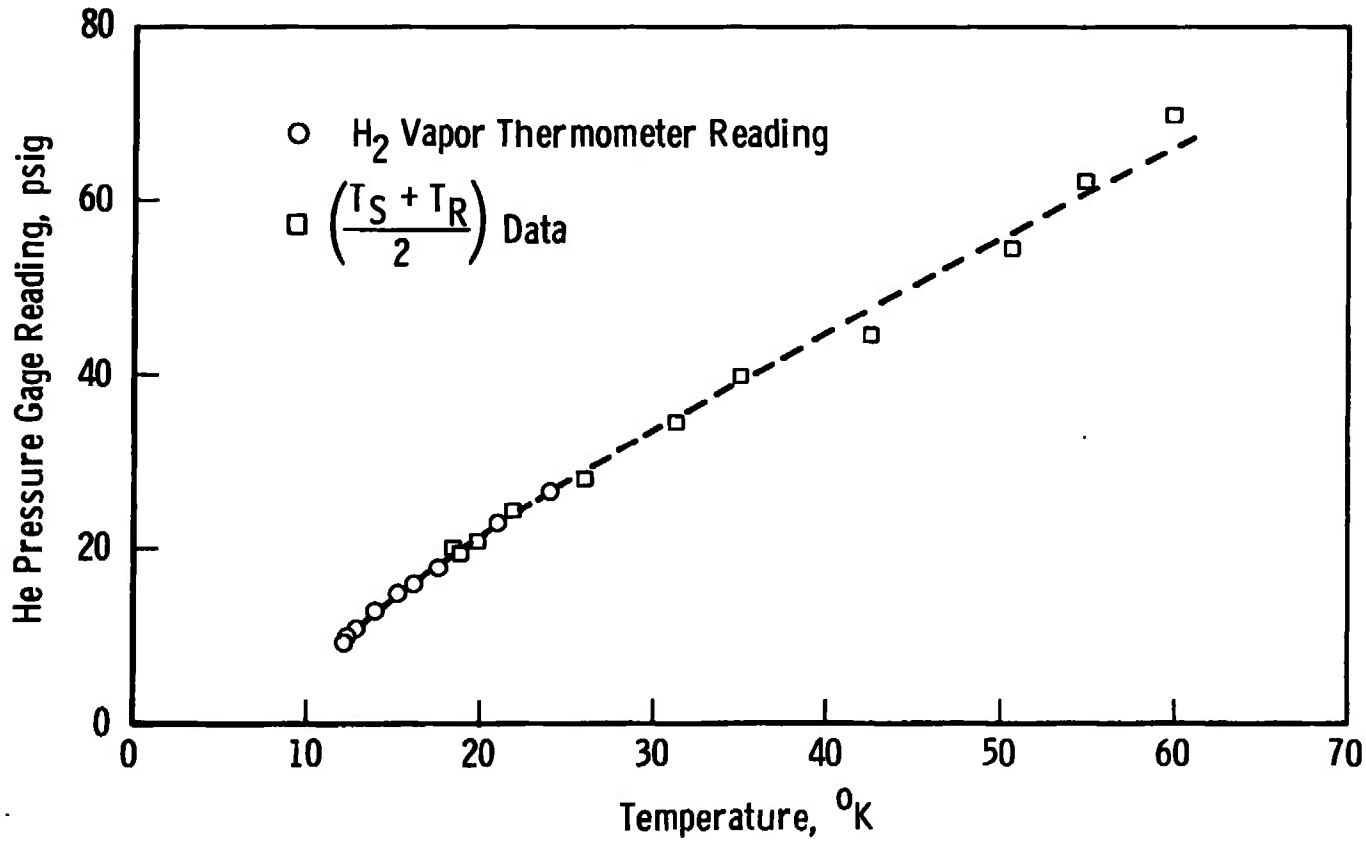

Figure 14. Calibration Curve for the Helium Gas Thermometer.

CHAPTER IV

PROCEDURES AND CALCULATIONS

I. SORPTION TEST PROCEDURES

Prior to each series of sorption pumping runs the molecular leak and pressure gage calibrations were carried out by the methods described in the preceding chapter. All runs were started by pumping the chamber to its base pressure level by the diffusion pump. The two gas addition systems were evacuated by their pumping systems and flushed several times with the gas to be used.

Next, the cryosurface was cooled by circulating cold gaseous helium from the cryostat through it. Its temperature was monitored by the hydrogen vapor thermometer and the supply and return temperatures at the refrigerator. At the maximum refrigerator capacity the cryosurface could be maintained at 12°K. By by-passing a portion of the cold helium the cryosurface temperature could then be adjusted to the desired temperature. When steady-state conditions were reached, the chamber was isolated from its pumping system and ready for admission of the sorbent gas.

1. Formation of Sorbent Frost

All of these tests were conducted by pre-depositing the frost sorbent before beginning the addition of hydrogen.

The sorbent gases used for these tests and their purities as given by the manufacturer (Matheson Chemical Co.) are:

Sorbent	Purity
CO_2	99.99%
SO_2	99.90%
CH_3Cl	99.50%

The reservoir of the sorbent gas addition system was filled to a particular forepressure which established the sorbent addition rate for a given leak. As the sorbent gas was admitted into the isolated chamber, the pressure rose to a level which depended upon the forepressure. Some typical values of conditions at which the CO_2 frost was formed are summarized in Table I.

TABLE I

FROST FORMATION CONDITIONS

Chamber Pressure During Formation P_{form}, torr	CO_2 Strike Rate $\dot{n}_{form}$	Frost Growth Rate $d\bar{\ell}/dt$
2×10^{-6}	6.3×10^{14} mol/cm^2-sec	0.0045 μ/min
2×10^{-5}	6.3×10^{15} mol/cm^2-sec	0.045 μ/min
2×10^{-4}	6.3×10^{16} mol/cm^2-sec	0.45 μ/min
1×10^{-3}	3.15×10^{17} mol/cm^2-sec	1.0 μ/min

Most of the sorbents were formed at different pressure levels or strike rates by varying the leak forepressure. However, a few were formed by pumping the chamber to its base pressure and then backfilling it with helium to pressures as high as 10^{-1} torr. The sorbent gas was then introduced into the chamber and the sorbent formed at relatively high helium partial pressure levels. Both the leak forepressure and chamber pressures were recorded continuously and held constant during the prescribed addition time. Then the helium was removed from the chamber by the diffusion pump.

The forepressure, together with the leak calibration, allowed measurement of the amount of sorbent added, Q_s. For convenience of discussion, the mean thickness of the sorbent frost was estimated from Q_s assuming that all of the sorbent gas added to the chamber was deposited on the cryosurface.

$$m_s = \frac{Q_s M}{kT_g} = m_f = \rho_f A_f \bar{\ell}_f$$

or

$$\bar{\ell}_f = \frac{M Q_s}{A_f \rho_f kT_g} \tag{5}$$

The density of the frost is needed to estimate the frost thickness. Densities of some species of frost used

for these tests are available, but the densities of others had to be estimated from the published values of their liquid density and the general trends between liquid and frost densities. Values of the liquid and solid densities of the various sorbents have been taken from References [38 through 41] (see Table II).

TABLE II

SORBENT DENSITIES IN THE LIQUID AND SOLID PHASES

Sorbent	ρ_L gm/cm^3	ρ_f gm/cm^3
CO_2	1.19	1.60
N_2	0.804	0.90
Ar	1.41	1.77
SO_2	1.46	1.80 estimated
CH_3Cl	1.00	1.20 estimated

Sorbent thicknesses from 0.1 to 4 microns were achieved by varying the flow rate and time of the sorbent addition.

2. Kinetic Pumping Measurements

Once the frost was deposited the sorbate gas was admitted to the chamber through its gas addition system; the chamber remained valved-off from its pumping system. Two different sorbate addition techniques were used:

a. Constant sorbate flow rate. The leak forepressure was held constant during the addition to maintain the sorbate addition rate constant at some desired value. Typical time histories of the chamber pressure and sorbate forepressure for this mode of operation are given in Figure 15. Preliminary tests demonstrated that when the chamber pressure had increased to about 3×10^{-4} torr the frost sorbent was essentially saturated with the sorbate and its pumping speed was reduced to a few liters/sec. This will be referred to hereafter as the saturation pressure. The test runs were terminated at this point by shutting off the sorbate flow.

b. Variable sorbate flow rate. For this operational mode the forepressure in the sorbate leak system was initially set at some value and the flow started which resulted in some corresponding value of the chamber pressure. Then, as the pumping speed of the frost characteristically decreased as it sorbed hydrogen, the forepressure on the leak and thus, the sorbate flow rate were steadily decreased in a manner to maintain a constant chamber pressure. Forepressure and chamber pressure time histories for this mode of operation are presented in Figure 16.

3. Adsorption Isotherm Measurements

Equilibrium adsorption isotherm data were obtained by pre-depositing the sorbent and introducing the H_2

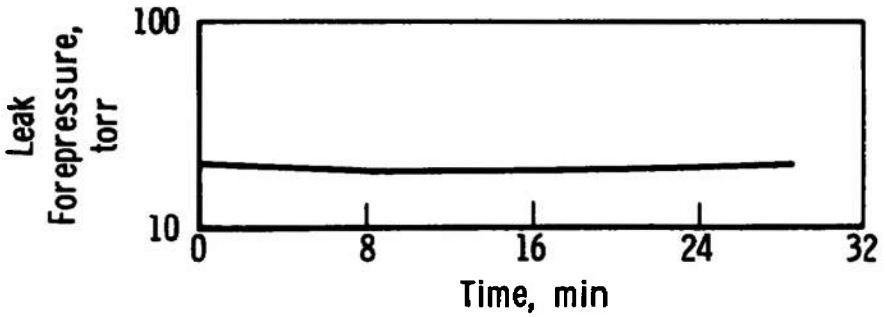

(a) Leak Forepressure

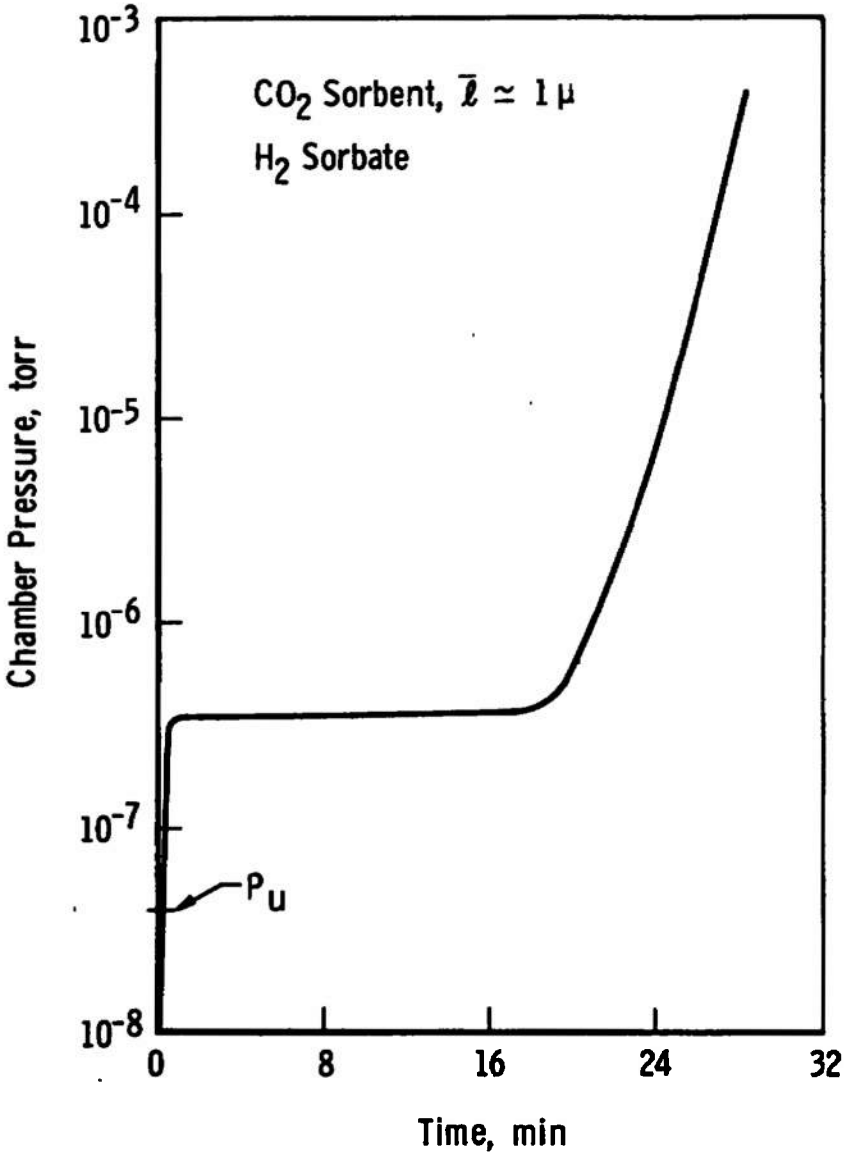

(b) Chamber Pressure

Figure 15. Typical Pressure History for a Test with Constant Sorbate Flow Rate.

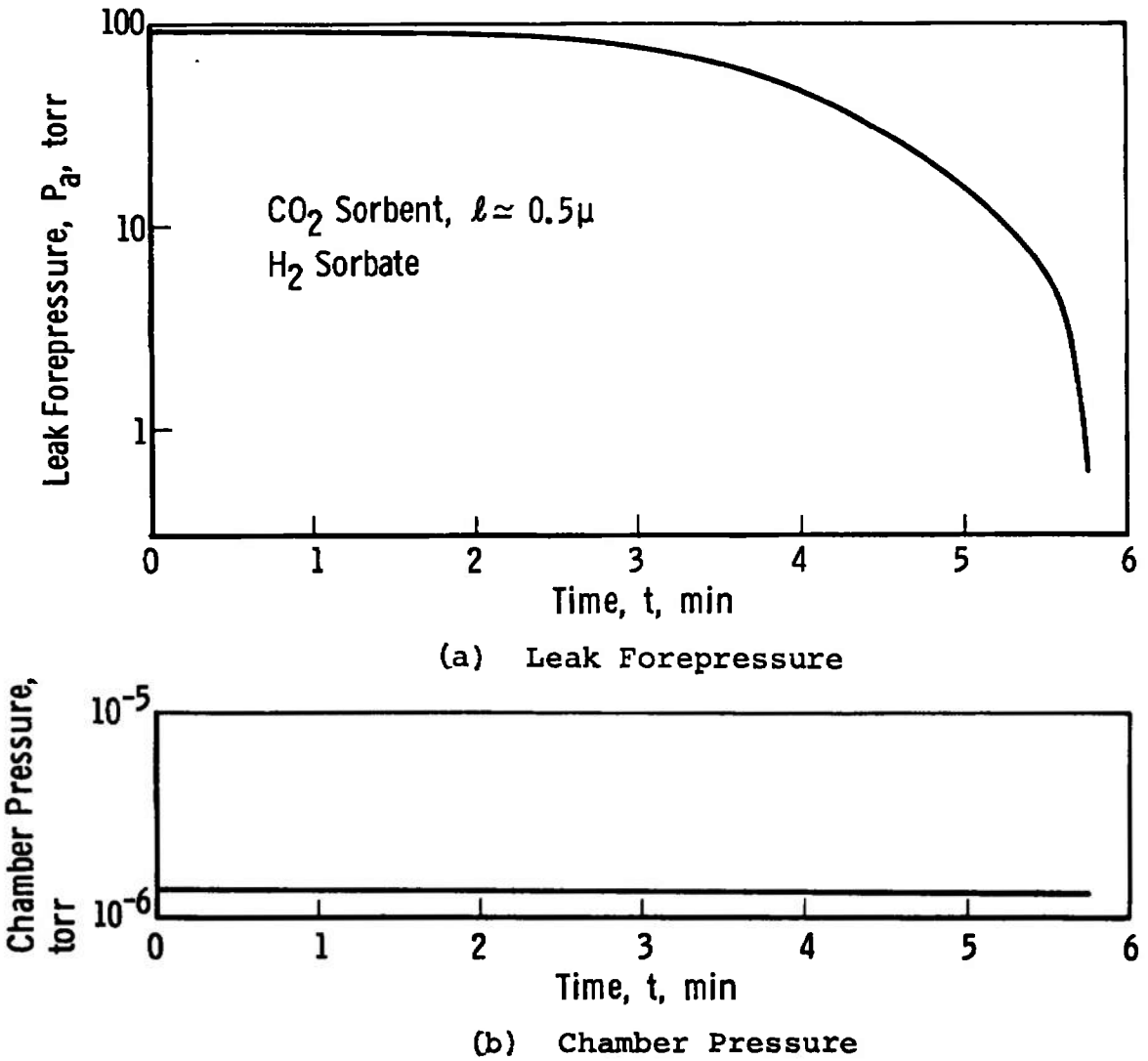

Figure 16. Typical Pressure History for a Test with Variable Sorbate Flow Rate.

sorbate in the constant flow rate mode. However, the H_2 flow was periodically interrupted and the chamber pressure allowed to reach its equilibrium value. After this occurred the sorbate flow was again initiated. This process was repeated several times until the saturation pressure was reached. A typical chamber pressure history during an adsorption isotherm test is given by Figure 17.

4. Desorption Isotherm Measurements

Figures 4, 5 and 6, pages 18, 22 and 23, indicate that after the frost is saturated it is possible to desorb some of the sorbate by decreasing the chamber pressure. This provides the basis for the measurement of equilibrium desorption isotherms. When the frost was completely saturated and the sorbate flow terminated, the diffusion pump was employed to decrease the chamber pressure to some predetermined level. Inasmuch as the pumping speed of the diffusion pump for H_2 was known, it was possible to estimate the amount of gas desorbed from the frost by a numerical integration of

$$Q_d = S \int_o^t P(t)dt$$

where P(t) is the measured pressure variation with time when the valve to the diffusion pump was opened.

Then, the chamber was valved off and allowed to reach equilibrium at which time the sorbate gas flow was

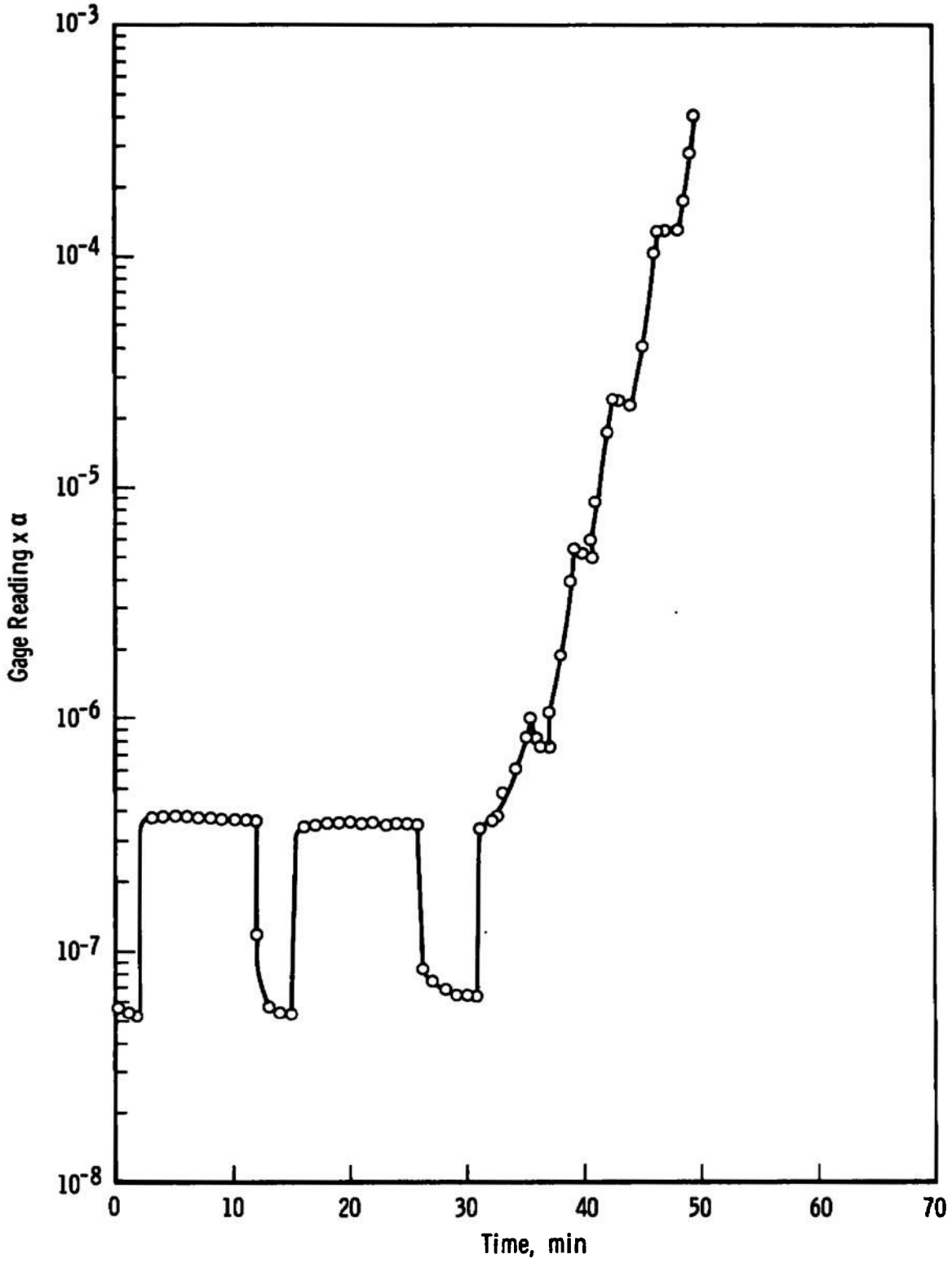

Figure 17. Typical Pressure Variation during Adsorption Isotherm Measurement with Interrupted Flow.

again started. The amount of sorbate gas needed to saturate the frost and restore the chamber pressure to the original saturation pressure was measured and found to be in good agreement with the amount of desorbed gas calculated from Equation 6, see Figure 18. This process was repeated for different pressure levels to define equilibrium isotherms for the desorption process.

5. Desorption by Warming the Sorbent

Isotherms measured at various sorbent temperatures (Figures 4 and 6, pages 18 and 23, for example) illustrate that the sorbed gas would also be desorbed if the frost temperature is increased. This could be achieved through by-passing some of the cold helium in the cryostat. As helium was by-passed, the chamber valve was opened so that the diffusion pump could remove the desorbed sorbate, and the cryosurface temperature was monitored with the gas and vapor thermometers. When the desired warm-up temperature was achieved, the by-pass valve was closed and the cryosurface temperature again decreased to the desired value in preparation for another sorption test.

II. CALCULATIONAL PROCEDURES

1. Pumping Speed

The definition of pumping speed has not been used in a consistent manner in the cryosorption literature. For example, Southerlan [11], Dawbarn [13] and Yuferov and

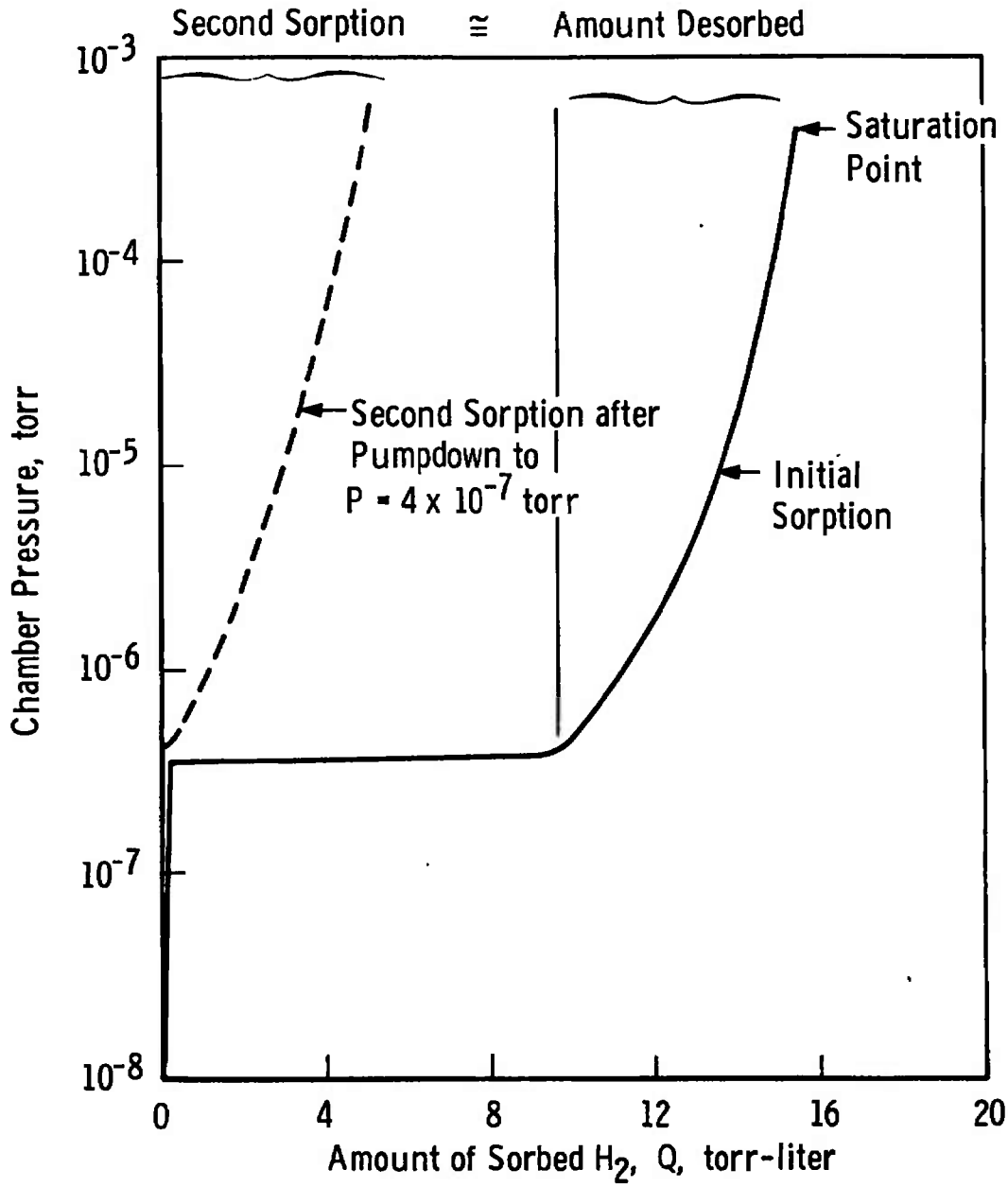

Figure 18. Typical Desorption Isotherm Measurement Data.

Busol [14] have each defined and calculated the pumping speed of frost sorbents in different ways. Other investigators have avoided the dilemma of defining the pumping speed by presenting only the chamber pressure histories during sorption tests [7, 21, 25 and 26].

The speed of a pump is generally defined as the volume of gas removed from the chamber per unit time at the existing pressure level. Then, the total gas load, $\dot{Q}$, handled by the pump is the product of the pumping speed and the pressure at the pump inlet.

$$\dot{Q} = PS$$

It is also given by

$$\dot{Q} = \dot{Q}_{add} + \dot{Q}_{out} - V_c \frac{dP}{dt}$$

where $\dot{Q}_{add}$ represents the intentionally added sorbate gas load, $\dot{Q}_{out}$ is the gas load due to chamber outgassing and leakage and V_c dP/dt represents the amount of gas which enters the chamber volume but is not pumped. If gas is not being intentionally added to the chamber ($\dot{Q}_{add} = 0$), the pump will reduce the chamber pressure to its ultimate value which would be fixed by outgassing and leakage. Thus, $\dot{Q}_{out}$ is given by,

$$\dot{Q}_{out} = P_u S$$

Combining these expressions results in,

$$S = \frac{\dot{Q}_{add} - V_c \frac{dP}{dt}}{(P - P_u)} \tag{7}$$

Equation 7 has been employed to calculate the pumping speeds presented here. To provide meaningful values, the pressure measurement location was such that it sensed the flux of molecules striking the sorption surface. Values of dP/dt were obtained by manually taking the slopes of a pressure-time plot and $\dot{Q}_{add}$ was determined from,

$$\dot{Q}_{add} = P_a K$$

2. Frost Sorption Capacity

The amount of gas pumped by a frost sorbent or a molecular sieve has also been reported in a variety of ways. A nondimensional method is employed here.

The amount of gas added to the chamber to form the sorbent was computed from,

$$Q_{sorbent} = t \cdot [P_a K]_{sorbent} \tag{8}$$

where Q has as convenient dimensions, torr-liters. When the sorbate was added at a constant rate, the amount added may be similarly determined from,

$$Q_{sorbate}\Big]_{P_a = const} = t \cdot [P_a K]_{sorbate} \tag{9}$$

For tests where the sorbate addition rate was varied to hold the chamber pressure constant the amount of sorbate gas was computed from,

$$Q_{sorbate}\Big]_{P_c = const} = K\Big]_{sorbate} \cdot \int P_a(t)dt \qquad (10)$$

The integration was carried out manually on figures such as Figure 16, page 54, by use of a planimeter.

The sorption capacity of the frost is defined as,

$$C \equiv \frac{Q\Big]_{sorbate}}{Q\Big]_{sorbent}} \qquad (11)$$

The quantity C is referred to as the "mole ratio" by some investigators [13, 16 and 17], and the "concentration" by others [14 and 18]. It is merely a convenient nondimensional way to express the amount of gas which has been sorbed and is referred to here as the capacity[9]

[9]The volume of gas sorbed in cm^3 divided by the mass of the sorbent in grams is also quite frequently used in literature to describe the quantity of gas sorbed by a porous medium. This parameter is analogous to the factor C employed here.

CHAPTER V

MEASUREMENT OF EQUILIBRIUM SORPTION CAPACITY OF HYDROGEN BY FROSTS

Some of the preceding has served to illustrate that if improvements could be made in the effectiveness of cryosorption pumps, they would primarily be made in the area of increased equilibrium sorption capacity. This chapter describes the results of a number of equilibrium isotherm measurements carried out to define factors which influence the sorption capacity of frosts and to determine if and how the amount of sorbed H_2 could be increased.

I. ISOTHERM MEASUREMENTS

1. Sorption Isotherms

The variation of the test chamber pressure which occurred as 300°K hydrogen was continuously being sorbed by a 1 μ thick layer of CO_2 cryodeposit at 12.4°K is shown by the dashed line in part a of Figure 19. Because a constant sorbate addition rate was used, this figure also represents a typical chamber pressure history as a constant hydrogen gas load is being pumped. If the sorbate flow was stopped, the chamber pressure would decrease to the lower equilibrium values shown by the symbols. These points define then the equilibrium sorption isotherm for a 12.4°K CO_2 cryodeposit, which was formed at a strike

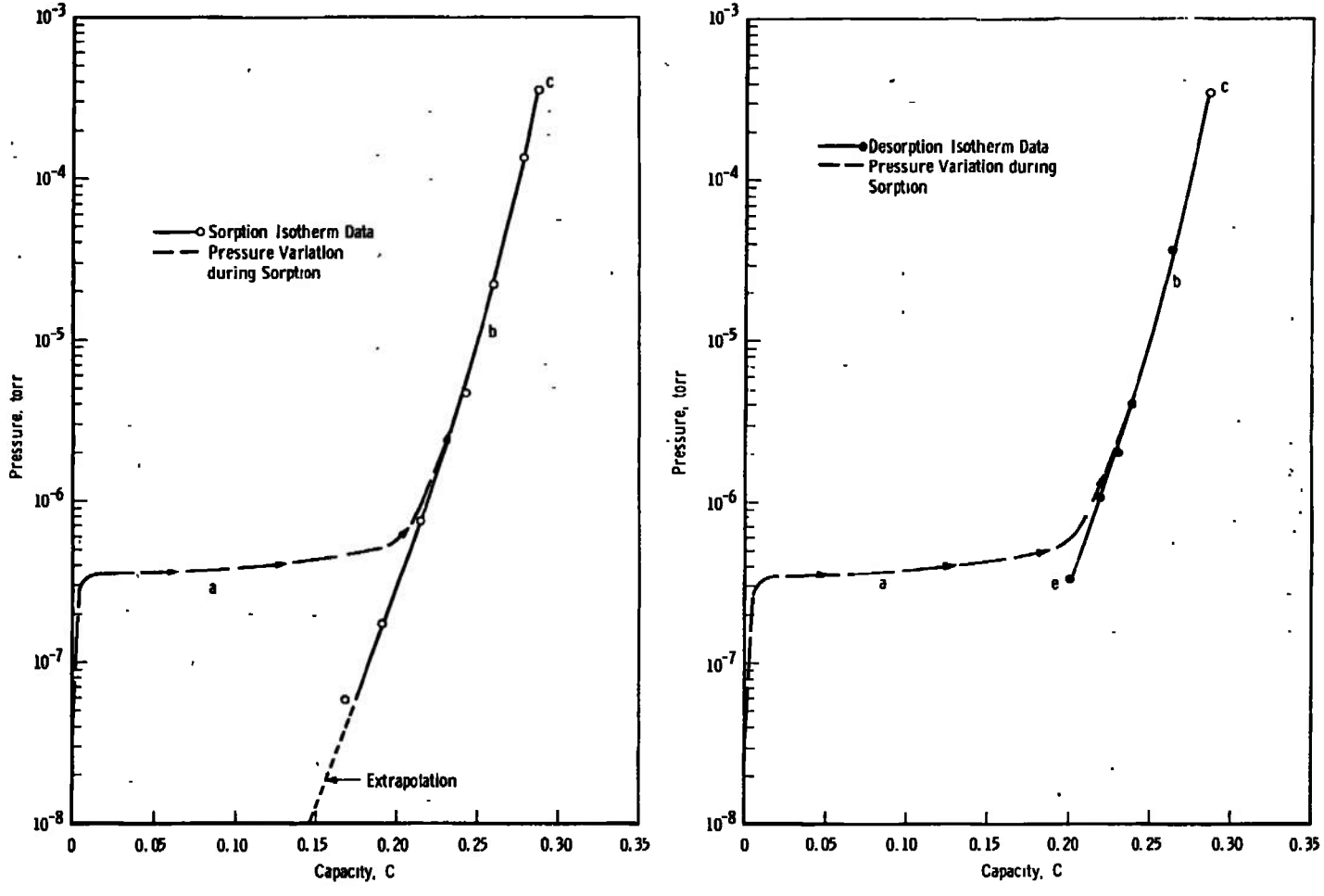

(a) Sorption Data for H_2 on CO_2 Frost at 12.4°K

(b) Desorption Data for H_2 from CO_2 Frost at 12.4°K

Figure 19. Equilibrium Isotherms for H_2 on CO_2 Frost Formed at $P_{form} = 2 \times 10^{-5}$ torr and $T_f = 12.4°K$.

rate of 6.3×10^{15} molecules/cm^2-sec. Data obtained at the lower values of capacity are not presented because the measured pressures are governed by the chamber in-leakage and outgassing and do not define the isotherm. The sorbate flow was always finally stopped at a pressure level corresponding to point (c), the saturation pressure where the frost was fully saturated for all practical purposes.

2. Desorption Isotherms

After the saturation pressure was reached via path abc in part a of Figure 19, the sorbed hydrogen could be desorbed from the frost by opening the valve to the diffusion pump and lowering the chamber pressure (for example, point b in part b of Figure 19). The amount of H_2 sorbate then needed to again saturate the frost corresponded to the change in capacity b to c. This point is illustrated by Figure 20 which compares the measured amount of H_2 required to re-saturate the frost to the amount desorbed as calculated by means of Equation 6. Equilibrium desorption isotherms were obtained by repeating this process at various pressures, a typical example is given by the solid line in part b of Figure 19. Comparison of the sorption and desorption isotherms in parts a and b of Figure 19 shows that they are essentially identical. Desorption isotherms for cryosorption on frosts have not been published previously.

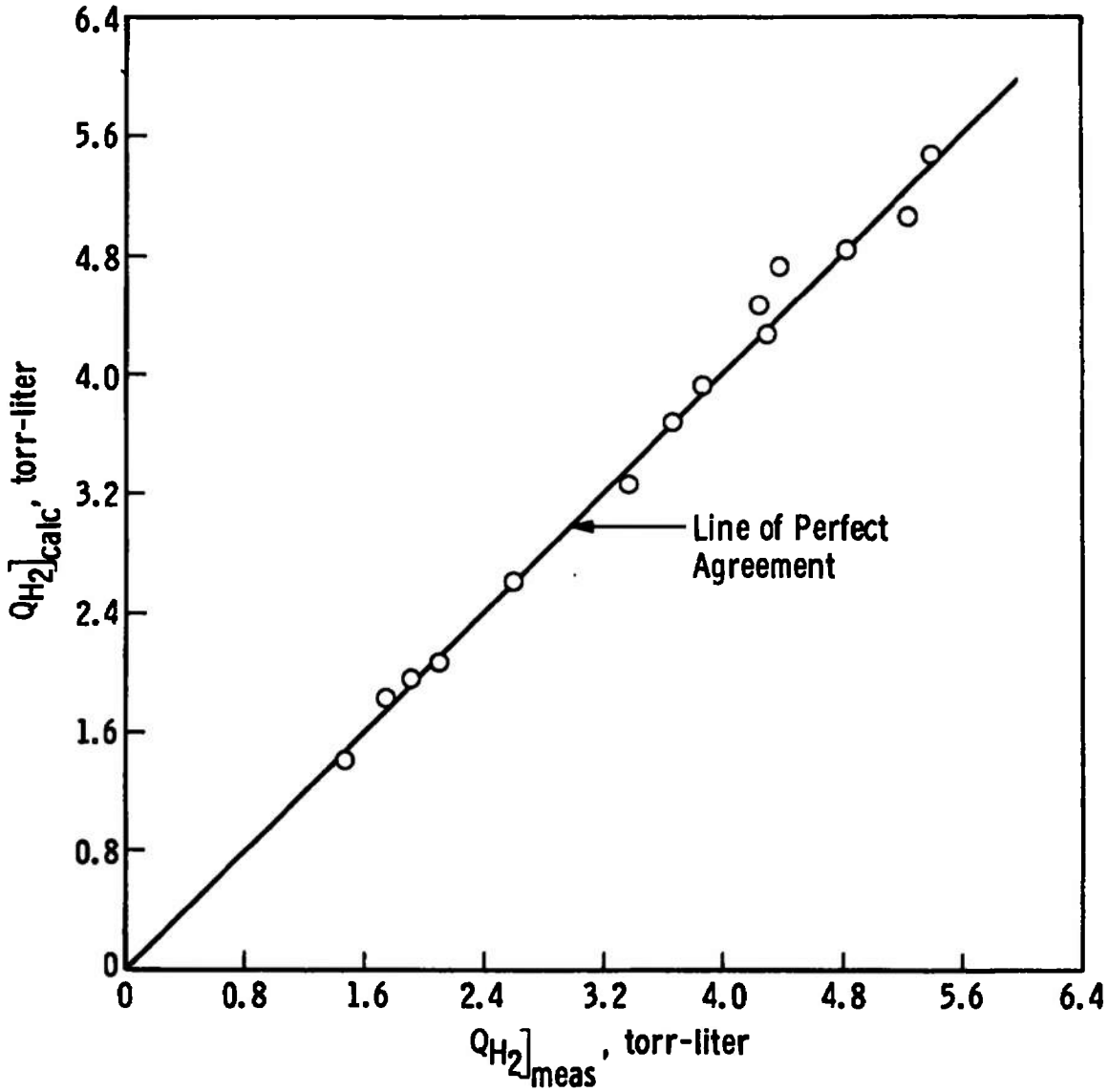

Figure 20. Comparison of Measured and Calculated Amount of Sorbate Desorbed during Warm-up of Frost.

During the desorption process the pressure could be reduced in a few minutes to about point e of part b in Figure 19' with the available diffusion pump. At this point an equilibrium between frost adsorption and desorption and chamber outgassing and pumping was established and continued pumping for several hours did not produce a significant decrease in pressure. Thus, it was not possible to completely desorb the H_2 from the frost. However, these tests demonstrated that CO_2 frost can with intermediate desorption be used over and over to pump hydrogen. If this desorption method is employed the re-use capacity of a frost for subsequent cryosorption pumping would be only roughly a third of its initial capacity for the present test apparatus. In view of subsequent tests in this series this residue capacity, however, may be fixed by the nature of the frost structure. This point will be discussed in more detail later.

3. Comparison with Other Investigations

Measured equilibrium isotherms for the sorption of H_2 by CO_2 frost at temperatures of 12.4°, 16.5° and 21.5°K are summarized in Figure 21. These data were obtained for frosts formed at the same temperature at which the subsequent cryosorption pumping took place and at a strike rate of 6.3×10^{15} molecules/cm^2-sec. Additional isotherm measurements have also been made in which the frost was: (1) formed in the same fashion but at

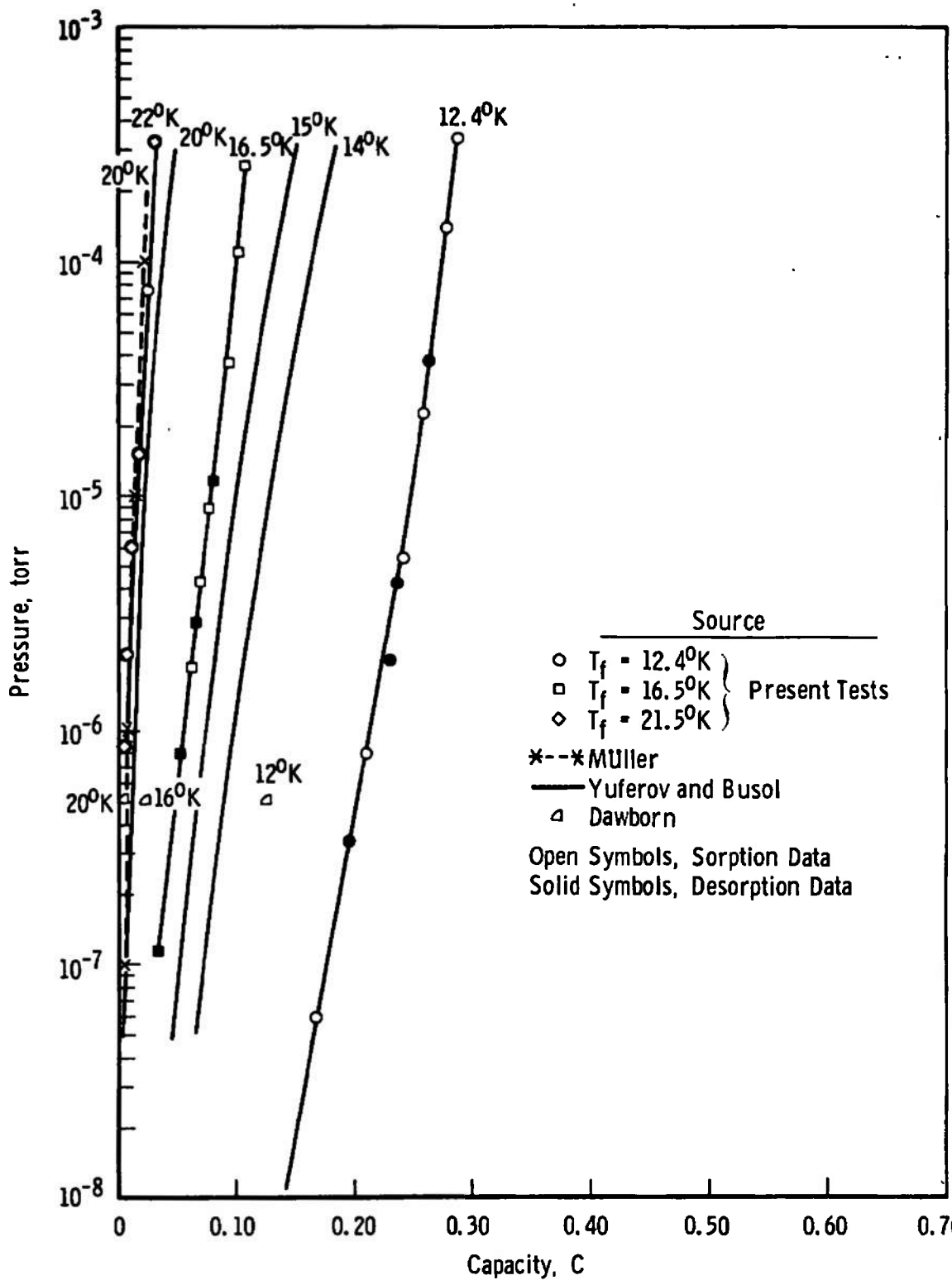

Figure 21. Comparison of Measured H_2 Equilibrium Sorption Isotherms of CO_2 Frost at Various Temperatures with Those of Other Investigations.

different thicknesses, and (2) allowed to "age" for several hours. Increasing the frost thickness, of course, allows a greater amount of H_2 to be sorbed but on the dimensionless basis of capacity, different thickness frosts produced the same isotherms. This may not hold true for much thicker frosts than employed for these tests which would have larger temperature gradients and higher surface temperatures because of their finite thermal conductivities. Allowing the frosts to age did not alter their isotherms. Thus, it is believed that no long-term reorientation of the frost structure occurs after it is deposited.

It is generally stated that the adsorption and desorption energies are approximately the same although only a few measurements are reported in the literature (see [42], Figure 9-2, for example). Because the sorption and desorption isotherms for frost are coincident, it follows that the sorption and desorption energies for this sorbent-sorbate system must be equal. The present test results agree with those reported by Yuferov and Busol [14] and correspond to a heat of sorption or desorption of about 1200 cal/mole, as will be shown later.

The present isotherm data appear to agree with those published previously by Yuferov and Busol [14], but it will be seen later that this result is fortuitous. Frosts used in the present tests, however, exhibited considerably higher saturation capacities than those

investigated by Dawbarn [13] and Müller [15], as well as higher capacities than those studied by Hunt, et al. [10] and Southerlan [12]. These latter data are not shown in Figure 21, page 67, because Hunt and Southerlan did not report the equilibrium chamber pressure at saturation. The reasons for all of these differences were not immediately evident, but were subsequently attributed to differences in the frost structure.

II. THE FROST STRUCTURE

1. The Known Structure of Solid CO_2

When formed from the liquid state CO_2 crystals are face-centered cubics and in the temperature range of this study the lattice constant would be about $a_o = 5.54\text{Å}$ [43]. Additional information concerning the structural defects of solid CO_2 formed from a liquid are contained in a paper by Coucoulos and Gregory [44]. These investigators report that, at atmospheric pressure, solid CO_2 at a temperature of 77°K has a polycrystalline structure. Also, as the solid is allowed to warm to room temperature it undergoes various structural changes.

Very little is known about the structure of CO_2 cryodeposits, but the generally held speculation is that solidified gases in the form of cryodeposits are amorphous. Graf and Paulon [45] have reported the results of two X-ray diffraction measurements indicating the

structure of CO_2 cryodeposit formed on a surface at about 80°K. When the deposit was formed at a pressure level of about 4×10^{-3} torr the diffraction patterns show that the cryodeposit possessed a definite cubic structure. However, when the cryodeposit was formed at a higher pressure of 10^{-1} torr, no diffraction patterns existed. These investigators believed that the deposit formed at the higher pressure was amorphous while the one formed at 4×10^{-3} torr was polycrystalline.

2. Effect of Frost Temperature on Its Structure

At pressure levels of about 10^{-7} torr, carbon dioxide will begin to condense on a surface when its temperature is decreased to about 80°K[10]. If a cryodeposit is formed at this temperature or just below, one would expect the surface-captured molecules to be rather mobile. They may migrate over the surface until they find positions of minimum potential energy with respect to other captured molecules which would correspond to lattice positions in some crystalline state. However, if the cryosurface temperature is well below that required for condensation, the captured molecules would be much less energetic after capture. As a result, they may not move very far from their random adsorption sites before being

[10]This corresponds to a temperature slightly lower than specified by the vapor-pressure curve at $P = 10^{-7}$ torr. For convenience it is defined (Chapter II) and referred to as the condensation temperature of CO_2.

covered by other captured molecules which strike the surface at random positions. Consequently, forming a cryodeposit on a surface at well below the condensation temperature would be in the direction to produce a more crystalline-like structure. Carbon dioxide cryodeposits used in this and other cryosorption investigations were formed at temperatures between about 12 and 20°K which is considerably below the condensation temperature of about 80°K. As a result they would be expected to be more disordered than the frost structures examined by Graf and Paulon [45], for example.

Previous investigators have observed that sorbed H_2 may be quite effectively desorbed by increasing the frost temperature. The isotherms (Figure 21, page 67) show that a CO_2 frost warmed to 20°K would contain only a small amount of residual hydrogen. Consequently, warming the frost would appear to provide a better means of desorbing it than lowering the chamber pressure. However, the effect of raising the frost temperature on its structure must be considered.

When a cryodeposit is warmed to a higher temperature, then its molecules become more mobile and they would tend to reorientate themselves toward a more orderly polycrystalline or crystalline state. Cooling the frost back to its original temperature would not restore the original more disordered structure, because decreasing the frost

temperature decreases the molecular mobility. This would have the effect of locking the more-ordered structure corresponding to the higher temperature in place. Similarly, if a cryodeposit formed at one temperature is subsequently cooled to a lower temperature, it should retain the type of structure characteristic to the higher initial temperature.

The effect on sorption capacity of warming a frost to some higher intervening temperature is shown in series of equilibrium isotherms in Figure 22. In all cases except one the frosts were initially formed at the temperature at which the isotherms were measured 12.4°, 16.5° or 21.5°K and at a strike rate of 6.3×10^{15} molecules/cm^2-sec. After the frost was saturated with H_2, its temperature was increased and the desorbed H_2 removed from the chamber by the diffusion pump. Then, the frosts were cooled again to their initial temperatures, and resaturated. Inspection of the isotherms in Figure 21, page 67, shows that a saturated 12.4°K frost when warmed to 20°K would retain a slight amount of residual H_2. If there were no changes in the frost's sorption properties due to warming, the subsequent saturation capacity of the desorbed frost would be only slightly less than its initial saturation capacity.

Isotherm data in Figure 22 indicate that this is not the case. For example, part a of Figure 22 shows

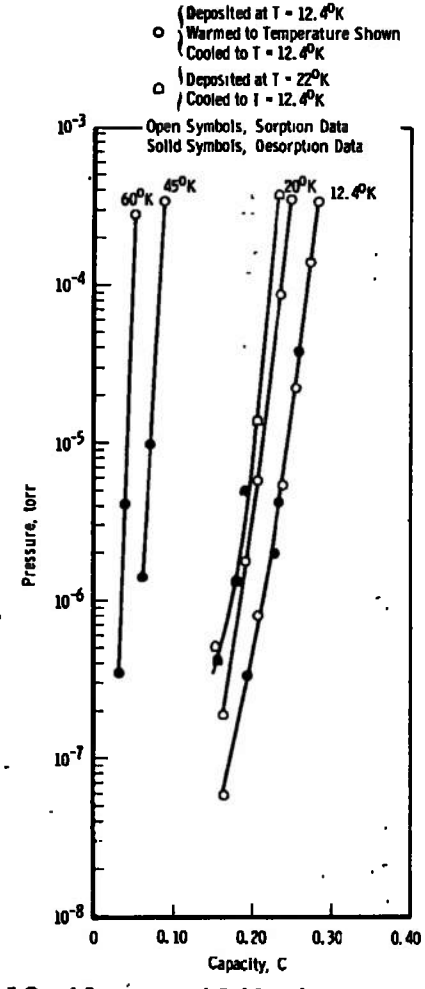

(a) 12.4°K Equilibrium Isotherms

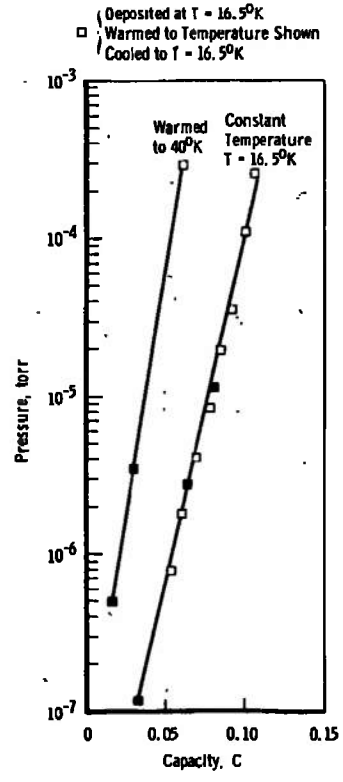

(b) 16.5°K Equilibrium Isotherms

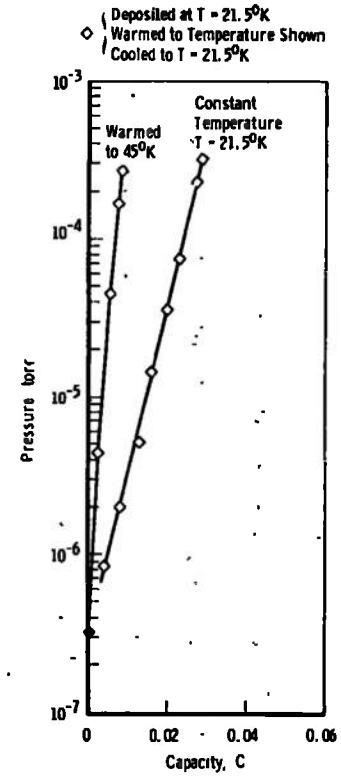

(c) 21.5°K Equilibrium Isotherms

Figure 22. Effect of Higher Intermediate Temperatures on the H_2 Equilibrium Sorption Isotherms of CO_2 Frost Deposited at a Strike Rate of 6.3×10^{15} molecules/cm^2-sec and at Various Temperatures.

that warming a 12.4°K carbon dioxide frost to 20°K and recooling it to 12.4°K resulted in reductions in the subsequent sorption capacity which were several times larger than expected. Furthermore, it is evident by inspection of the remaining isotherms in Figure 22 that the higher the temperature used to desorb the frost, the greater the loss in subsequent saturation sorption capacity. When the frost was warmed to 60°K and then cooled back down to 12.4°K, its saturation capacity was only 20 percent of the original value. Although fewer data were obtained, the re-use capacities of 16.5°K and 21.5°K CO_2 frosts were also significantly reduced when they were warmed to intervening temperatures of about 40°K (see parts b and c of Figure 22, respectively). Similar experimental results have been published by Yuferov, et al. [46], for a CO_2 frost at a temperature of 20.4°K. In that investigation the frosts were warmed to between about 80° and 100°K and cooled again to 20.4°K. Generally, the losses in the subsequent sorption capacity were not proportionally as great as shown in Figure 22. Those investigators also, by use of X-ray diffraction measurements, were able to detect changes in the frost structure from an amorphous to a more ordered state as the frost was warmed.

These reductions in the sorption capacity are not due to partial desorption as occurred when the frost was

desorbed by lowering the chamber pressure, but rather they reflect: (1) the change in the frost structure as it is warmed [46], and (2) the varying capacities of different types of frost structures to sorb a gas.

An equilibrium isotherm for a CO_2 frost which was deposited at a temperature of 22°K and then cooled to 12.4°K is also contained in part a of Figure 22. It is of interest to compare it to the isotherm for a frost deposited at 12.4°K, and saturated with H_2, warmed to 20°K to desorb the H_2[11], and then recooled to 12.4°K. The frost formed at 22°K has a somewhat lower capacity, thus, it would appear that frost formed at some higher temperature may be somewhat more ordered than frosts which are warmed to that temperature. In any case, it is apparent that the frost capacity is strongly dependent upon the maximum temperature which it has experienced.

Hengevoss [47] has recently reported somewhat similar findings for a limited number of tests of the sorption of hydrogen at a temperature of 77°K by very thin layers of condensed argon. His results, although quite sketchy, also imply that the sorption effectiveness of argon frost depends upon its temperature history. He also found that

---

[11]Additional measurements have shown that saturating and desorbing the frost plays no detectable role in the capacity changes. A frost (1) deposited at 12.4°K, (2) warmed to 20°K, (3) cooled to 12.4°K, and then saturated produced the same isotherm as a frost whose temperature was increased to 20°K to desorb it.

an argon frost formed at 20°K and then cooled to 9°K possessed a somewhat lower capacity than one formed at 9°, warmed to 20° and cooled again to 9°K.

Figure 22, page 73, also illustrates that even though structural changes take place which decrease its capacity, warming the frost is a superior way to desorb it. It is clear that the frost temperature increase should be as small as possible, consistent with desorbing most of the H_2. Regardless of the cryosorption pumping temperature there appears to be no advantage to raising the frost temperature above about 20 to 22°K. This will provide a re-use capacity of about 85 to 90 percent of the original value in contrast to the 30 percent re-use capacity when the frost was desorbed by lowering the pressure. As will be seen in a subsequent figure, the frost temperature should not be raised beyond about 30°K if it is to be re-used.

3. Effect of Frost Formation Rate on Its Structure

Since the measured isotherms suggested that frosts which were formed in a manner to make them more porous or amorphous or polycrystalline were superior sorbents, additional measurements were made for frosts which were intentionally formed in a manner to make them more disordered. When a cryodeposit is formed at a relatively high chamber pressure and hence a high strike rate, the captured molecules would have much less time to wander over the surface

in search for lattice positions before being buried and entrapped by other condensing molecules, than if the deposit were formed at a low strike rate. Consequently, forming the frost at high strike rates is in the direction to produce a more disordered or porous-type structure. This idea is consistent with Graf and Paulon's X-ray diffraction measurements of the structure of CO_2 cryodeposits formed at different pressure levels as mentioned earlier in this chapter.

Equilibrium isotherms for CO_2 frosts formed at different strike rates and chamber pressure levels are given in Figure 23. They demonstrate that, as expected, frosts formed at higher strike rates have significantly greater sorption capacities. For example, a frost formed at a strike rate of 6.3×10^{16} molecules/cm^2-sec had anywhere from a 35 to 100 percent higher sorption capacity at various chamber pressures, than a frost formed at a strike rate of 6.3×10^{15} molecules/cm^2-sec.

As the CO_2 strike rate is increased there is also an attendant increase of the chamber pressure level at which the cryodeposit is formed and an increase of the actual growth rate of the frost as summarized in Table I, page 49. In an attempt to isolate some of these variables, equilibrium isotherms of CO_2 cryodeposits formed in a helium background of 1×10^{-1} torr were also obtained and are shown in Figure 23. In this case the strike rate of

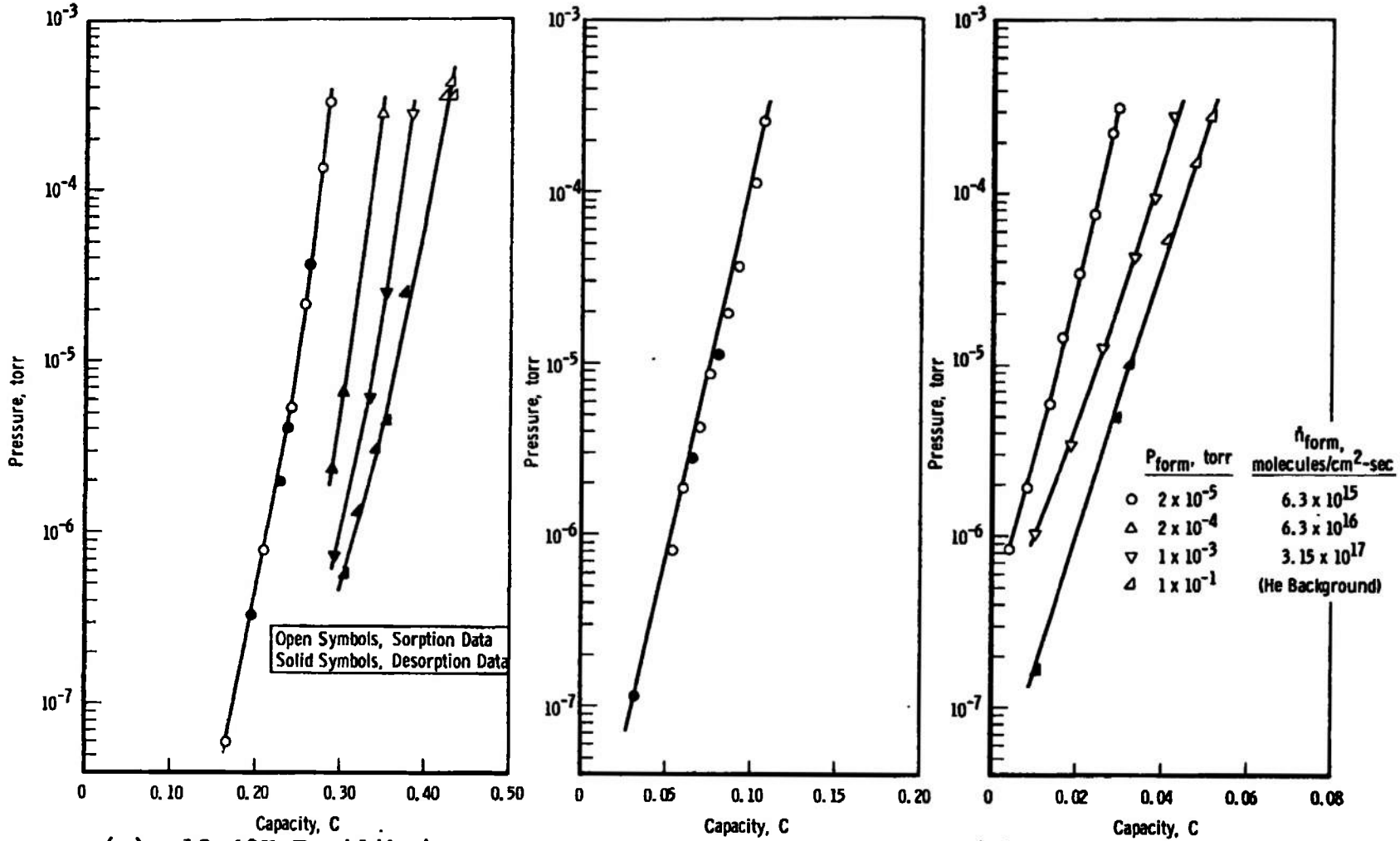

(a) 12.4°K Equilibrium Isotherms

(b) 16.5°K Equilibrium Isotherms

(c) 21.5°K Equilibrium Isotherms

Figure 23. Effect of Formation Rate on the H_2 Equilibrium Sorption Isotherm of CO_2 Frost at Various Temperatures.

CO_2 molecules and the actual growth rate of the frost were the same as for frosts formed at a pressure of 2×10^{-5} torr. These frosts exhibited still greater sorption capacities. This effect could possible be due to the high strike rate of noncondensible helium atoms on the condensing surface retarding surface migration of the captured CO_2 molecules. Another possibility is that buried and trapped He atoms were subsequently desorbed leaving voids in the structure. In any case, it is apparent that forming the frost in this manner resulted in a more porous structure.

This series of tests demonstrated how the sorption capacity of frosts may be readily improved. Saturation sorption capacities for CO_2 were obtained which were as much as an order of magnitude greater than achieved during any previous cryosorption investigation. The maximum capacities measured in this investigation indicated that 43 H_2 molecules may be sorbed for each 100 CO_2 molecules in the frost. Further improvements in capacity are undoubtedly possible by forming the cryodeposit at still greater rates; the upper limit could not be determined with the present test apparatus.

Frosts formed at higher strike rates were also subject to a reduction in their subsequent capacity if they were warmed to higher temperatures for desorption purposes (see Figure 24). This reduction was proportionally

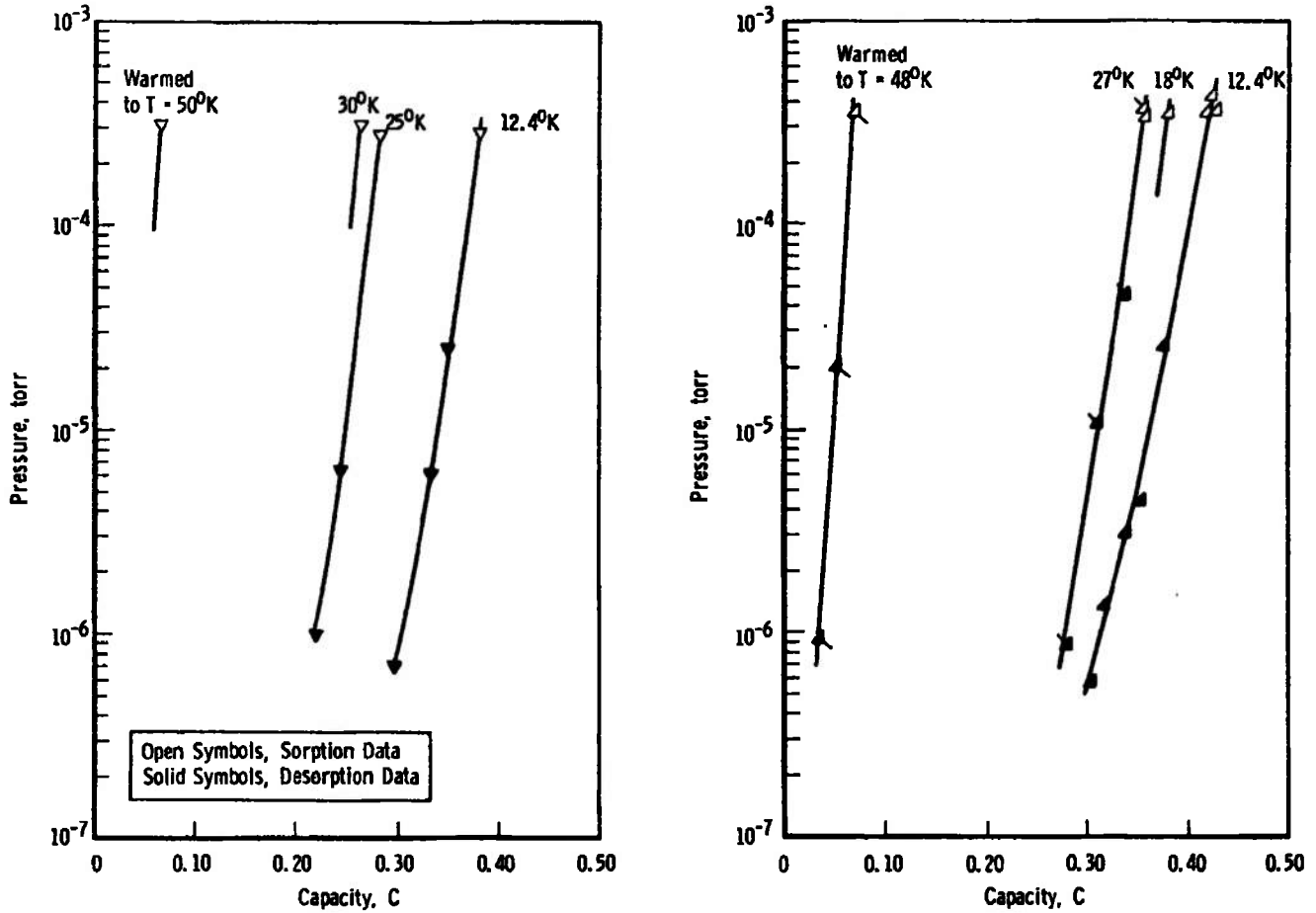

(a) Frost Formed at P = 10^{-3} torr and $\dot{n}$ = 3.15 × 10^{17} molecules/cm^2-sec

(b) Frost Formed in Helium Gas Background of 10^{-1} torr

Figure 24. Effect of Higher Intermediate Temperatures on the H_2 Equilibrium Sorption Isotherms of CO_2 Frost Deposited at Different Strike Rates and at a Temperature of 12.4°K.

greater than that suffered by frosts formed at lower strike rates. This probably occurs because the structure of frosts formed at high strike rates is more disordered. Their re-use capacity, however, is about 80 to 85 percent of their initial capacities if the frost temperature is not increased above 20°K to desorb the hydrogen.

A review of some of the gettering experiments in which H_2 and other gases were chemisorbed on metallic films has revealed that similar phenomena were observed. Clausing [5] found that titanium films which were formed at a high evaporation rate, or formed in the presence of an inert gas (He or Ar), were superior chemisorbents. He related this improved sorption capacity with a pronounced change in the visual appearance and structure of the deposited metal film. Further, he stated that the better sorbing films were "poorly crystallized" and possessed a greater effective active surface area.

4. Sorption Capacity of Different Sorbent Species

Ten to fifteen different sorbents have been previously investigated, but no one has as yet attempted to explain why some are better sorbents than others. The present tests, although not definitive, do, in a general way, shed some light on this subject.

Isotherms given in Figures 22 and 23, pages 73 and 78, consistently demonstrate that frosts which are formed in a way to make them more amorphous or porous have greater

sorption capacity. Depositing the frost at a temperature much below its condensation temperature limits the surface mobility and migration of molecules away from their random adsorption sites and produces more porous deposits. Consequently, the sorption capacity of a frost should be at least roughly related to the difference between the condensation temperature and the temperature at which the cryosorbent is formed. Since cryosorption pumping of H_2 normally will require frost temperatures between 10° and 20°K, sorbent gases which have condensation temperatures in the range between 20° and 30°K, such as N_2, O_2, Ar or CO, will tend to produce more crystalline-like structures and will inherently be poorer sorbents. Gases which have much higher condensation temperatures such as CO_2 and H_2O should have considerably better sorption capacity if they are deposited at low temperatures (in the 10 to 20°K range).

Previous cryosorption investigations which studied several types of sorbents tend to verify this idea (see Figures 1, 3 and 5, pages 10, 17 and 22). Carbon dioxide and water frosts always exhibited far greater capacities than N_2, O_2 and Ar sorbents. Yuferov and Busol [12, 14] also tried gasoline, alcohol and other hydrocarbons as sorbents. They did not publish sorption capacity data for these substances but stated that they were far inferior to CO_2. Because they all have high condensation

temperatures, this would appear to contradict the proposed importance of the condensation temperature. Thus, a high condensation temperature is a necessary but not completely sufficient condition for high sorption capacity. Two other sorbents which have relatively high condensation temperatures, sulphur dioxide, SO_2, and methyl chloride, CH_3Cl, were also examined in this investigation. Both provided interesting results.

Equilibrium isotherms measured while pumping H_2 with a SO_2 frost are summarized in Figure 25. Its capacity, although somewhat less than that of CO_2 (compare Figure 22, page 73, and Figure 25), is relatively high. Furthermore, where SO_2 frost is warmed to desorb the H_2, its loss in subsequent sorption capacity parallels that exhibited by CO_2 frost. Obviously, as a sorbent, SO_2 is in the same class as CO_2.

Methyl chloride frost on the other hand appeared to possess a low sorption capacity. However, when the CH_3Cl sorbent gas was introduced into the chamber, the ion gages and mass spectrometer, tuned to a mass number of 2, indicated a steady pressure increase as shown in Figure 26. One might attempt to explain the increased mass spectrometer readings in terms of the cracking pattern of CH_3Cl but this would not explain the higher ion gage readings. Since the cryosurface temperature was about 12°K, it would pump any gas impurities being added to the chamber except

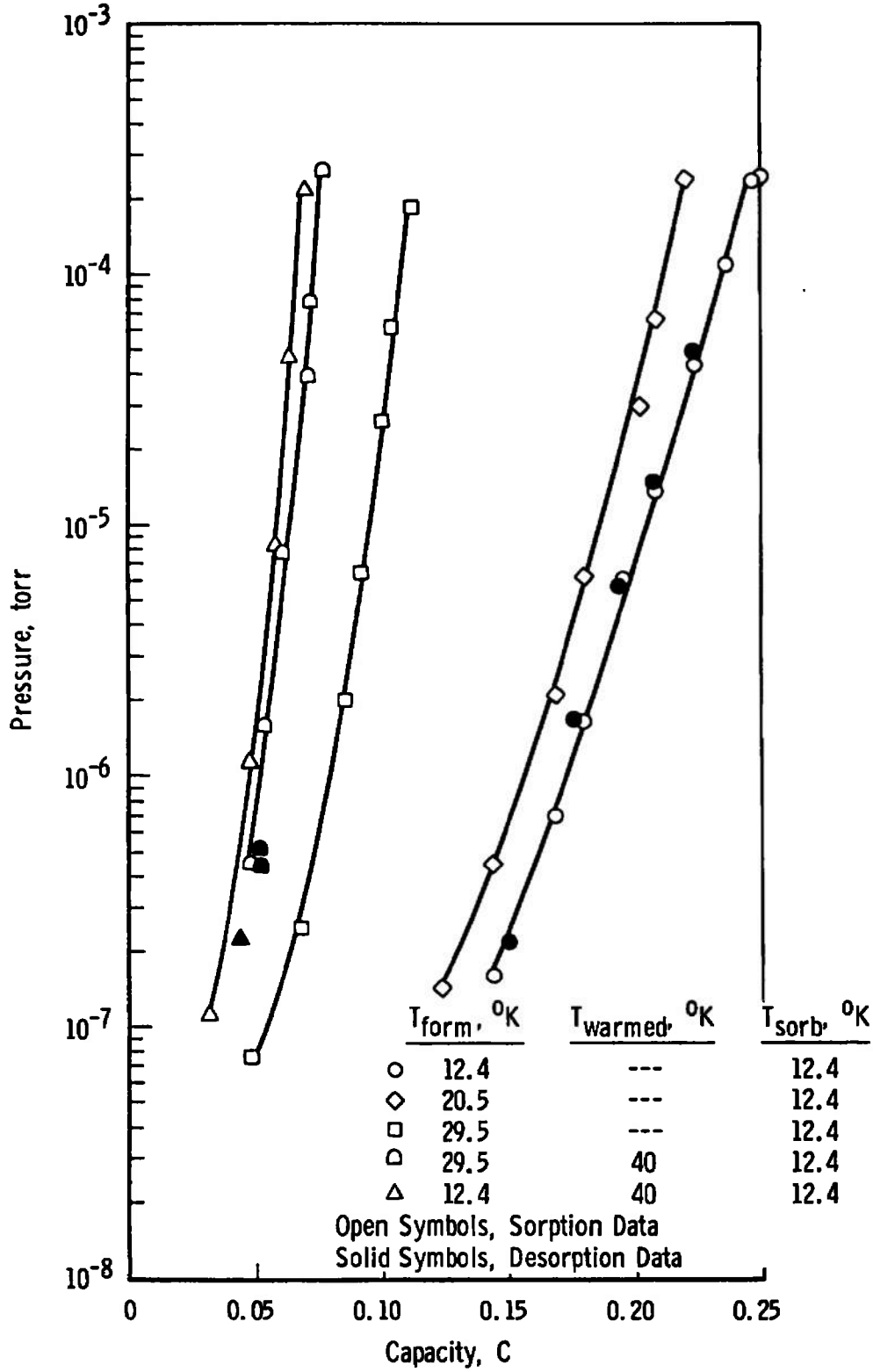

Figure 25. Equilibrium Sorption Isotherms for H_2 and SO_2 Frost at a Temperature of 12.4°K and Formed at a Strike Rate of 6.3×10^{15} molecules/cm^2-sec.

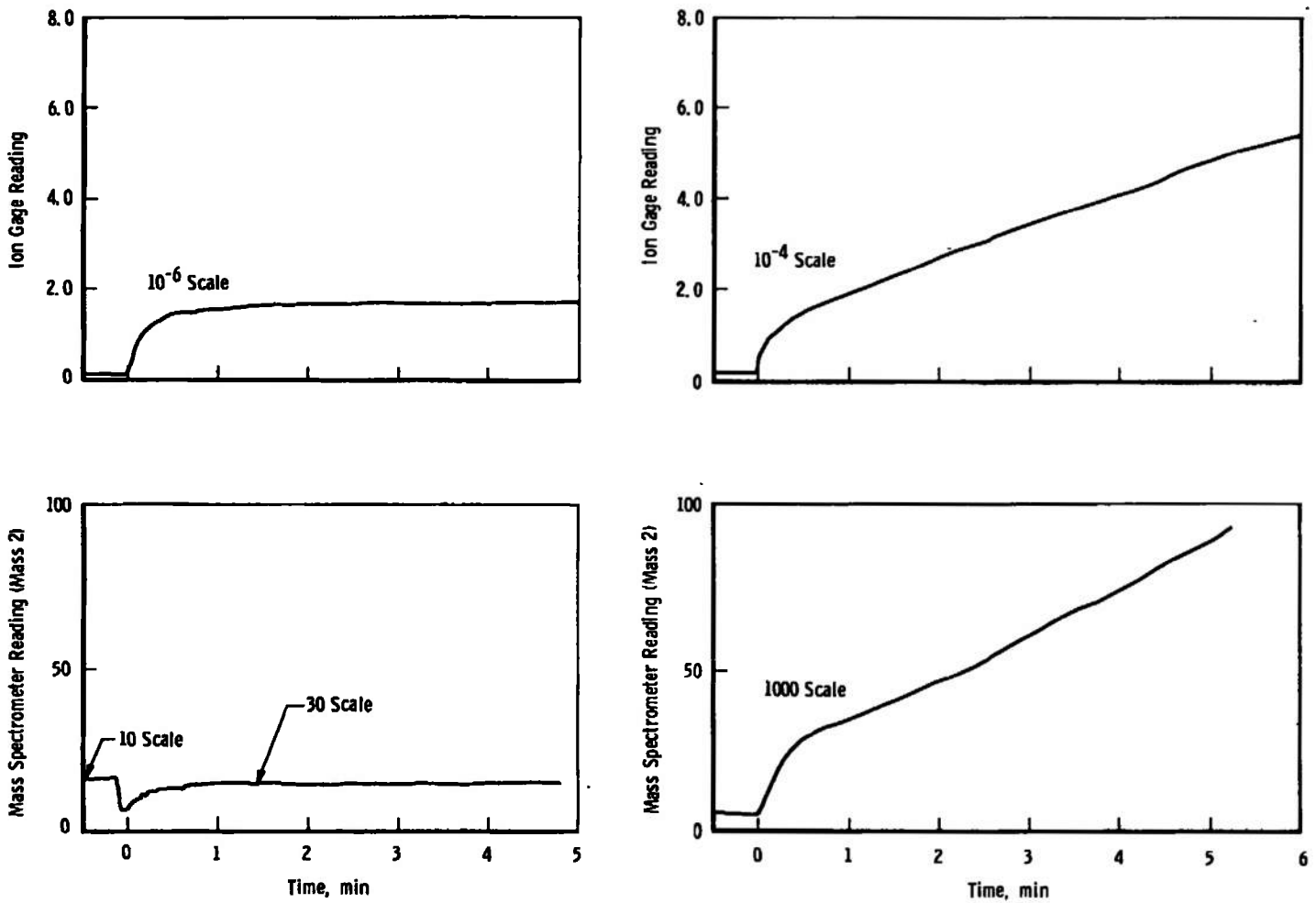

(a) Chamber Pressure Histories during CO_2 Sorbent Addition

(b) Chamber Pressure Histories during CH_3Cl Sorbent Addition

Figure 26. Ion Gage and Mass Spectrometer Readings during Sorbent Gas Additions.

H_2, He or Ne. The latter two gases could not be detected with the mass spectrometer. The only possible conclusion was that hydrogen was entering the chamber along with the CH_3Cl. A chemical analysis of the bottled CH_3Cl did not detect the presence of H_2. Consequently, it is believed that: (1) the hot ion gage filaments break down a portion of the CH_3Cl forming H_2, or (2) the room temperature methyl chloride may partially decompose when it enters the chamber at a pressure of less than 10^{-7} torr, releasing H_2 which in turn is sorbed by the CH_3Cl (and/or its decomposition products) frost. As a result the frost was partially saturated with H_2 before the test H_2 was intentionally admitted into the chamber. If this conclusion is correct it may explain why some of the previously tried sorbents, such as gasoline, alcohol, acetone and other complex polyatomic molecules containing hydrogen, had rather poor sorption capacities. They may also break down in hot gages, etc., or at very low pressure.

III. SUMMARY AND APPRAISAL OF SORPTION CAPACITY MEASUREMENTS

1. A Summary View of the Frost Structure

Isotherm measurements presented in this chapter have resulted in the identification of several factors which influence the sorption capacity and permit the process of cryosorption pumping to be put in better perspective.

The maximum H_2 sorption capacities of CO_2 frosts at a temperature of 12.4°K as functions of: (1) the maximum temperature which the frost has experienced, and (2) the pressure at which the frost was formed are presented in Figure 27. This figure clearly illustrates the advantages of forming the frost at high pressure levels or strike rates and maintaining the frost at low temperature. It also shows that there is no advantage of depositing a frost at a lower temperature than the temperature at which the subsequent cryosorption pumping is to take place. Regardless of the formation strike rate the re-use capacity of the frost is reduced as its temperature is increased.

These tests consistently suggest that cryodeposits formed at a temperature well below that required to condense the gas and formed at high strike rates have rather disordered or amorphous structure. However, if the frost is formed at low strike rates or at temperatures approaching its condensation temperature, or if the frost is allowed to warm to higher temperatures, a much more ordered or crystalline structure results which has poorer sorption characteristics. Because the more porous frost structures are better sorbents, it follows that the diffusion mechanism must be one of surface diffusion into the pores, cracks or other defects in the frost. Interstitial or bulk diffusion of the sorbate into an ordered crystal structure is not the predominant diffusion mechanism in

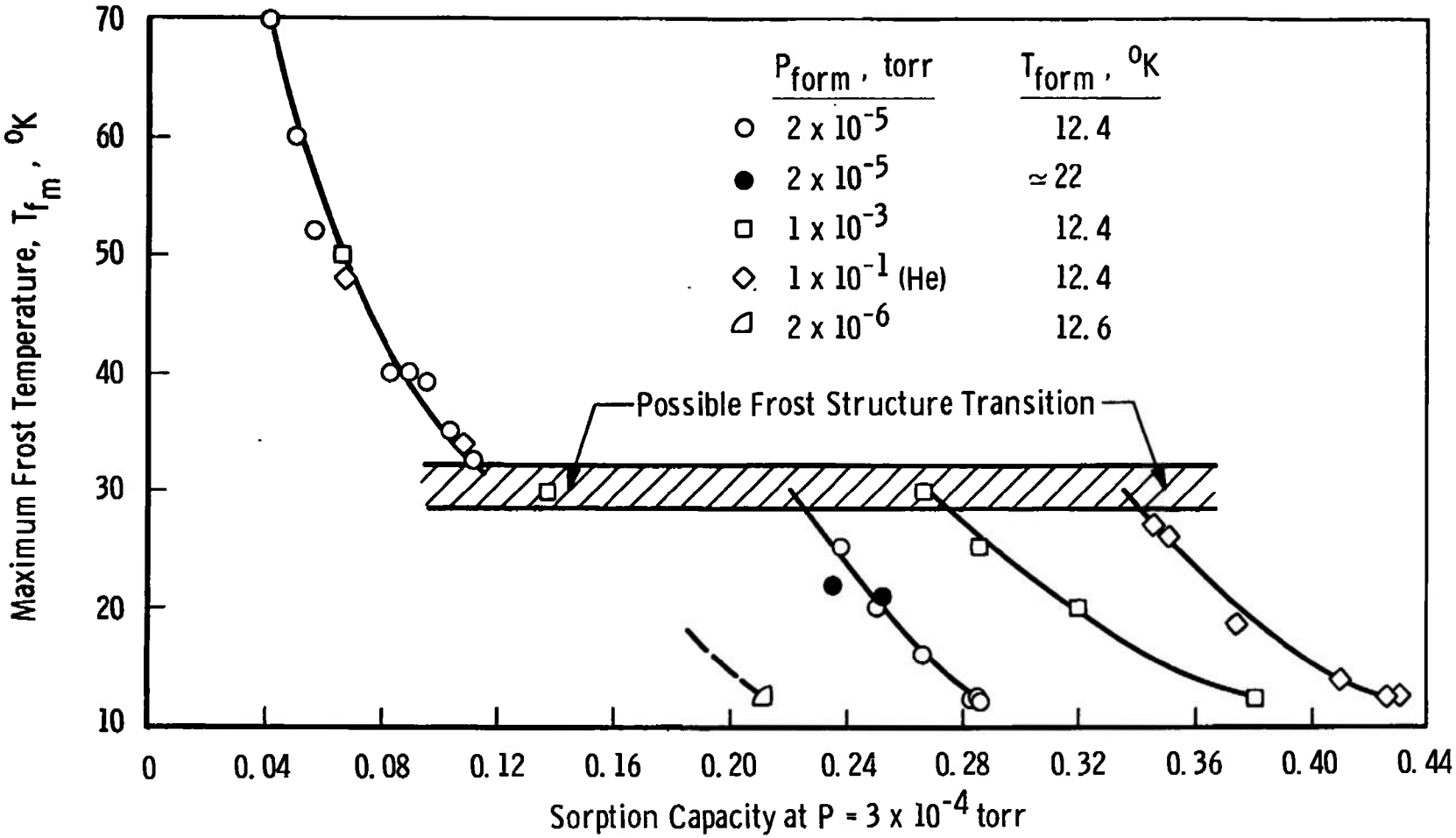

Figure 27. Summary of Maximum Equilibrium Sorption Capacities of CO_2 Frosts at a Temperature of 12.4°K as a Function of the Intermediate Warming Temperature.

frost cryosorption pumping. Yuferov, et al. [46] have also arrived at this conclusion based on their X-ray diffraction measurements of the CO_2 frost structure.

Figure 27 also shows an interesting characteristic of CO_2 frost. As the frost temperature was increased above about 30°K a sudden discontinuity occurred in the sorption capacity. This may indicate the occurrence of a transition in the frost structure, perhaps a large-scale reordering of the frost from an amorphous to some polycrystalline state. After passing through this transition region it appears that all CO_2 frosts had the same sorption characteristics independent of the conditions at which they were formed. Hence, they all may have changed to the same kind of structure. This phenomenon is the basis for the previous suggestion that if H_2 is desorbed by warming the frost, its temperature should not be increased above 30°K. Although fewer data were available, the same phenomenon occurs with SO_2 frost (see Figure 25, page 84). Phase transitions in this temperature range are reported in the literature for solid CH_4 and solid O_2 [48, 49], and other solidified gases exhibit similar transitions from one crystalline structure to another at other temperatures. However, no reference to this phenomenon could be found in the literature describing the properties of solid CO_2.

Figure 28 illustrates a point that was made earlier: the amount of H_2 sorbed at saturation was proportional to

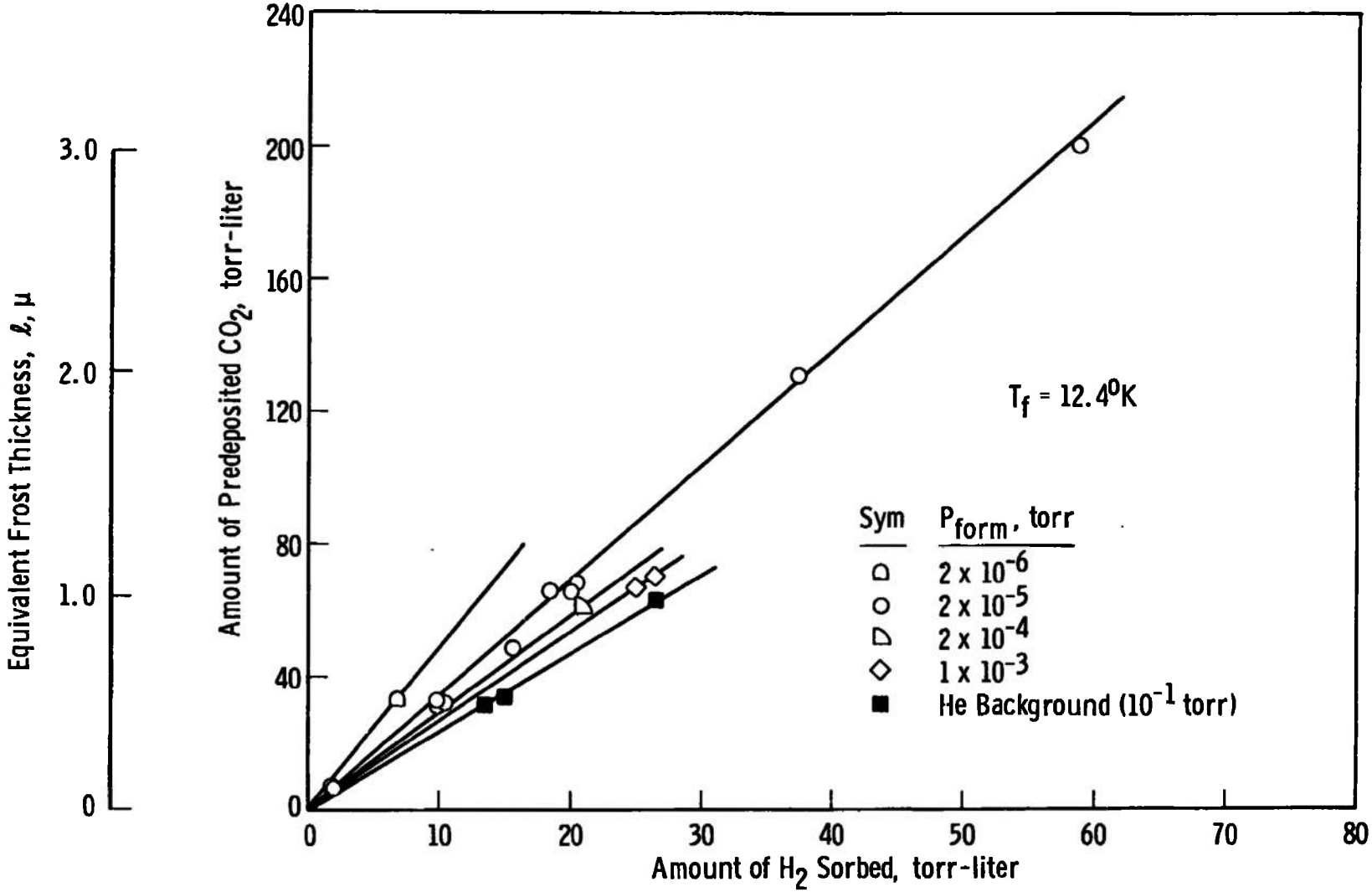

Figure 28. Variation of the Quantity of H_2 Sorbed with the Quantity of CO_2 Predeposited as a Sorbent.

the amount of CO_2 predeposited as the sorbent; regardless of how the frost was formed. Thus, the amount of gas sorbed is related directly to the frost thickness. Consequently, not only is the frost porous but its porosity is more or less uniformly distributed throughout its volume.

Müller, et al. [50] have shown that the optical properties of cryodeposits give some information about the physical properties of the deposit. Assuming a porous frost consists of: (1) the pure substance, and (2) vacuum voids, its effective refractive index, μ_e, is related to the refractive index of the pure substance, μ, and the volumes of the pure substance V_p and voids V_v (see [51] for details),

$$\frac{\mu_e^2 - 1}{\mu_e^2 + 2} = \left(\frac{V_p}{V_p + V_v}\right)\left(\frac{\mu^2 - 1}{\mu^2 + 2}\right)$$

Consequently, porous cryodeposits have lower refractive indices than their pure substance because of the unity refractive index of the vacuum voids. Kruger and Ambs [51] have measured the refractive indices of CO_2 and H_2O formed as solid thin films on 77°K and 4.2°K surfaces. Assuming that the refractive index of the 77°K film represents that of the pure substance, the above equation indicates that a 4.2°K CO_2 cryodeposit is composed of about 30 percent vacuum pores while only 5 percent of the

volume of a 4.2°K H_2O cryodeposit is void. These porosities would be larger than those of frosts with temperatures between 12° and 20°K. Unfortunately, refractive index data for frosts in this temperature range are not available. These estimates are also consistent with the capacity measurements of [10] for CO_2 and H_2O frosts and tend to support the picture of the frost structure which has emerged from this investigation.

2. Explanation of Inconsistencies between Previous Investigations

The results of this investigation now provide the means to explain some of the differences in test results obtained by other investigators. The large variation in the previously measured values of the sorption capacity (Figure 7, page 30) is, in general, due to the different ways in which the frosts were formed by the various investigators. Figure 27, page 88, shows that sorption capacity data are only useful and meaningful if they are accompanied by a description of how the frost was formed and a description of its previous temperature history. This may be illustrated by the following examples:

(1) Hunt, et al. [10] obtained unexpectedly low capacities (Figures 1 and 7, pages 10 and 30) for frost with temperatures near 11°K. This was due to the fact that they formed the frost at an extremely low strike rate, perhaps two

orders of magnitude less than the lowest rate employed in the present investigation. In view of the isotherm data presented in Figure 23, page 78, their low capacity measurements are not surprising.

(2) Southerlan [11] concluded that H_2O frost at 20.4°K sorbed H_2 better than CO_2 frost at 16°K, and his measured sorption capacities were lower than those obtained by other investigators (Figure 7, page 30). His unusual results stem from the fact that he, unaware of the consequences, warmed the CO_2 frost to 28°K and then recooled it to 16°K before saturating it with H_2. This procedure may have reduced its capacity by as much as 30 percent (see Figure 27, page 88) and made it appear inferior to H_2O frost when it is actually superior.

(3) Yuferov and Busol [14] measured isotherms which appear to agree quite well with those of this investigation (Figure 21, page 67). However, they formed all of their frosts at 20.4°K and then cooled them to 14° or 16°K before saturating them with H_2. Figure 27 demonstrates the importance of the temperature history of the frost and illustrates that this agreement is accidental.

(4) Müller [15] and Dawbarn [13] have also presented sorption capacity data for CO_2 frosts. However, since they give no information about how the frosts were formed, there is, in fact, no basis for comparison with the present tests.

3. Explanation of the "Poisoning" Effect of N_2 on a CO_2 Sorbent

Dawbarn [13] and Yuferov and Busol [14] mention that the presence of N_2 significantly reduced the sorption capacity of CO_2 frost. Dawbarn believed that it acted as a barrier retarding the diffusion of H_2 molecules away from their adsorption sites. The reasons for this behavior now seem clear.

For both of these investigations, N_2 was admitted to the chamber after the CO_2 and was cryopumped on top of the CO_2 frost. Since its condensation temperature is only a few degrees above that of the cryosurface, the N_2 frost layer would tend to be more ordered and inhibit the diffusion of adsorbed molecules into the CO_2. The N_2 frost itself has been shown to be poor sorbent (see Figure 1, page 10), and hence it would act as a surface barrier as Dawbarn proposed. Any other gas, however, which condenses at only a few degrees above that of the cryosorption surface should produce a similar barrier. It is significant to note that N_2 does not provide a barrier to the

sorption of helium by an argon frost at 4.2°K, but H_2 does [17]. Hydrogen will only be captured at temperatures below about 5°K; thus, it must form a well-ordered surface frost layer which retards the diffusion of helium.

CHAPTER VI

PREDICTION OF EQUILIBRIUM SORPTION ISOTHERMS OF FROSTS

Physical sorption is fundamentally a very complex phenomenon. Although it has been studied intensely over the past fifty years, it is still not well understood and no single theory can accurately describe the phenomenon. As a result thousands of isotherms for various sorbent-sorbate combinations have been measured and published. However, to avoid the measurement of frost isotherms for every case of interest, the ability to predict them is obviously worth seeking. The purpose of this chapter is to describe the usefulness of existing adsorption theories for correlating and predicting the measured H_2 sorption characteristics of CO_2 frost.

The purpose of most adsorption theories is to allow a prediction of the isotherm for a given sorbent-sorbate combination. Because of the unknown nature of the surface and the complex interaction between the surface and the sorbate molecules, such a general prediction is not possible at the present time. Consequently, the simpler problem of: (1) predicting isotherms for any gas on a particular sorbent, or (2) predicting the isotherms at various temperatures from an isotherm obtained at one temperature, has attracted considerable attention.

The sorption capacity of various kinds of porous sorbents (molecular sieves, charcoal, silica gel, etc.) is usually summarized in terms of equilibrium isotherm plots which have the simple functional form, (see footnote 6, page 16),

$$C = f(P)\Big]_T \tag{12}$$

The situation with frost sorbents is more complicated, because their cryosorption capacity is strongly influenced by additional factors,

(1) The strike rate and/or chamber pressure level at which the frost was formed.

(2) The cryosurface temperature at which the frost was formed.

(3) The temperature history of the frost.

Consequently, the isotherms for frost sorbents have the following dependence,

$$C = f[P, P_{form}, T_{form}, T_f(t)]\Big]_{T_f} \tag{13}$$

Because information about the various factors which govern the frost capacity was not given by previous investigators [10 through 19] those data are of little practical value for the design of frost cryosorption pumping systems. Isotherm data given in Chapter V are quite repeatable, if one forms the frost at the conditions specified, and are used here to test the applicability of several adsorption

theories. Brunauer [29] and Young and Crowell [42] have published excellent summaries of both the experimental work and available sorption theories, and de Boer [52] discusses in some detail the physical phenomena associated with adsorption. More recent work in this area is summarized, for example, in [53, 54, 55 and 56].

I. HENRY'S LAW AND THE FREUNDLICH EQUATION

For very small concentrations gases usually dissolve in solids according to Henry's law [42],

$$C = aP^m \tag{14}$$

where m = 1 for non-metals such as cryodeposits. It is a simple sorption isotherm equation and can be derived theoretically on the assumption that the gas in the solid is sufficiently dilute to obey the perfect gas law (see [42], page 105). It is quite useful in treating the problem of gas permeation through solids. Shupe [57] has presented a rather complete survey of the role of Henry's law in permeation phenomena.

Brunauer [29] states that Henry's law should hold for sorption at low pressures, but a more modern view is that it is the expected limit of every isotherm as $P \to 0$ (see discussion by Hobson [54]). If Equation 14 is obeyed, the measured isotherms of frost sorbents should provide a straight line with unity slope on plots of log C versus

log P. Some of the sorption isotherms from Chapter V, Figure 23, page 78, are replotted in Figure 29 in terms of log C and log P coordinates to check their agreement with Equation 14. It is apparent that the pressure levels employed in this study are not low enough for the sorption of H_2 by CO_2 frost to follow Henry's law. However, as the pressure decreased, the slopes of the isotherms given in Figure 29 increase and for a frost temperature of 21.5°K appear to approach the expected limit of 1. Thus, these trends suggest that cryosorption by frosts may obey Henry's law but only in the ultra-high vacuum range. Similar trends exist for low-pressure isotherm data for N_2 sorbed by porous glass and charcoal [55].

The empirical Freundlich equation,

$$C = a_1 P^{1/n} \tag{15}$$

one of the oldest isotherm equations, is similar to Henry's law and may be easily tested in the same way. The factors a_1 and n are defined to fit the experimental data. Although Equation 15 is empirical, it is widely used, particularly by those desiring to provide "engineering estimates." It has been used successfully, for example, for correlating the sorption characteristics of various gases in charcoal [29]. Equation 15 also produces straight lines on log C versus log P plots but with various slopes which depend upon the value of 1/n. Figure 29 also

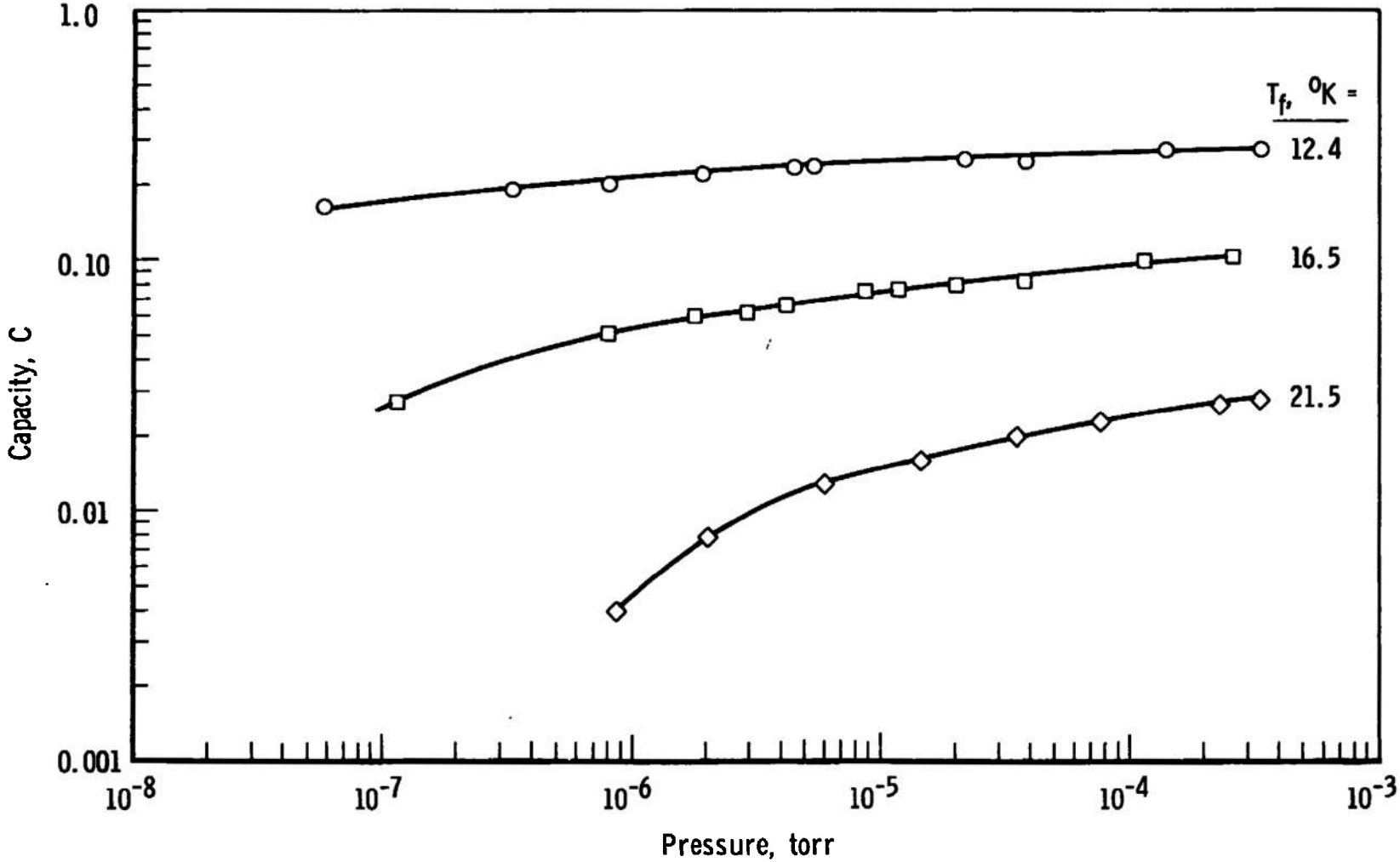

Figure 29. Equilibrium Sorption Isotherms Plotted in Log-Log Coordinates for CO_2 Frost Formed at a Strike Rate of 6.3×10^{15} molecules/cm^2-sec.

illustrates that the Freundlich equation would only provide a gross approximation to the isotherms of cryodeposits, and would not be particularly useful in correlating their isotherms.

II. THE LANGMUIR THEORY

The Langmuir equation resulted from one of the first theoretical treatments of surface adsorption and occupies a central position in the field of adsorption. Its derivation is given in detail by Brunauer [29]. Langmuir assumed that molecules which strike a bare surface have a certain probability of being adsorbed on the surface, but those which strike a site already occupied by an adsorbed molecule would be immediately re-evaporated. Thus, adsorption, as specified by the Langmuir model, is limited to monolayer coverage. The Langmuir adsorption model is often applied to porous media, but a hypothetical effective adsorption area is used. This area, which is experimentally found to be orders of magnitude greater than the geometric surface area, corresponds to the interior surface areas of the pores, cracks, crevices, etc.

Using the notation employed here, Langmuir's equation takes the form,

$$C = \frac{C_m \, b \, P}{1 + b \, P} \tag{16}$$

C_m and b are not empirical constants but have well-defined physical significance. C_m represents the monolayer sorption capacity of the frost at saturation; b is given by,

$$b = \frac{\alpha_o \, e^{E_a/kT}}{k_o (2\pi m \, k \, T)^{1/2}} \tag{17}$$

and is a coefficient of adsorption (see [30] for additional details). In practice both C_m and b are determined from experimental isotherm data; however, they must have reasonable values which are consistent with their physical meaning.

Equation 16 can be readily put into the following two forms,

$$\frac{P}{C} = \frac{P}{C_m} + \frac{1}{bC_m} \tag{18a}$$

and

$$\frac{1}{C} = \frac{1}{C_m} + \frac{1}{bPC_m} \tag{18b}$$

Consequently, a plot of Equation 18a in P/C and P coordinates would provide a straight line with an intercept of $1/bC_m$ and a slope of $1/C_m$. Alternatively, a plot of 1/C against 1/P will also give a straight line (Equation 18b).

Such plots, but in particular the former, are commonly used to determine if experimental isotherm data follow Langmuir's equation. Young and Crowell [42] do not recommend use of the latter method because they state it places too much emphasis on the low-pressure part of the isotherm. Inasmuch as the low-pressure end of the isotherm is of paramount interest here, this latter method should provide the better test of Equation 16.

Isotherm data from Figure 23, page 78, replotted in Figure 30 in terms of 1/P and 1/C coordinates produce highly non-linear curves. Consequently, the sorption mechanism must be more complicated than simple monolayer coverage and the Langmuir theory does not appear to be applicable to frost cryosorption at low pressures. This conclusion is in accord with the findings of Hobson [55] who has investigated the sorption of H_2 by porous glass and charcoal at low pressure, and with the conclusion of Danner [58] who has studied sorption by cold molecular sieves. However, in much earlier investigations, Schmidlin, et al. [59], and Haygood [60] concluded that the Langmuir model is valid for low-pressure cryotrapping of H_2 by water. These test data were quite limited and as Hobson points out, the sorption process with continuous deposition of the sorbent may lead to quite different results. In any case, Langmuir's equation clearly will

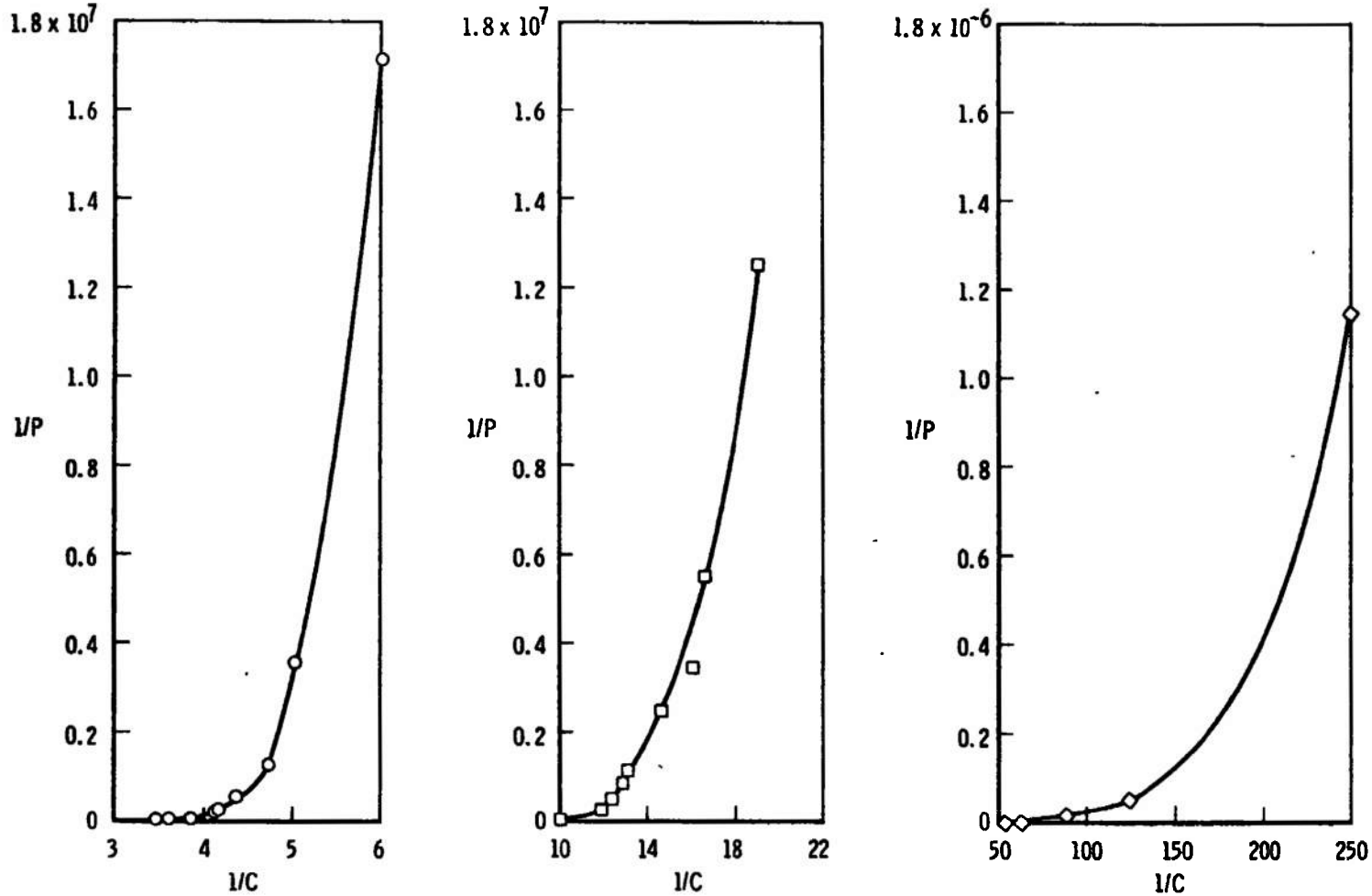

Figure 30. Equilibrium Sorption Isotherms Plotted in Langmuir Coordinates for CO_2 Frost Formed at a Strike Rate of 6.3×10^{15} molecules/cm^2-sec.

not predict the isotherms for pre-deposited frost sorbents at low pressures.

It is of interest to note that when the usual P/C and P coordinates were used, the frost isotherm data of Figure 23, page 78, produced slightly concave but relatively linear lines. However, it is repeatedly emphasized ([29], for example) that obtaining a straight line is a necessary but not a sufficient condition for guaranteeing that the data in question obey Langmuir's equation. Values obtained for C_m and b from P/C versus P plots of the present isotherm data were not at all reasonable and when used together with Equation 16 did not produce isotherms which even approximated the measured ones. Thus, with very low pressure isotherm data the coordinates suggested by Equation 18b are recommended as a more straightforward test of the applicability of Langmuir's model.

III. THE BET THEORY

Brunauer has classified experimentally measured isotherms into the five basic shapes sketched in Figure 31. The Type I isotherm is characteristic of monolayer adsorption and is the shape predicted by Langmuir's equation (which has already been shown to be inappropriate for frost sorbents). Types II to V represent multi-layer or multi-molecular adsorption.

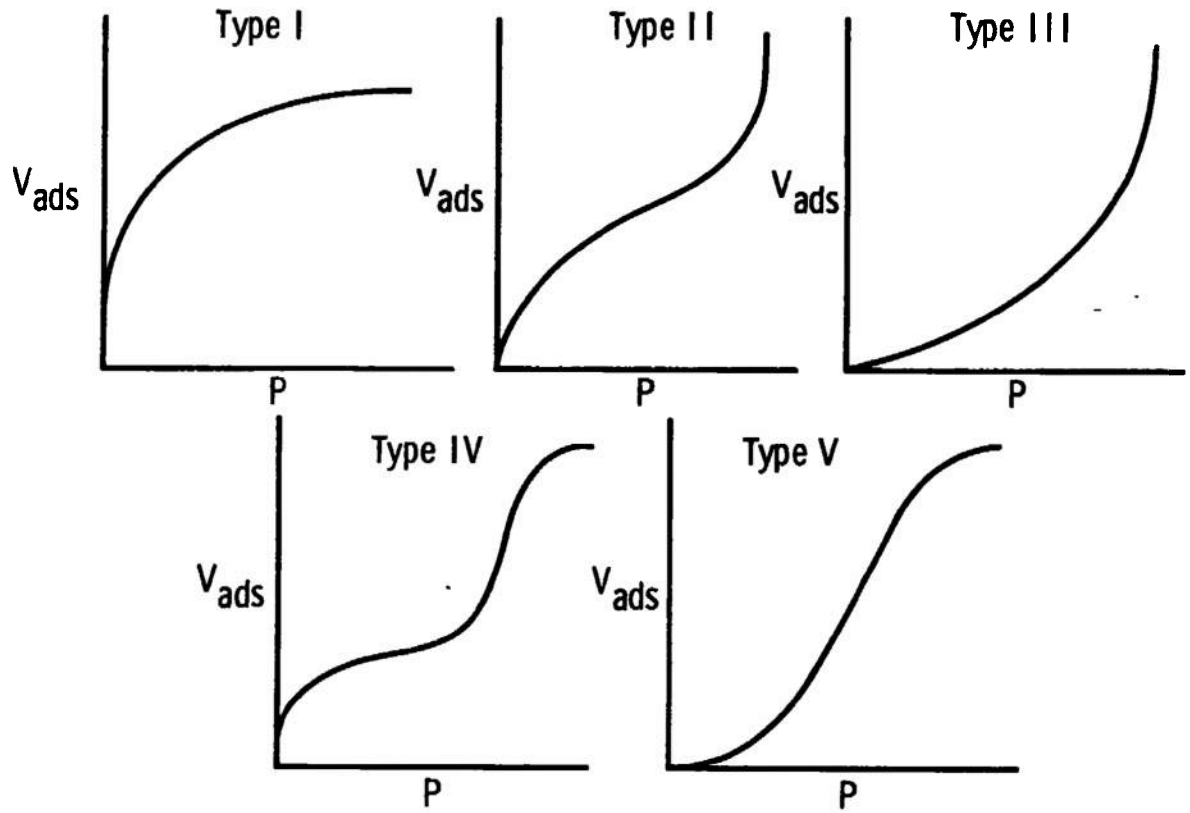

Figure 31. Brunauer's Classification of Adsorption Isotherms.

Microporous sorbents such as charcoal [29, 61], porous glass [61], silica gel [29, 61 and 62], and others generally exhibit Type IV or V isotherms with adsorption-desorption hysteresis (the equilibrium desorption isotherm is displaced to lower pressures than the adsorption isotherm). It is generally agreed that this behavior which usually occurs at higher pressures than of interest here is associated with condensation in small capillaries or in narrow-necked micropores. Inasmuch as no sorption-desorption hysteresis is observed with frost sorbents (see Figure 21, page 67) the capillary condensation theory [63] is probably not applicable in predicting equilibrium isotherms for cryofrosts.

A more general adsorption theory by Brunauer, Emmett and Teller (see [29], page 149), commonly called the BET theory, extends Langmuir's approach to the case of multilayer adsorption. The basic assumption of the BET theory is that molecules in the first layer can serve as adsorption sites for molecules in a second layer and so on. Moreover, there is a balancing of condensation and evaporation rates of molecules between layers. It is further assumed that the first layer will have some value for the heat of adsorption, E_a, but for all succeeding layers the adsorption energy, is assumed equal to the heat of vaporization of the sorbate, E_L. The resulting isotherm equation may be expressed,

$$C = \frac{C_m \beta P}{(P_o - P)\left[1 + (\beta - 1)\frac{P}{P_o}\right]} \tag{19}$$

for multi-molecular adsorption on a free surface. P_o is the vapor pressure of the sorbate and β is defined below.

$$\beta = \exp(E_a - E_L)/kT \tag{20}$$

If multi-layer adsorption does not occur on a free surface but is limited to say n layers because of space limitation imposed by opposing walls of a crack or pore, Equation 19 is replaced by,

$$C = \frac{C_m \beta P/P_o}{(1 - P/P_o)}\left[\frac{1 - (n+1)(P/P_o)^n + n(P/P_o)^{n+1}}{1 + (\beta - 1)(P/P_o) - \beta(P/P_o)^{n+1}}\right] \tag{21}$$

Equations 19 and 21 can reproduce all five isotherm shapes given in Figure 31, page 106, with appropriate values for C_m, β and n. Consequently, the BET theory has rather widespread application.

Inasmuch as the results discussed in Chapter V clearly indicate that the frosts are porous, one would expect that Equation 21 would more likely apply. However, at the very low pressures at which frost cryosorption takes place, $P/P_o \ll 1$, and hence,

$$(P/P_o)^{n+1} < (P/P_o)^n << P/P_o << 1$$

for all values of n greater than 1. Consequently, one may neglect the $(P/P_o)^{n+1}$ and $(P/P_o)^n$ terms in Equation 21 in which case it reduces to Equation 19. This conclusion is also borne out by the calculated BET isotherms for various values of n [28, 42]. For the case of n = 1, Equation 21 reduces to the form of Equation 16 which has already been shown to be inappropriate for the prediction of the isotherms for frosts. Thus, at very low pressures the simpler form of Equation 19 represents limited-multilayer adsorption.

Equation 19 may be transformed into,

$$\frac{P}{C(P_o - P)} = \frac{1}{C_m\beta} + \left(\frac{\beta-1}{\beta}\right)\frac{1}{C_m}\frac{P}{P_o}$$

which shows that the BET equation is a straight line for a $P/C(P_o - P)$ and P/P_o coordinate system, has intercept of $1/C_m\beta$ and a slope of $(\beta-1/\beta)\ 1/C_m$. Some of the Chapter V isotherm data are replotted in these coordinates in Figure 32 and produce curves quite similar in shape to those which resulted when the isotherm data were plotted in terms of the usual Langmuir coordinates suggested by Equation 18a. In this case the linear approximation to the 12.4°K isotherm data curve (Figure 22, page 73) yields a slope and intercept of

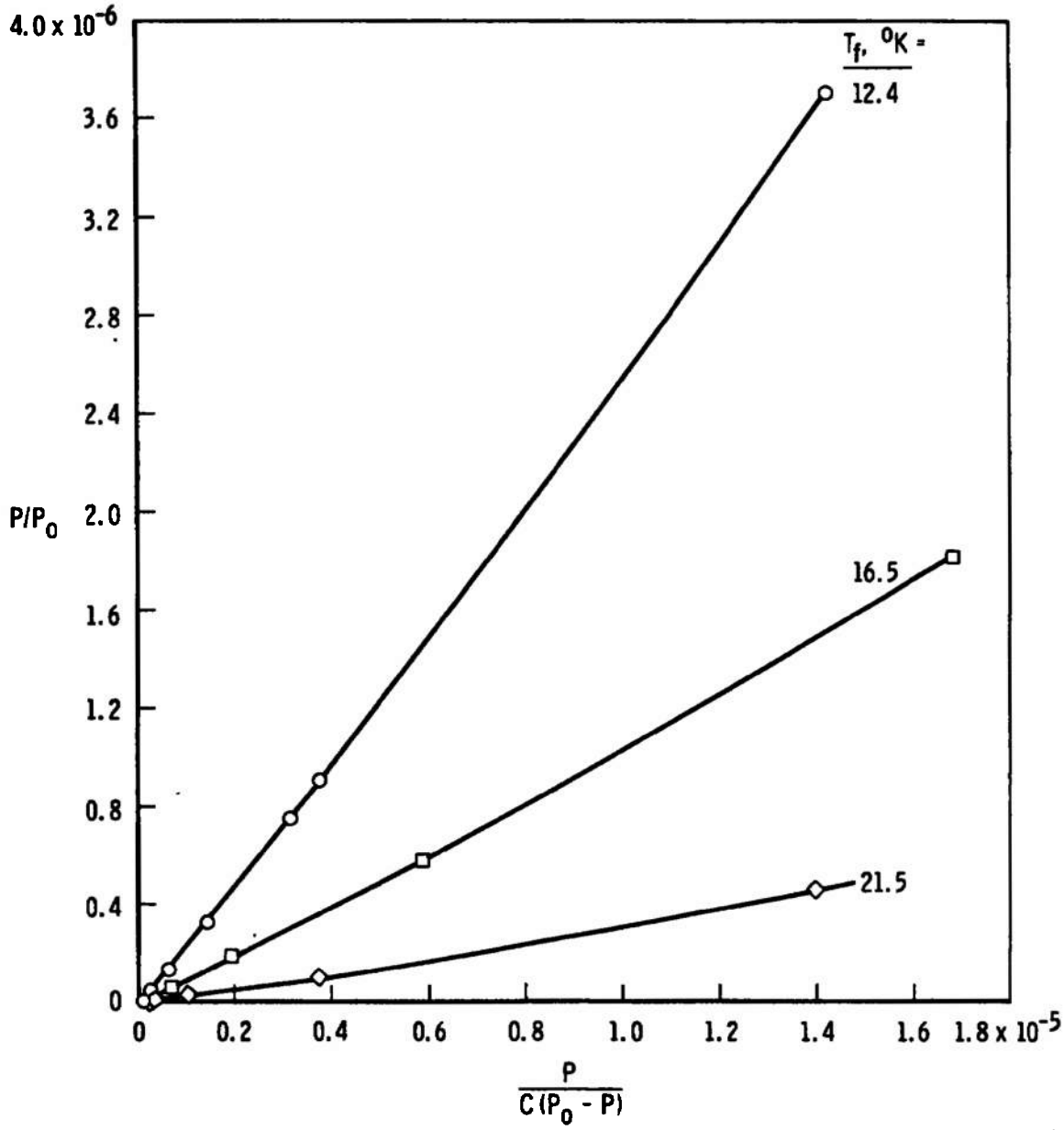

Figure 32. Equilibrium Sorption Isotherms Plotted in BET Coordinates for CO_2 Frost Formed at a Strike Rate of 6.3×10^{15} molecules/cm2-sec.

$$\left(\frac{\beta-1}{\beta}\right)\frac{1}{C_m} = 4.25$$

$$\frac{1}{C_m\beta} = 6.0 \times 10^{-8}$$

which in turn lead to values of

$$\beta = 0.71 \times 10^{8} \quad \text{and} \quad C_m = 0.234$$

These values, however, are highly unreasonable. First, C_m represents the maximum sorption capacity and the value obtained from Figure 32 is less than actual measured values. Secondly, the heat of adsorption for H_2 on CO_2 frost has been shown to be about 1200 cal/mole (Chapter II). Since the heat of vaporization of H_2 is 216 cal/mole, Equation 20 indicates that β for a 12.4°K frost, must be approximately,

$$\beta = e^{(1200-216)/(1.98)(12.4)} \simeq 3 \times 10^{17}$$

rather than the value required to fit the data.

Inasmuch as reasonable values for these physical parameters were not obtained, the necessary criteria required for the applicability of the BET theory cannot be satisfied. Consequently, it cannot accurately predict isotherms for frost cryosorption at pressures below 10^{-4} torr.

IV. THE POTENTIAL THEORY AND THE DUBININ-RADUSHKEVICH ISOTHERM EQUATION

The potential theory originally developed by Polanyi provides another approach to multi-layer adsorption (see [29, 42] for complete discussions). It considers that an interaction potential field exists near the surface of the sorbent and because of it the sorbate molecules are bound to be sorbent like an atmosphere is bound to a planet. The adsorbed layers are treated as being more compressed at the surface of the sorbent and decrease in density outward. The potential theory offers no explicit isotherm equation. Rather, if one imagines a number of equipotential surfaces, ε, above the sorbent surface, then each adjacent pair of these surfaces encloses some volume, V, of adsorbed gas. There is a definite relationship between the gas-surface interaction potential and the adsorbed gas volume. Since ε and V can, in principle, be expressed in terms of pressure and temperature (see [29]) the characteristic equation is equivalent to an isotherm equation.

When the sorbent temperature is less than the critical temperature of the sorbate, it is further assumed that the adsorbed film may be treated as an incompressible liquid. Then the energy required to compress a vapor from some pressure P to the vapor pressure of the bulk liquid at the temperature of the sorbent, P_o, is given by,

$$\varepsilon = - kT \ln \frac{P}{P_o} \tag{22}$$

Also, the volume filled in the sorption space or equivalently the volume of the condensed sorbate would be given by: Mass of condensed sorbate in liquid phase = Mass of sorbed gas, or

$$V_L \rho_L = V_a \rho_g \tag{23}$$

Calculation of an isotherm by means of the potential theory is a complex process. Consequently, Dubinin and his co-workers have simplified matters by developing an isotherm equation within the framework of the Polanyi potential theory[12]. Dubinin writes the characteristic equation as,

$$V_L = f(\varepsilon) \tag{24}$$

and his experiments have shown that Equation 24 has the form,

$$V_L = V_o e^{-\phi \varepsilon^2} \tag{25}$$

---

[12]Most of the original papers by Dubinin and his co-workers were not available to the present author; the one exception is [64]. In addition, discussions of the sorption work by this Russian group are contained in [55, 58, 65 and 66].

where for porous solids V_o is taken to be the pore volume and ϕ reflects a distribution of the pore volume according to size [58]. Equation 25 is semi-empirical and was first used to describe the sorption of gases by charcoal at much higher pressures than those of this investigation. It has been subsequently shown to be valid for molecular sieves at low temperatures [58] and other porous media at low temperature and low pressure [55]. Also, Ross and Olivier [67] use functions of this type for the development of other isotherm equations. They reasoned that a random distribution of adsorption energies would be appropriate for a solid which has a random distribution of cracks, pores, and other defects. The present author knows of no further theoretical justification for Equation 25, yet the fact remains that it describes a wealth of experimental data [55, 58, 65, 66, 68 and 69].

Combining Equation 22 through 25 results in the expression for the Dubinin-Radushkevich isotherm equation (hereafter referred to as the D-R isotherm equation),

$$\log V_a = \log \frac{V_o \rho_L}{\rho_g} - \phi k^2 T^2 [\log \frac{P}{P_o}]^2 \qquad (26)$$

In the notation employed herein Equation 26 may be rewritten as

$$\log C = \log C^o - A^o T^2 [\log \frac{P}{P_o}]^2 \qquad (27)$$

where for a given sorbate, C^o and A^o reflect the geometric porosity characteristics of the frost. If the experimental isotherm data are represented by Equation 27, they would produce a straight line when plotted with log C and $[\log (P/P_o)]^2$ coordinates with an intercept equal to log C^o and a slope A^oT^2. Consequently, the frost isotherms were plotted in terms of these coordinates as shown in Figures 33 and 34.

It is observed that the isotherm data for CO_2 frost formed at a pressure level of 2×10^{-5} torr are reasonably well approximated by straight lines (Figure 33). Moreover, the slopes of all of the curves in Figures 33 and 34 result in the same value of A^o ($A^o = 3.42 \times 10^{-5}$ $1/°K^2$). Consequently, the D-R isotherm equation properly predicts the dependence of the experimental isotherms on frost temperature, which itself is a notable achievement. In addition, the C^o intercepts which are an index of the total available sorption volume (in terms of the dimensionless capacity parameter) are a little larger than the maximum measured values and hence reasonable. As might be expected, the intercepts for frosts formed at different pressure levels change significantly because the frosts have different structures.

The only other set of isotherm data for H_2 sorbed by CO_2 frost (obtained by Yuferov and Busol, [14]) were also tested to see if they followed the D-R isotherm

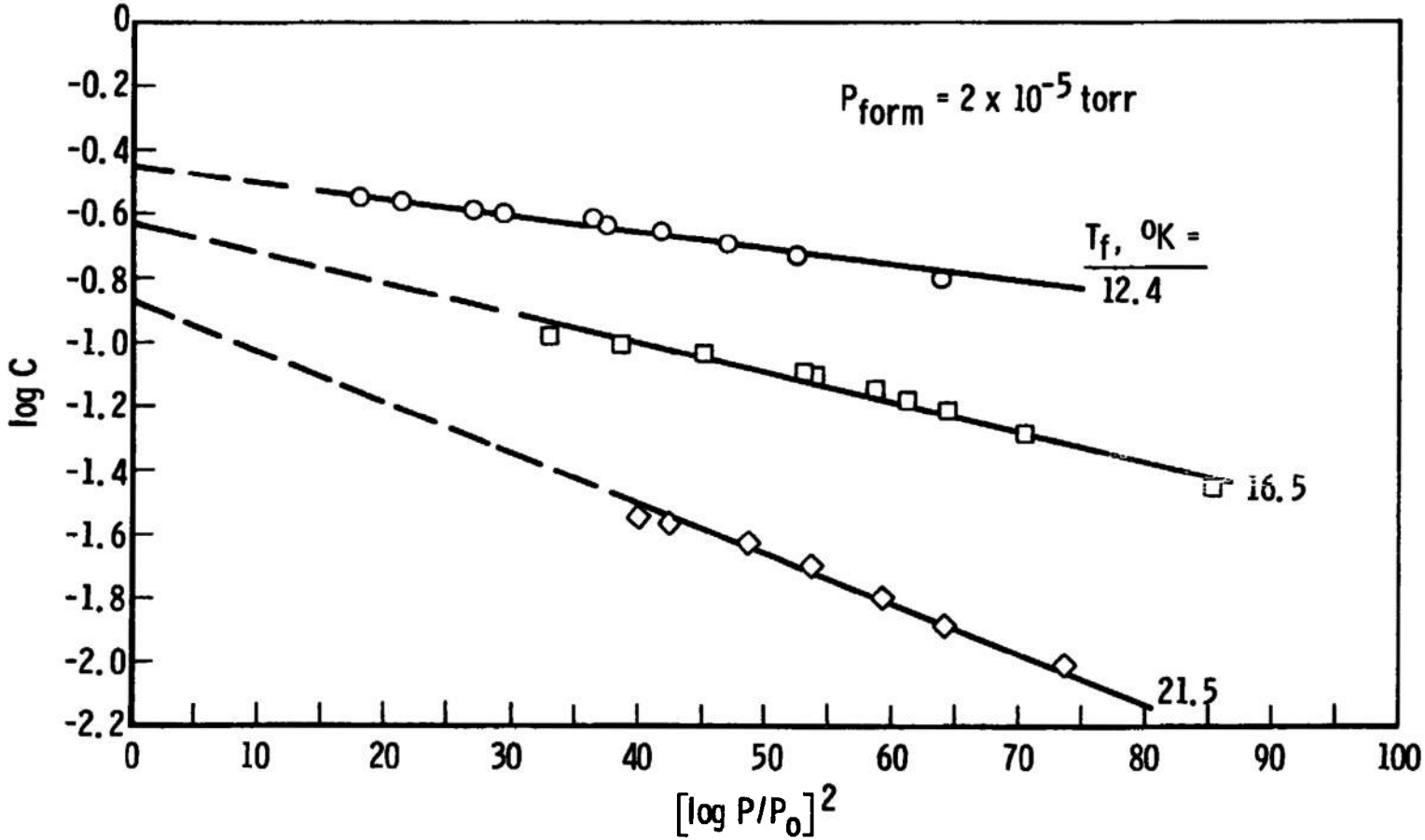

Figure 33. Equilibrium Sorption Isotherms Plotted in D-R Coordinates for CO_2 Frost Formed at a Strike Rate of 6.3×10^{15} molecules/cm^2-sec and at Different Temperatures.

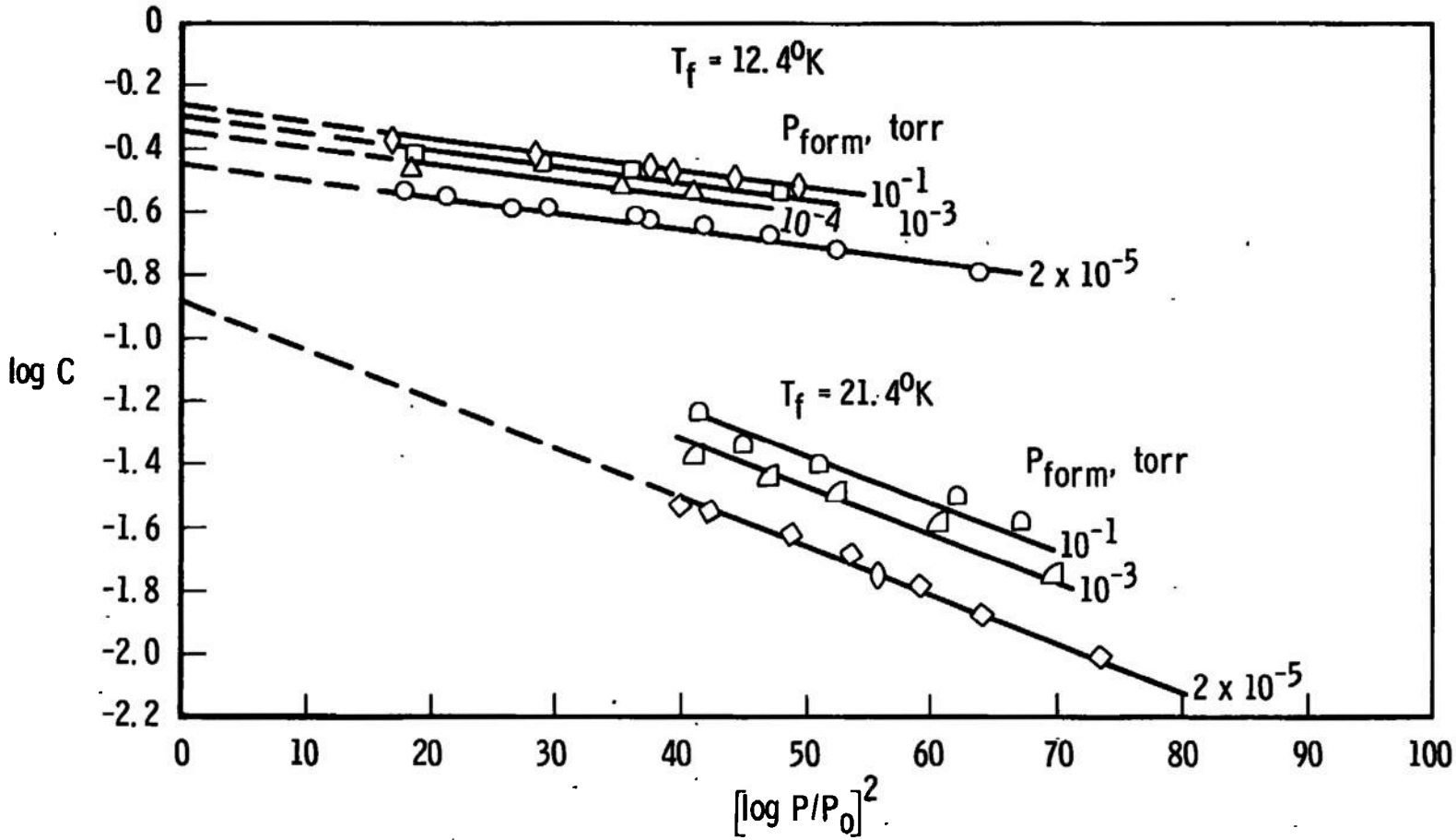

Figure 34. Equilibrium Sorption Isotherms Plotted in D-R Coordinates for CO_2 Frost Formed at Different Pressures.

equation; the results are shown in Figure 35. Again straight line isotherms were obtained at all temperatures with the D-R coordinates. Yuferov and Busol formed the CO_2 frost at an unknown pressure and at 20.4°K. They then cooled it to lower temperatures. Consequently, values of A^o or C^o obtained from Figure 35 have no common basis for comparison with corresponding values for isotherms obtained during this investigation.

Figures 33, 34 and 35 demonstrate that the D-R isotherm equation (Equation 27) is useful in predicting the equilibrium sorption characteristics of cryodeposits, even though its foundation is, in part, empirical. It can clearly account for the temperature dependence of the isotherm for H_2 on CO_2 frost. A value of $A^o = 3.4 \times 10^{-5}$ per $°K^2$ characterizes CO_2 frosts formed over a wide range of pressures and temperatures. Values of C^o, which are indices of the maximum sorption capacity are specified by the intercepts on the ordinates in Figures 33 and 34 and are summarized in Figure 36 for CO_2 frosts formed in various ways. They may be used in Equation 27, together with the previously determined value of A^o to estimate the sorption capacity of CO_2 frosts over ranges of temperature and chamber pressure. Thus, application of the D-R isotherm equation requires that an isotherm be measured at one temperature to determine, A^o, and that single sorption data points be obtained at one or more

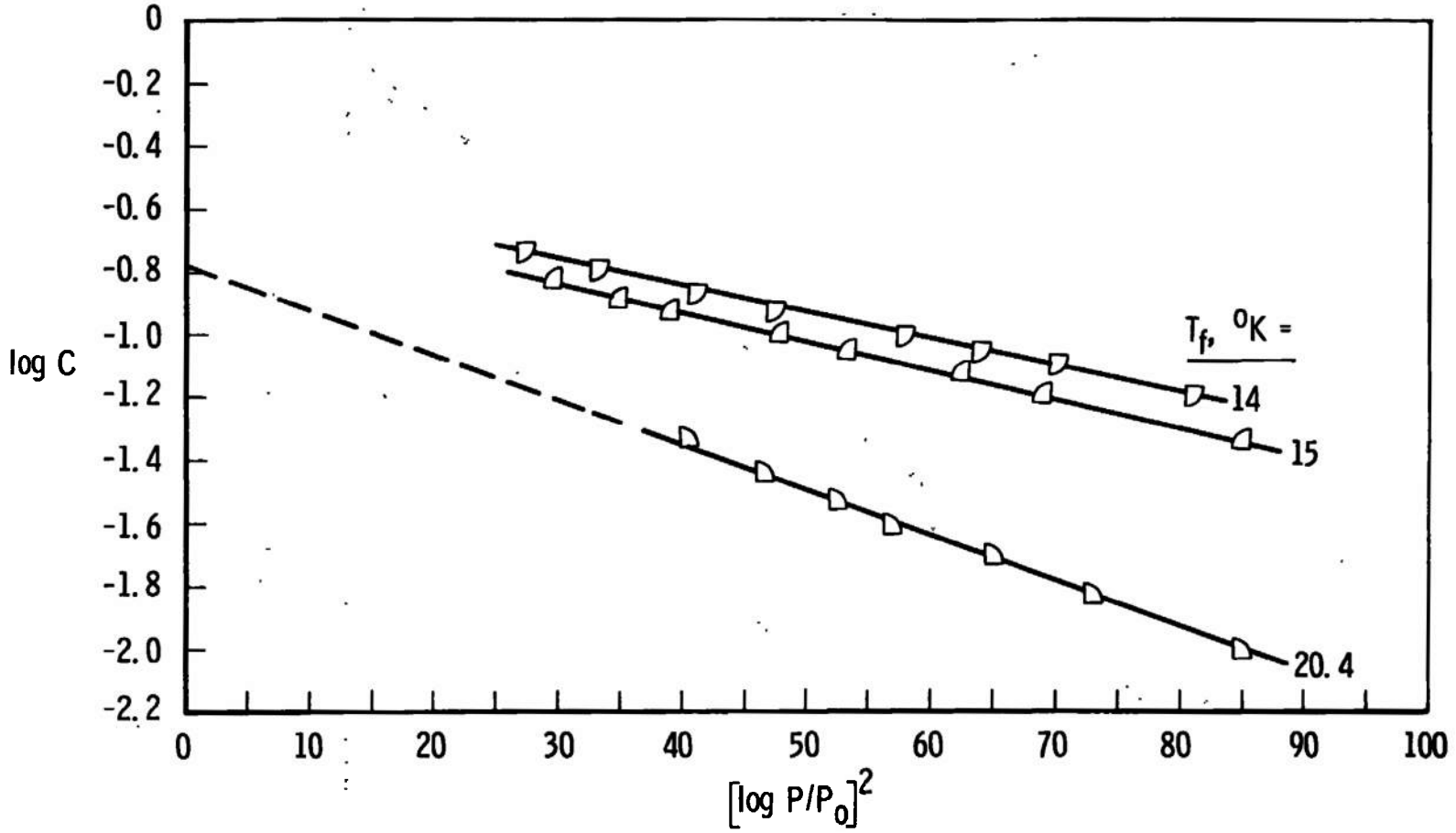

Figure 35. Equilibrium Sorption Isotherms Obtained by Yuferov and Busol Plotted in D-R Coordinates.

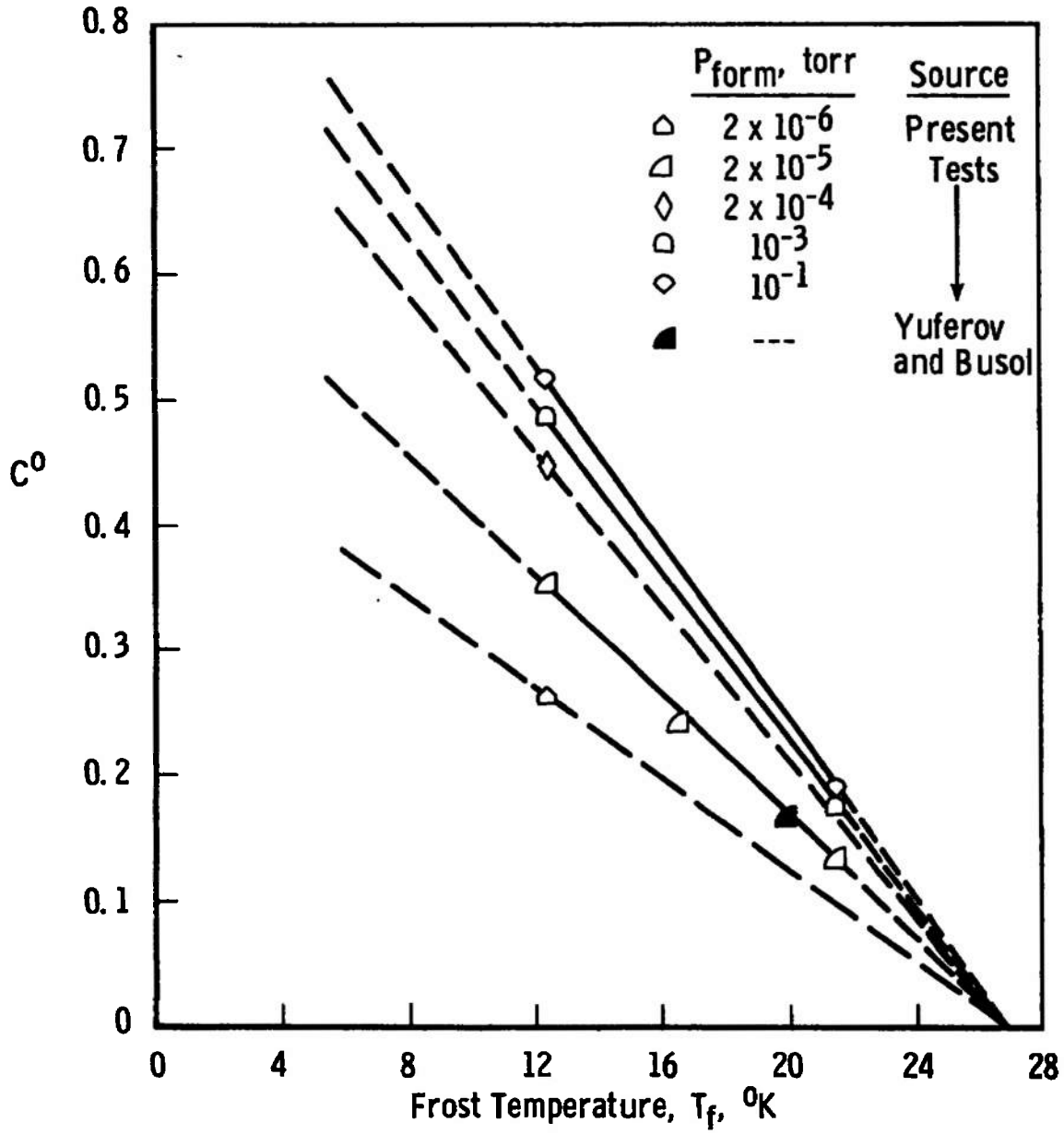

Figure 36. Experimentally Determined Values of C^O in the D-R Isotherm Equation of H_2 Sorbed by CO_2 Frost.

different frost temperatures to define $C^{o}(T_f)$. With this information, a complete family of isotherms at various chamber pressures and sorbent temperatures may be estimated. The results of such a series of calculations are described in the following section.

V. PREDICTION OF H_2 SORPTION BY CO_2 FROST

Taking $A^{o} = 3.4 \times 10^{-5}$ per $(°K)^2$ and values of C^{o} from Figure 36 for frosts formed at a pressure level of 2×10^{-5} torr, a series of isotherms was calculated from Equation 27 for a wide range of chamber pressures and for frost temperatures from 8°K to 24°K. The results of these calculations are shown by the solid lines in Figure 37. They represent isotherm predictions for frosts formed at a pressure of 2×10^{-5} torr and at the same temperature at which cryosorption takes place. Measured isotherms for frost formed at the same conditions are also given in the figure. They are observed to agree quite well with the calculations. The agreement exhibited in Figure 37 is not unexpected because the 21.5°K isotherm and single points on the other two isotherms were in effect used to define A^{o} and C^{o}, respectively. It should also be noted that varying shapes of the isotherms exhibited in Figure 21, page 67, for frosts at different temperatures are, in general, also predicted by the D-R equation.

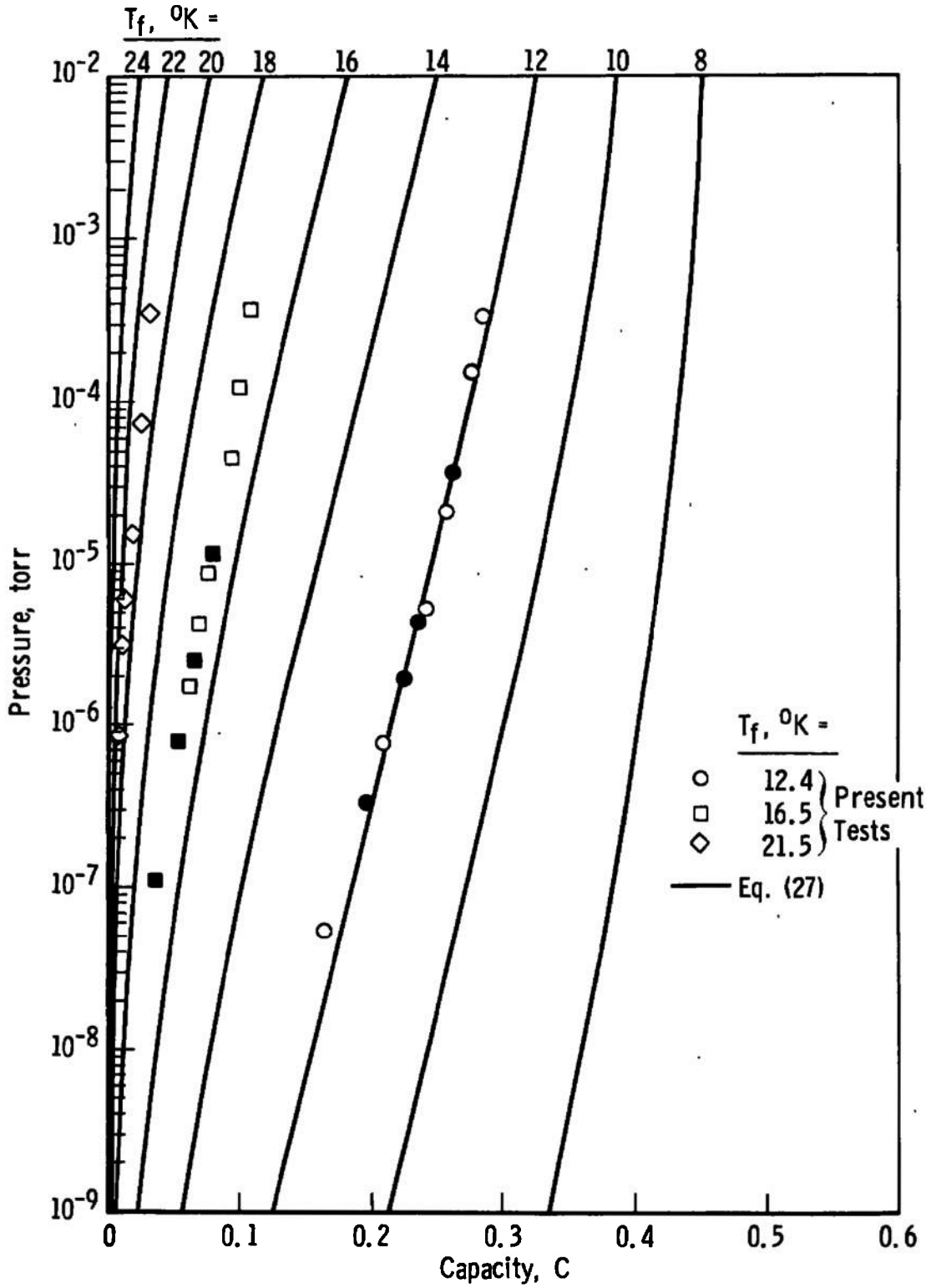

Figure 37. Comparison of Calculated H_2 Equilibrium Isotherms for the D-R Equation for CO_2 Frost Formed at a Strike Rate of 6.3×10^{15} molecules/cm^2-sec.

A complete set of equilibrium isotherms of CO_2 frosts formed at various strike rates have been predicted using Equation 27. In all cases the value of A^o was taken as 3.4×10^{-5} and C^o values were obtained from Figure 36, page 120. Computations were made for frost temperatures from 6° to 26°K and chamber pressures from 10^{-9} to 10^{-2} torr. These predictions are given in Figure 38.

Subsequent to the calculations, additional isotherm data were obtained at a temperature of 16.5°K and for a frost formed at a pressure of 1×10^{-3} torr. They are plotted together with the calculated isotherms in part d of Figure 38. The calculated isotherms are completely independent of these data. It is apparent that this isotherm was accurately predicted by the D-R isotherm equation. Sufficient information is given here to allow prediction of the H_2 sorption capacity of CO_2 frost at temperatures between 20° and 12°K to within ±10 percent. The accuracy of Equation 27, outside of this frost temperature, and in particular at lower temperatures, is not known. It would be of some practical interest to pursue sorption capacity measurements for frosts at temperatures below 12°K to determine the accuracy of the D-R equation in this range. In any case, the calculated families of sorption isotherms given in Figure 38 may be used to estimate the H_2 capacity of cryosorption pumping systems which would employ CO_2 frost as a cryosorbent.

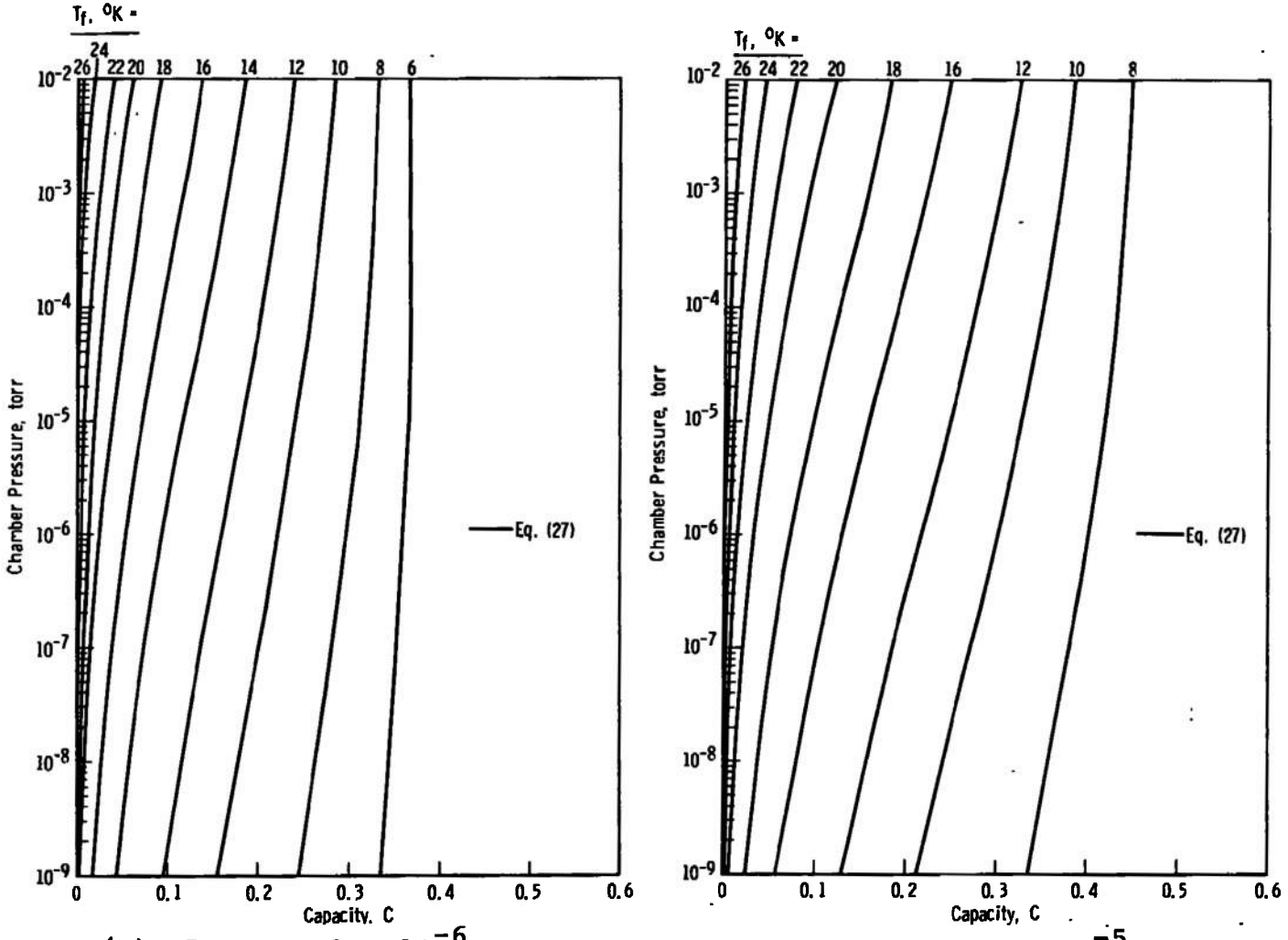

(a) $P_{form} = 2 \times 10^{-6}$ torr (b) $P_{form} = 2 \times 10^{-5}$ torr

Figure 38. Calculated Equilibrium Isotherm Design Charts for the Sorption of H_2 by CO_2 Frosts Formed at Various Conditions.

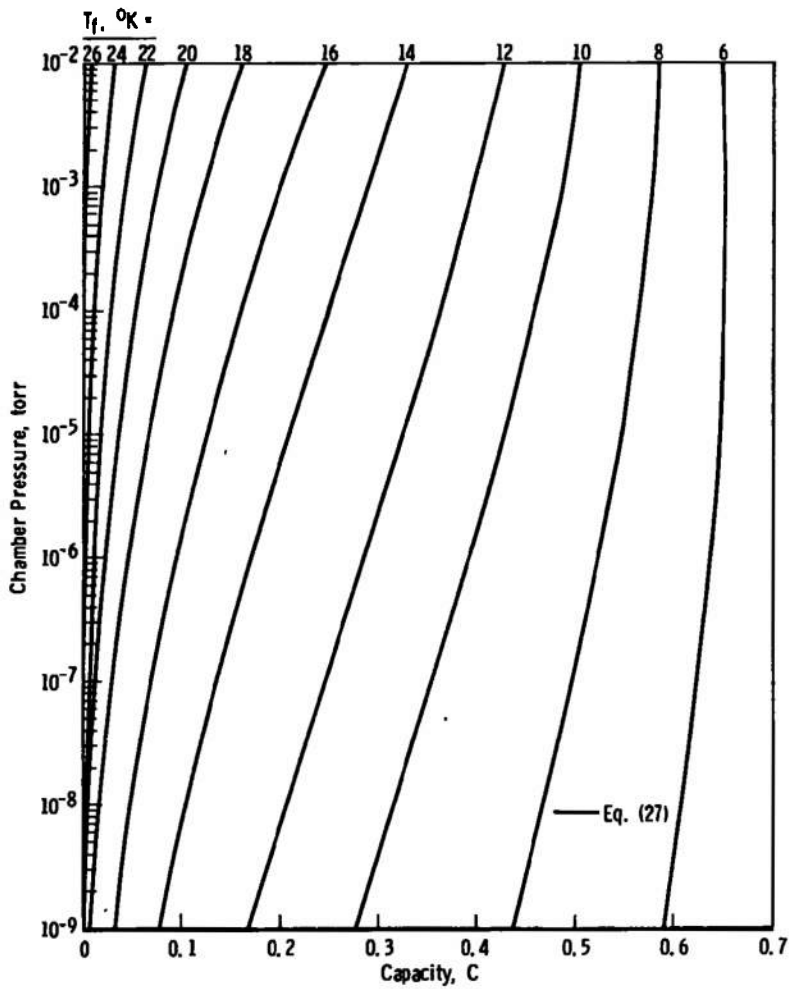

(c) $P_{form} = 2 \times 10^{-4}$ torr

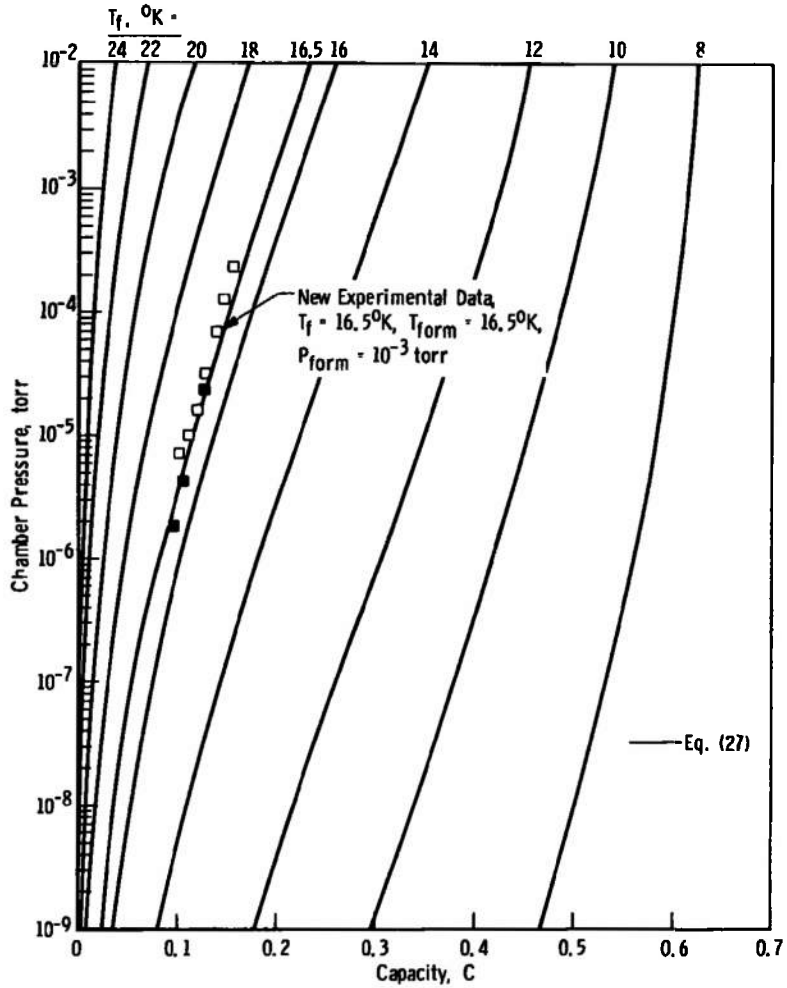

(d) $P_{form} = 1 \times 10^{-3}$ torr

Figure 38. (continued)

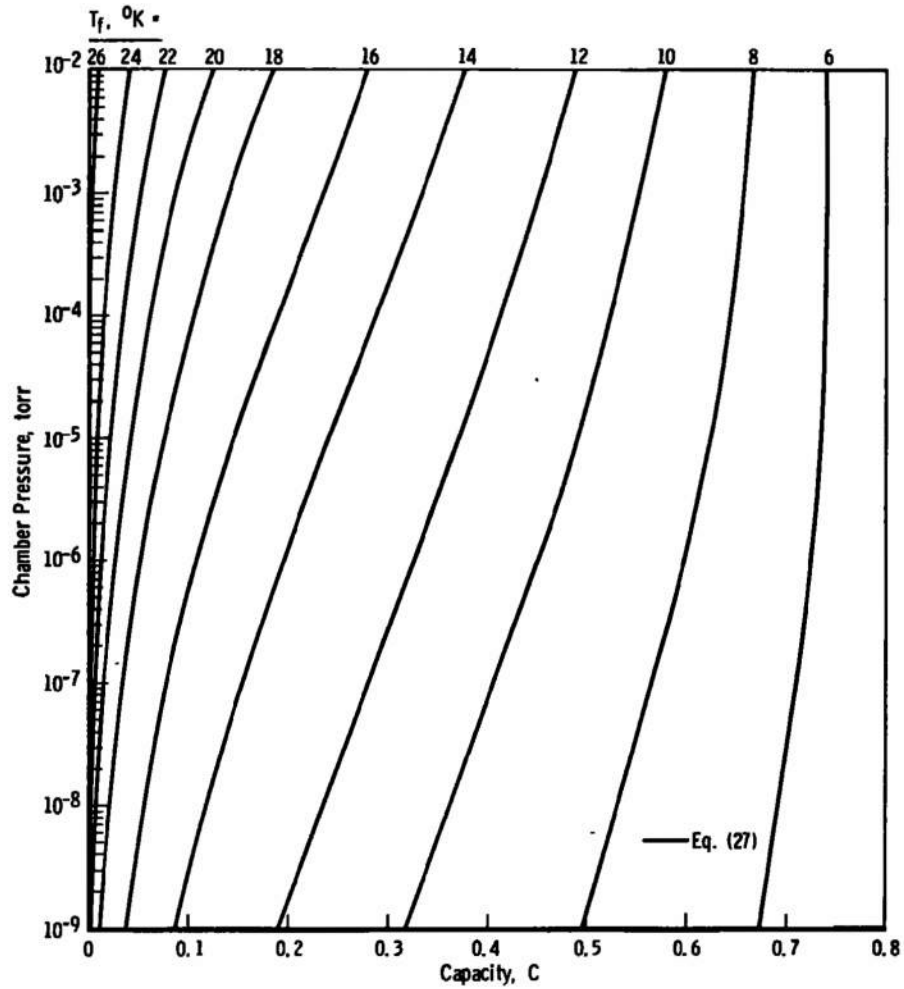

(e) $P_{form} = 1 \times 10^{-1}$ torr

Figure 38. (continued)

These isotherm curves may be cross-plotted in the form of isosteres and then the sorption energy obtained from the Clausius-Clapeyron equation,

$$E_d = 4.57 \left[\frac{d(\log P)}{d(1/T)} \right]_C \quad \text{cal/mole}$$

for P in torr and T in °K. The results of such calculations are given in the following table,

TABLE III

CALCULATED DESORPTION ENERGIES

C	E_d, cal/mole		
	$\dot{n}_{form} = 6.3 \times 10^{15}$	$\dot{n}_{form} = 6.3 \times 10^{-16}$	$\dot{n}_{form} = 3.5 \times 10^{17}$
0.05	1320	1360	1375
0.10	1165	1295	1320
0.15	1050	1240	1265
0.20	970	1170	1215
0.30	- -	1050	1115

Note that E_d decreases somewhat with increasing C. This characteristic is exhibited by a variety of porous sorbents ([29], Chapter VII).

CHAPTER VII

MEASUREMENT OF THE SORPTION DYNAMICS OF FROSTS

There are two aspects of sorption: (1) the conditions for equilibrium, and (2) the dynamics of sorption. The first has been considered in the previous two chapters and establishes how much gas can be sorbed when equilibrium is attained. The second, which involves a description of how this equilibrium condition is achieved, is treated in this chapter and the next. Thus, the equilibrium isotherm data given previously describes the final condition of a dynamic sorption process.

I. HYDROGEN PUMPING SPEED MEASUREMENTS

The pumping speed of the "bare" cryosurface at a temperature of 12.4°K is given in part a of Figure 39. It appears that the stainless steel surface has a high pumping speed for several seconds and sorbs appreciable quantities of H_2. However, this is not the true picture. The chamber pressure decreases about a decade as the cryosurface is cooled to 12°K. Consequently, the surface is actually covered with a thin layer of cryodeposit from the residual and desorbed gases in the chamber ($\ell \simeq 0.015\mu$) and the "bare surface" pumping effect is due to cryosorption.

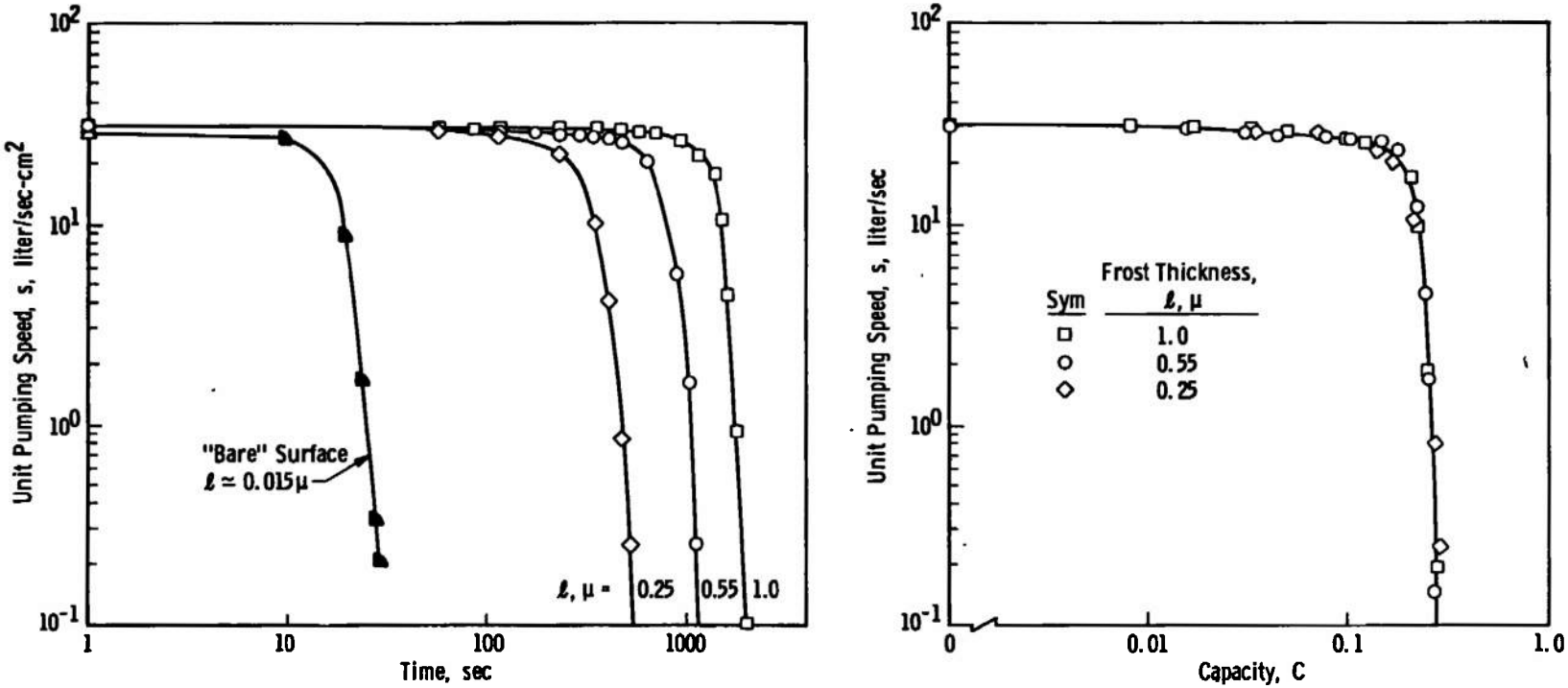

(a) Pumping Speed versus Time

(b) Pumping Speed versus Capacity

Figure 39. Dynamic H_2 Pumping Speed Curves for Various Thicknesses of 12.4°K CO_2 Frost Formed at a Chamber Pressure Level of 2×10^{-5} torr on a 12.4°K Surface - Constant H_2 Sorbate Addition Rate.

Dynamic pumping speed curves for 12.4°K CO_2 frost layers of three different thicknesses, but otherwise formed in the same manner, are also shown in Figure 39, part a. The curves are displaced by time intervals which are proportional to the frost thickness. Consequently, if these data are replotted in terms of the dimensionless capacity parameter, C, they produce essentially a single pumping curve as shown in part b of Figure 39.

A similar series of sorption pumping curves are given in part a of Figure 40 in which the sorbate flow rate was varied in order to maintain a constant chamber pressure during sorption. Because the sorbate flow rate is continuously decreasing, the pumping speed is shown as a function of the amount of H_2 sorbed. Again, on the basis of the dimensionless frost capacity the pumping curves collapse into essentially a single curve (part b, Figure 40), although the scatter is somewhat greater, particularly in the vicinity of the knee in the curve.

The trends shown in these figures are similar to those obtained by Hunt, et al. [10] for the sorption of H_2 by a CO_2 frost (Figure 1, page 10). The pumping speed of CO_2 frost decreases slowly from its initial value as H_2 is sorbed. Then it falls off very rapidly as saturation is approached. The present tests further illustrate two important points.

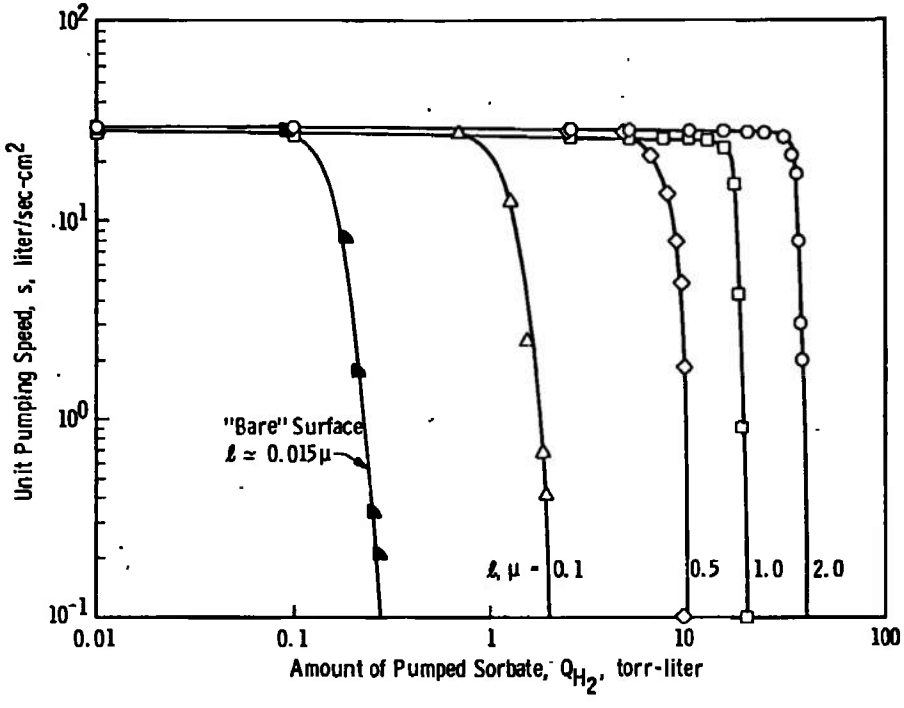

(a) Pumping Speed versus Amount of H_2 Sorbed

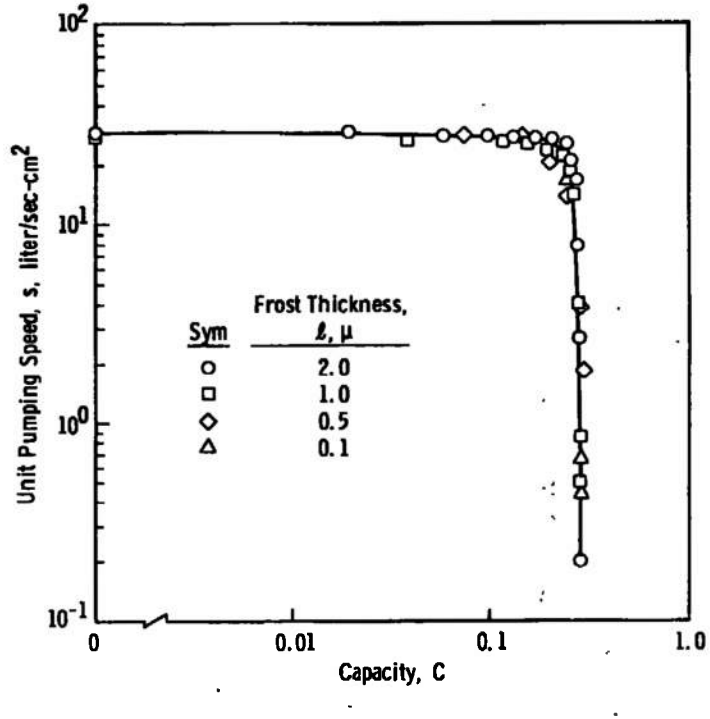

(b) Pumping Speed versus Capacity

Figure 40. Dynamic H_2 Pumping Speed Curves for Various Thicknesses of 12.4°K CO_2 Frost Formed at a Chamber Pressure Level of 2×10^{-5} torr on a 12.4°K Surface - Pumping at Constant Chamber Pressure.

First, the initial pumping speed of the frost is independent of the volume of the frost. Additional tests with a cryosurface of different geometry and the pumping speed results of other investigators show that the initial pumping speed is proportional to the geometric area[13] of the frost. Thus, while the sorption capacity is governed by the volumetric or bulk characteristics of the frost (Chapter V), the initial pumping speed depends primarily on the interaction of the sorbate molecules with the sorbent surface. The nature of the complex sorbate-sorbent interaction is discussed later.

Secondly, the present tests have shown (Figure 28, page 90) that at equilibrium, the amount of H_2 sorbed by a CO_2 frost was directly related to the frost volume (or thickness for a given frost surface area). The dynamic pumping curves further demonstrate the important fact that this situation exists throughout the pumping process. Consequently, a pumping speed curve measured for a frost at one thickness can be used to estimate the dynamic pumping characteristics of frosts formed at the same conditions but having different thicknesses, if the frosts are not sufficiently thick to produce significant temperature gradients.

---

[13] In this case this denotes the spherical surface area of the pumping surface. Because of the complex network of pores, cracks, crevices, etc., the physical surface area of a porous frost may be many times greater than its apparent geometric area.

1. Effect of Frost Temperature

Pumping speed versus capacity curves for CO_2 frosts formed at two pressure levels and temperatures are given in Figure 41. Higher temperature frosts are observed to have lower initial pumping speeds. This agrees with pumping speed data obtained previously by Dawbarn (Figure 2, page 14) and is associated with the lower sticking probability and higher desorption rate of the warmer frosts. The present tests, however, more completely characterize the pumping process for different frost temperatures. They demonstrate that as the frost temperature increases, the capacity range or time interval over which the pumping speed remains relatively high is reduced.

2. Effect of Frost Formation Rate

Dynamic pumping speed curves for frosts formed at various strike rates are summarized in Figure 42. Forming the frost at a higher rate, which as shown previously made it more disordered and increased its equilibrium capacity, also resulted in a small decrease in its initial pumping speed. This trend was also exhibited by higher temperature frosts (for example, compare T_f = 21.5°K and T_f = 16.5°K curves in Figure 41).

Figure 42 also illustrates that the increase in equilibrium sorption capacity achieved by forming a more disordered frost at higher strike rates occurs over the entire pumping speed range. It is apparent that the

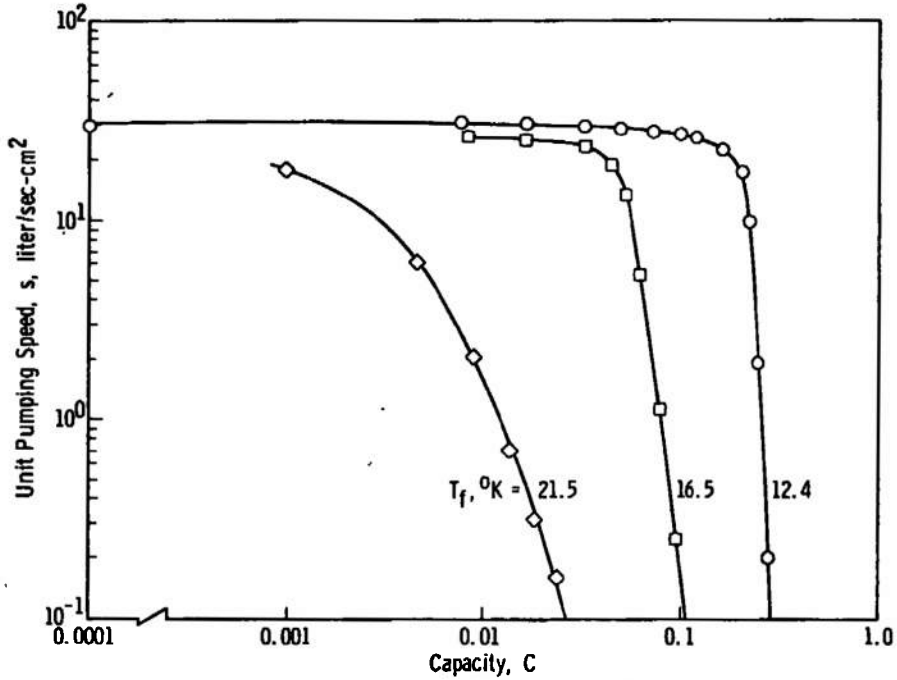

(a) $P_{form} = 2 \times 10^{-5}$ torr

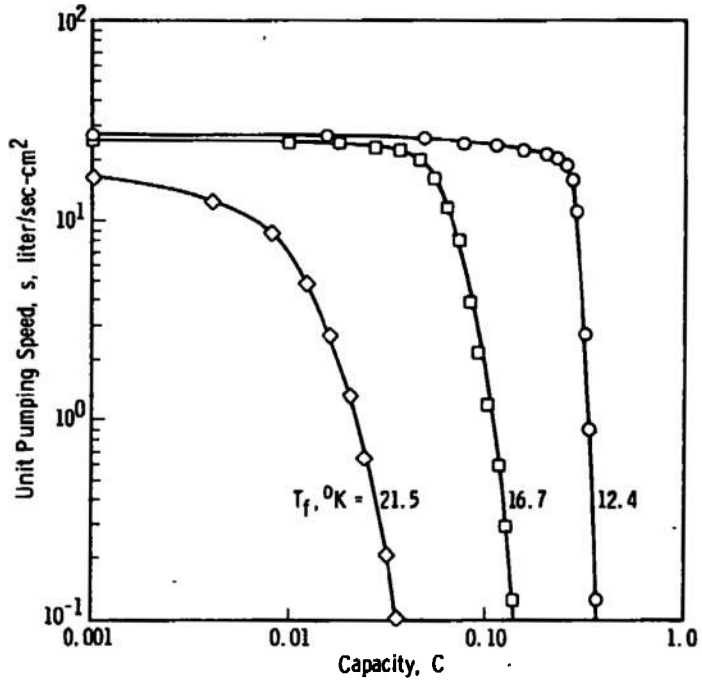

(b) $P_{form} = 1 \times 10^{-3}$ torr

Figure 41. Dynamic H_2 Pumping Speed Curves for CO_2 Frosts at Various Temperatures - Constant H_2 Sorbate Addition Rate.

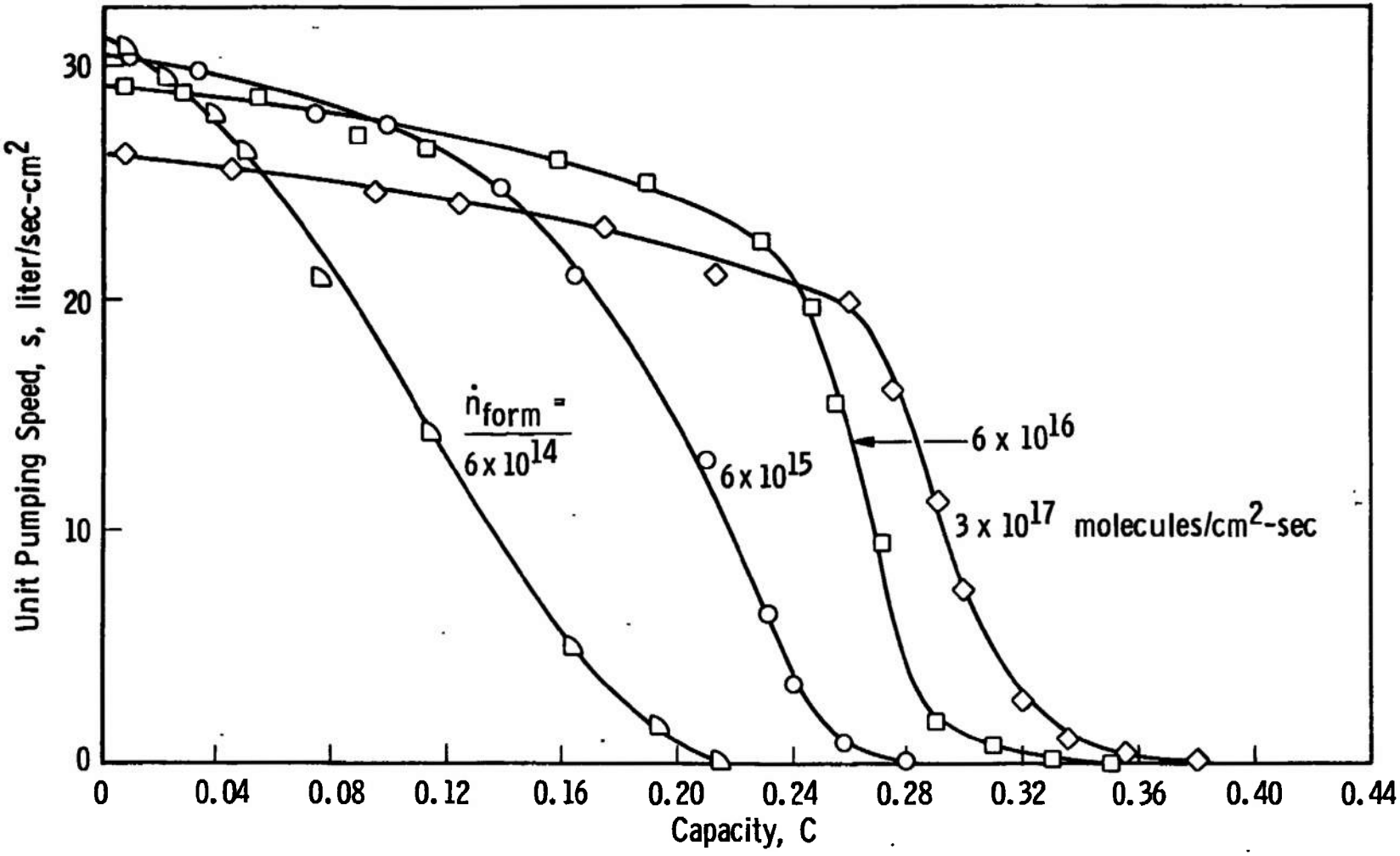

Figure 42. Dynamic H_2 Pumping Speed Curves for 12.4°K CO_2 Frost Formed at Different Strike Rates.

advantage gained in increased sorption capacity by forming a porous frost greatly outweighs the modest decrease in pumping speed.

3. Effect of Warming the Frost

It was previously demonstrated that intermediate warming of the frost decreased its equilibrium sorption capacity. Figure 43 further shows that when a frost is cycled through some temperature range its dynamic pumping speed curves are essentially shifted to lower capacity, but warming the frost also produces a small increase of the initial pumping speed. Although an intermediate temperature increase of the frost may grossly alter its structure, it obviously does not significantly alter the interaction character of its surface.

4. Different Sorbents

Dynamic pumping speed curves for SO_2 and CH_3Cl sorbents are compared to that of CO_2 in Figure 44. All of these frosts were formed at essentially the same conditions. All of the curves have similar shapes but somewhat different values of initial pumping speed and saturation capacity. The CH_3Cl frost exhibited the highest pumping speed of those investigated in this study. The differences in their sorption capacities at saturation are discussed in detail in Chapter V.

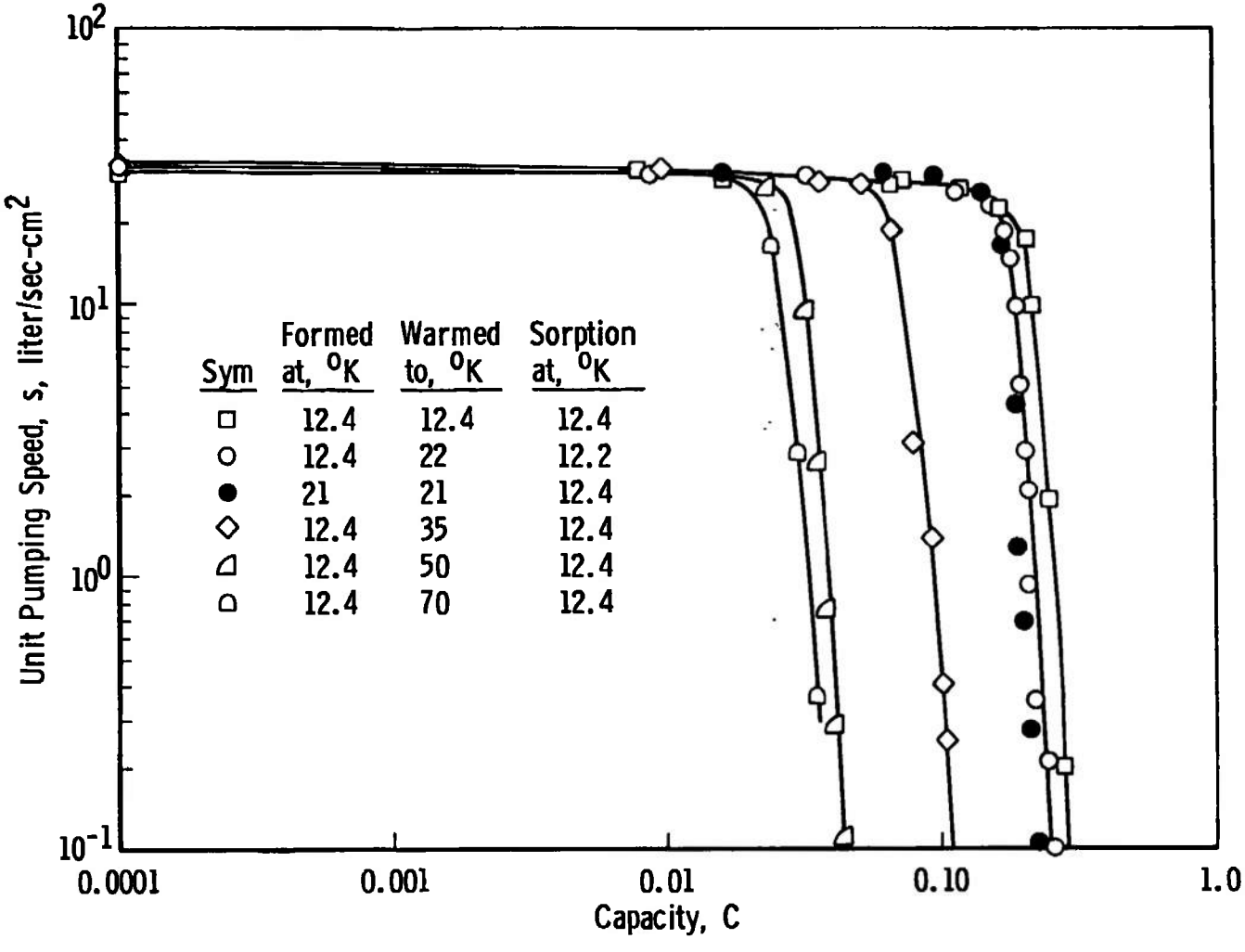

Figure 43. Dynamic H_2 Pumping Speed Curves for CO_2 Frost Formed at a Strike Rate of 6.3×10^{15} molecules/cm^2-sec and a Temperature of 12.4°K but Warmed to Higher Intermediate Temperatures.

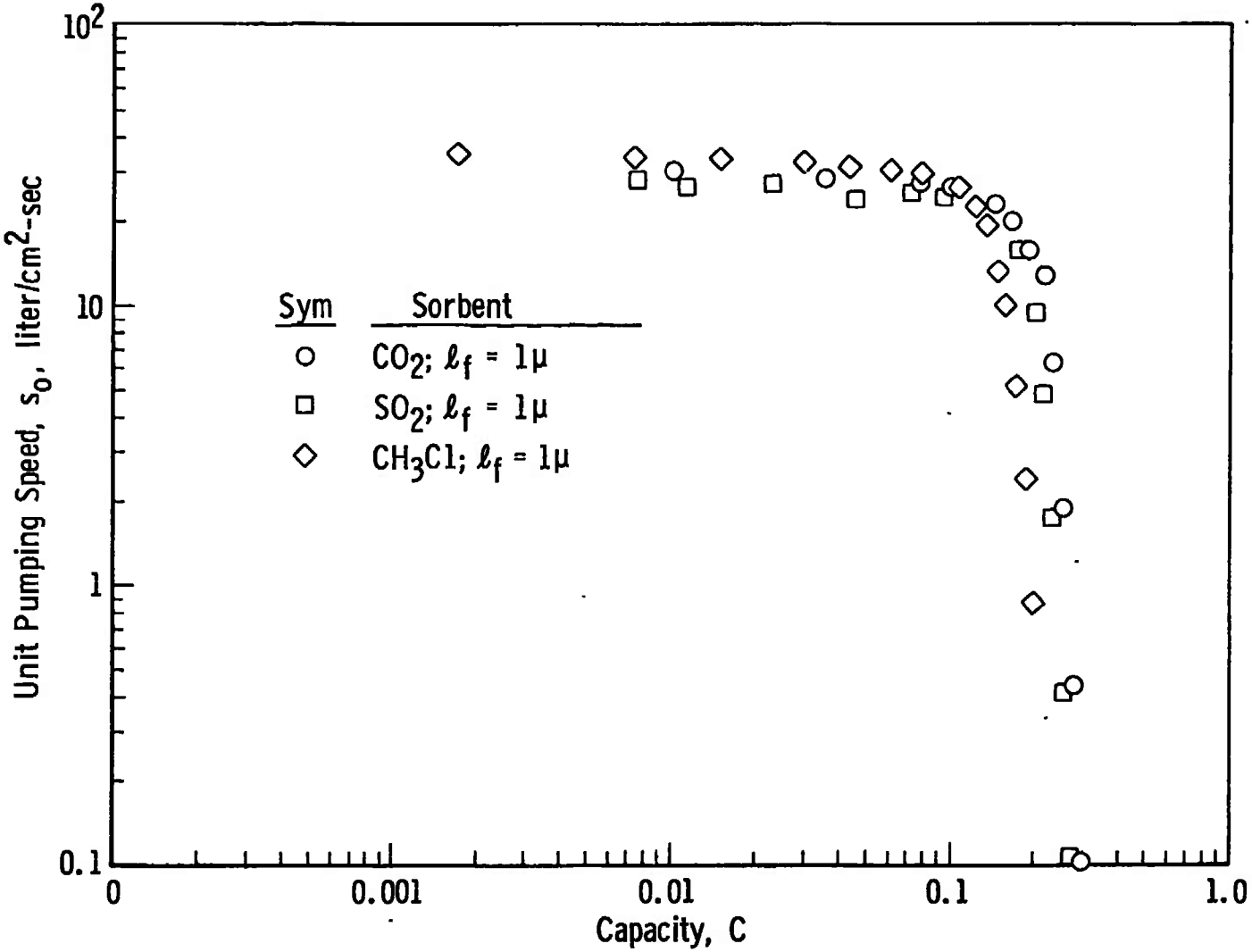

Figure 44. Dynamic H_2 Pumping Curves of Several Sorbents at a Temperature of 12.4°K and Formed at the Same Conditions.

5. Comparison with Other Investigators

Unit pumping speeds of about 30 liter/sec-cm^2 measured during this investigation for CO_2 frost (Figures 39 through 43, pages 129, 131, 134, 135 and 137) appear to be somewhat greater than those published by other investigators (see Figure 7, page 30). The differences, however, are largely due to the way in which the pumping speed is defined. The fact that in a closed chamber the frost is also pumping a gas load due to outgassing and inleakage has not always been considered. Equation 7 employed to compute all of the pumping speeds presented here, credits the frost for handling this additional gas load, and more realistically represents the true frost pumping speed. Others have generally reported "system" pumping speeds, and the present pumping speed results are actually quite consistent with those obtained previously. The shape of the dynamic pumping curves are quite similar to those obtained by Hunt, et al. [10] and Yuferov and Busol [14], and the reduction in pumping speed attendant to higher frost temperatures as previously noted by Dawbarn [13] was also verified.

The strike rate of 300°K H_2 on a surface corresponds to a theoretical maximum pumping speed of about 44 liter/sec-cm^2. This implies that the maximum effective capture coefficient of the CO_2 frost for H_2 varies between about 0.55 and 0.70 for the various kinds of frost structure

formed in this investigation. These values are in the same range as those reported previously [9].

No other investigators have examined SO_2 of CH_3Cl frost sorbents. It is apparent that they have pumping speeds comparable to CO_2 but somewhat lower saturation capacities.

Frosts which were formed in a manner to make them more disordered, thus giving them more irregular surfaces, exhibited higher capacities but had slightly lower initial pumping speeds (Figure 41, page 134). In contrast, warming and recooling the frost promotes a more ordered and smoother surface and increases the initial pumping speed (Figure 42, page 135). These two effects are consistent, and suggest frost cryosorbents with smoother surfaces will have higher initial pumping speeds. This may occur because a smoother frost surface may: (1) result in a stronger total interaction with the sorbate molecules, and/or (2) result in conditions which decrease the flux of desorbed molecules.

CHAPTER VIII

ANALYSIS AND THEORY OF THE SORPTION DYNAMICS OF FROSTS

I. THE SORPTION PROCESS

When a gas molecule collides or interacts with a solid surface it may: (1) reflect elastically, (2) reflect inelastically, in which case the energy exchange may be characterized by the energy accommodation coefficient, or (3) it may lose sufficient energy that it is physically adsorbed at least for a short time. In a survey paper, Stickney [71] has shown that the details of the gas-surface interaction are governed by the interaction potential between the gas and surface material, the nature of the surface, the gas and surface temperatures and several other factors. Once the particle is adsorbed: (1) it may remain (or accumulate) on the surface for long times by condensation or chemisorption mechanisms, (2) it may be desorbed, or (3) it may diffuse over the surface or into the substrate material. Because cryodeposited sorbents are amorphous, it is apparent that diffusional processes could play an important role in sorption pumping. Moreover, it was suggested in Chapter V that cryofrosts are so porous that the diffusion mechanism is one of surface

diffusion into pores, cracks or other defects in the frost rather than interstitial diffusion.

1. Physical Adsorption

Because the physical character of the surfaces of frost cryosorbents is unknown and the interaction potential is extremely complex [71 through 74], one can form, at best, only an idealized qualitative picture of the sorbate-sorbent interaction [75, 76], as sketched in Figure 45. For simplicity only the dimension normal to the surface is shown. A free molecule in the gas phase has some energy at point (a); and, as it approaches the surface it experiences an attractive force. If in the interaction the molecule gives up some of its energy to the surface, it may not have sufficient energy to escape from the potential well. Once caught at some energy level in the well, say point (b), the molecule may undergo a relaxation process and attain thermal equilibrium with the solid [70]. If the solid is cooled this would result in the molecule residing near the bottom of the well (point c). At this point it is physically adsorbed. It will remain adsorbed in the potential well until it receives enough energy from the surface or from other incident molecules to escape. Frenkel [77] has deduced from statistical considerations, that on the average the parti- will reside on the surface for the time,

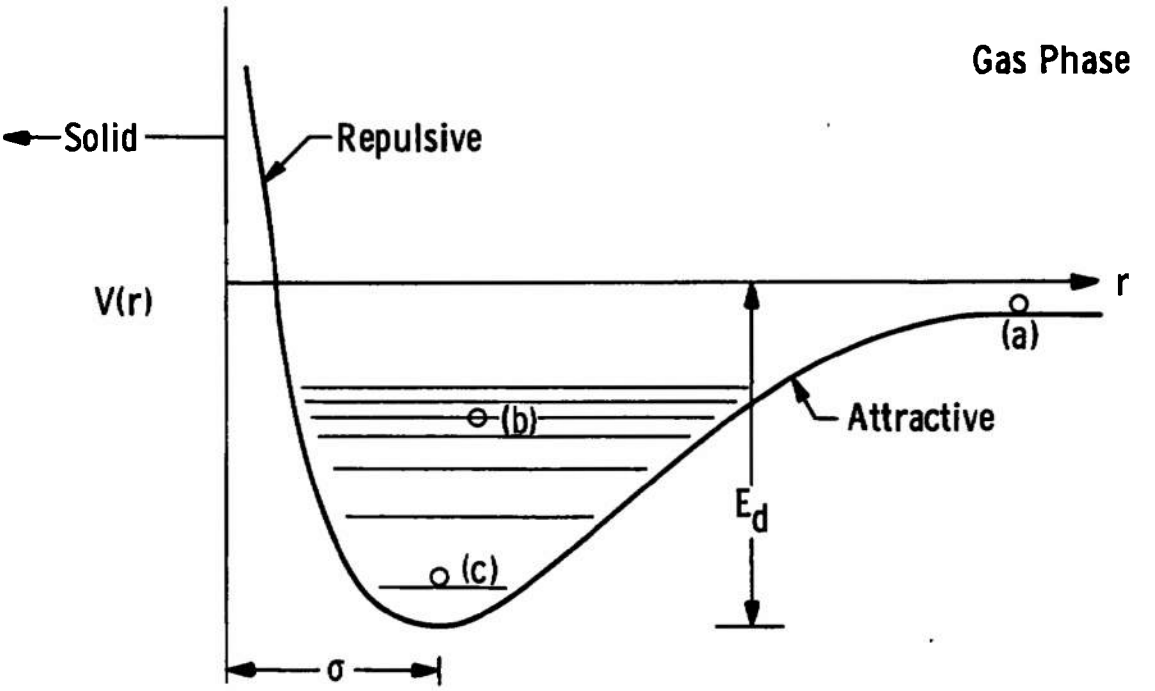

(a) Potential Plot for Physical Adsorption

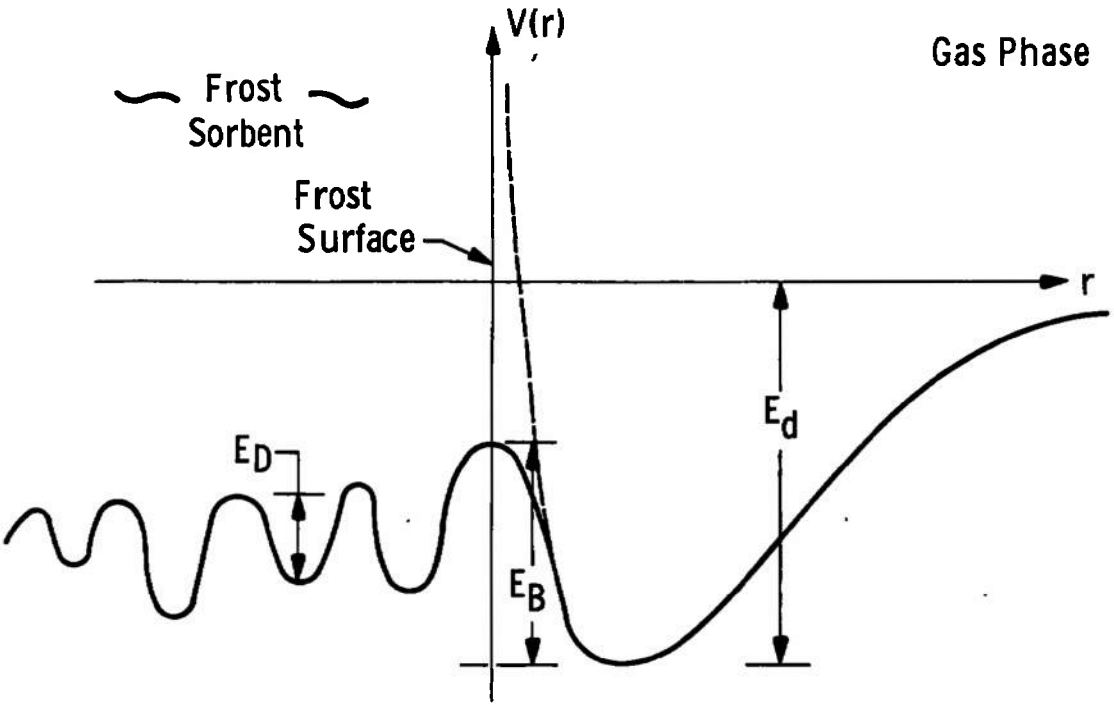

(b) Potential Plot for Frost Cryosorption

Figure 45. Potential Energy Distribution for Physisorption and Frost Cryosorption.

$$t_r = \tau\, e^{E_d/kT} \tag{28}$$

The residence time on the surface, t_r, can obviously be increased by decreasing the surface temperature. In this case the adsorbed molecules would reside near the bottom of the well with a smaller statistical change of receiving enough energy from the surface to be desorbed. This is, or course, the basis of cryopumping. In this case surface temperature is reduced to less than the vapor-pressure temperature [2] so that adsorbed molecules have a very low probability of being desorbed and remain in a condensed, solidified form on the surface. Gas can be continuously pumped as long as the frost surface is maintained at or below the required temperature.

2. Cryosorption

The situation for cryosorption pumping is somewhat different. Experimental cryosorption test results show that physically adsorbed molecules are not bound to the surface but diffuse or migrate into the cryosorbent. This has the effect of removing the repulsive part of the interaction normally imposed by a solid surface and may be depicted by the gas-surface interaction potential distribution sketched in part b of Figure 45.

The adsorbed molecule may have to overcome a potential barrier, E_B, in order to migrate away from its adsorption site and into the sorbent. This barrier must

be considerably less than the depth of the adsorptive potential well, if sorption is to be much more probable than desorption. As a sorbed molecule diffuses further into the sorbent it must overcome various diffusion potential barriers (E_D). These internal barriers may have different heights than those near the surface because the forces retarding diffusion away from the surface may be considerably different than those retarding diffusion within the porous structure of the sorbent. This occurs because the adsorbed molecule interacts with sorbent molecules in a two-dimensional sense on the surface while a sorbed molecule will interact with sorbent molecules in three dimensions within small pores in the sorbent. For cryosorption pumping the surface temperature obviously need not be low enough to cryopump the sorbate gas, but it must be low enough so that the adsorbed molecules have a low probability of gaining enough energy to be desorbed.

Consequently, the rate at which sorbate molecules are removed from the gas phase and the dynamic sorption characteristics of frosts are governed by one or some combination of the following factors:

(1) The rate at which sorbate molecules are adsorbed on the frost surface.

(2) The rate at which the adsorbed molecules migrate away from their adsorption site and penetrate the interior of the frost.

(3) The rate at which the sorbed molecules diffuse through the frost structure.

A simple analysis indicates how these various factors affect the pumping speed. The rate at which sorbate molecules strike the surface is given by,

$$\frac{dN_i}{dt} = \frac{A_f\ P}{\sqrt{2\pi mkT_g}} \tag{29}$$

Some of these incident molecules will stick and be adsorbed while others are immediately reflected. Assuming a sticking probability, c, the rate at which molecules are directly reflected from the surface is,

$$\frac{dN_r}{dt} = (1-c)\ \frac{dN_i}{dt} = (1-c)\ \frac{A_f\ P}{\sqrt{2\pi mkT_g}} \tag{30}$$

and, hence the rate at which they are adsorbed would be,

$$\frac{dN_a}{dt} = \frac{dN_i}{dt} - \frac{dN_r}{dt} = \frac{c\ A_f\ P}{\sqrt{2\pi mkT_g}}. \tag{31}$$

The rate at which particles are desorbed is equal to the number of molecules on the surface, N_o divided by their mean residence time, or,

$$\frac{dN_d}{dt} = \frac{N_o}{t_r}$$

Since the mean residence time is given by Equation 28,

$$\frac{dN_d}{dt} = \frac{N_o\, e^{-E_d/kT_f}}{\tau} \tag{32}$$

Then, the rate at which molecules are pumped may be obtained from Equations 31 and 32 as,

$$\dot{N}_p = \dot{N}_i - \dot{N}_r - \dot{N}_d = \frac{c\, A_f\, P}{\sqrt{2\pi mkT_g}} - \frac{N_o\, e^{-E_d/kT_f}}{\tau} \tag{33}$$

($\dot{N}_p$ is proportional to the measured pumping speeds.)

Desorption energies were obtained from the equilibrium sorption isotherms (Chapter VI) and shown to depend upon the amount of gas sorbed. Yuferov and Busol [14] have reported a similar dependence. Thus,

$$E_d = E_d(N_o)$$

Also, the sticking probability decreases as the amount of gas sorbed increases

$$c = c(N_o)$$

This occurs because as more and more H_2 is sorbed, the incident H_2 molecules interact with the frost specie and an increasing amount of previously sorbed H_2. Since H_2 interacts more strongly with the sorbent specie than with other H_2 molecules the sorbent-sorbate interaction

potential decreases as the H_2 is sorbed. Thus, Equation 33 in its more general form is,

$$\frac{dN_p}{dt} = \frac{c(N_o)\ A_f\ P(t)}{\sqrt{2\pi mkT_g}} - \frac{N_o}{\tau}\ e^{-E_d(N_o)/kT_f} \tag{34}$$

where the gas phase pressure, P, may also vary with time. Although it is possible to infer from the experimental dynamic sorption pumping data reasonable variations of E_d and c with the amount of gas sorbed, there is no way to uniquely determine their functional variation. Because of these unknown functions, Equation 34 has limited use to directly determine the rate at which the sorbate gas is pumped.

Equation 34 was developed by considering a balance of particles from and to the gas phase at the frost surface, but the rate at which molecules are pumped is also given by,

$$\frac{dN_p}{dt} = \frac{\partial N(\ell,t)}{\partial t} + A_f\ D\ \frac{\partial n(\ell',t)}{\partial x}$$

where $n(\ell',t)$ represents the number density of sorbed molecules just inside the frost, and $N_o = N(\ell,t)$ the number of molecules adsorbed on the surface. It is convenient to express the latter term as an effective number density of adsorbed molecules on the surface $n(\ell,t)$ and rewrite this expression as,

$$\frac{dN_p}{dt} = (A_f \ell^*) \frac{\partial n(\ell,t)}{\partial t} + A_f D \frac{\partial n(\ell',t)}{\partial x} \qquad (35)$$

The first term on the right side of Equation 35 accounts for the fact that some of the adsorbed molecules may accumulate on the frost surface while the second term represents the rate at which other adsorbed molecules cross the frost surface and enter into and diffuse through the frost[14]. It is necessary to distinguish between the concentration of molecules on the surface $n(\ell,t)$ and that just inside the surface $n(\ell',t)$ to account for the possibility of a penetration barrier E_B, at the surface and a particle number gradient across it. If there is no penetration barrier at the surface then $n(\ell,t)$ and $n(\ell',t)$ would be the same.

Conjectural variations of the different rate mechanisms which make up the sorption process are sketched in part a of Figure 46 for the case of constant pressure. The rate at which molecules strike the surface ($\dot{N}_i$) is constant since the pressure is constant. The rate at which the incident molecules are reflected ($\dot{N}_r$) is shown to increase with increasing amount of gas sorbed because of the previously mentioned decrease in sticking probability with an increasing amount of gas sorbed. Inasmuch as $\dot{N}_d$

[14] In the most general case molecules may be adsorbed onto the surface at a different rate than they are sorbed by the frost.

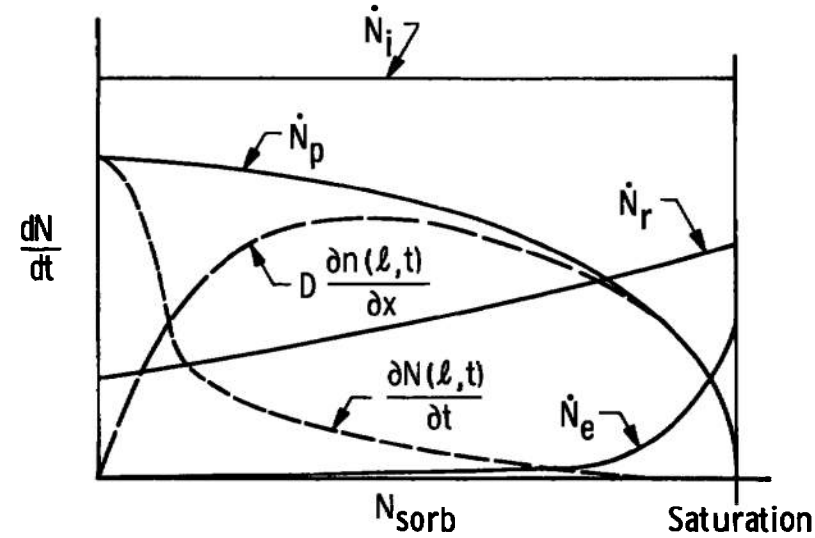

(a) General Case

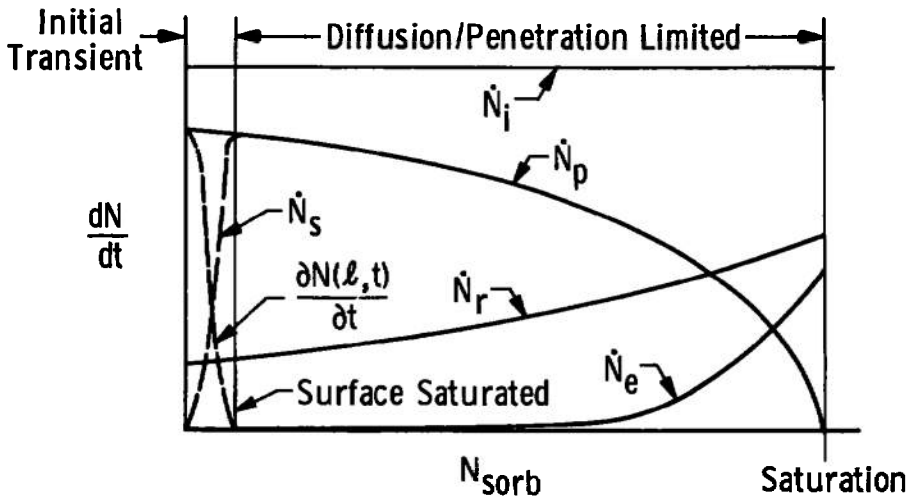

(b) Diffusion/Penetration Limited Case

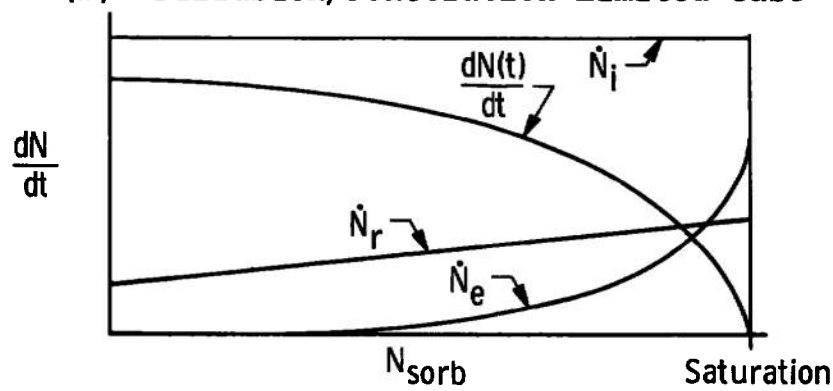

(c) Adsorption Rate Limited Case

Figure 46. Schematic of the Molecular Strike or Flow Rates for Various Types of Sorption Pumping.

varies exponentially (Equation 32) and E_d also decreases with an increasing amount of gas sorbed, $\dot{N}_d$ would be small during the initial stages of sorption but increase significantly during the latter stages. The variation of $\dot{N}_p$ is typical of the measured dynamic sorption curves for rather porous CO_2 frost presented in Chapter VII. The variations of $\dot{N}_r$ and $\dot{N}_d$ are arbitrary; but they must satisfy Equation 33. Arbitrary variations of $\frac{\partial N(\ell,t)}{\partial t}$ and $D\frac{\partial n(\ell',t)}{\partial x}$ are also sketched in part a of Figure 46. It is only known that they must satisfy Equation 35.

II. FORMULATION OF A GENERAL SORPTION THEORY

It was previously suggested that sorbate molecules are first adsorbed on the frost surface and then by surface diffusion they migrate into the disordered, porous interior of the frost. To account for the penetration of adsorbed molecules into the frost as well as their subsequent diffusion, the diffusion process may be thought of as occurring in two steps,

(1) Diffusion away from the surface adsorption site (i.e., penetration into the frost).

(2) Further diffusion into the pores, cracks, grain boundaries, etc., of the frost.

As suggested previously and depicted in part b of Figure 45, page 143, the diffusion barriers an adsorbed molecule must overcome to migrate away from its adsorption site are

different from those which resist diffusion within the frost. Consequently, consistent with this model of sorption pumping, the cryosorbent frost may be thought of as consisting of two regions: (1) a very thin layer near the surface with an effective thickness of ℓ_1, and (2) the remaining bulk frost layer of thickness ℓ_2 as sketched below,

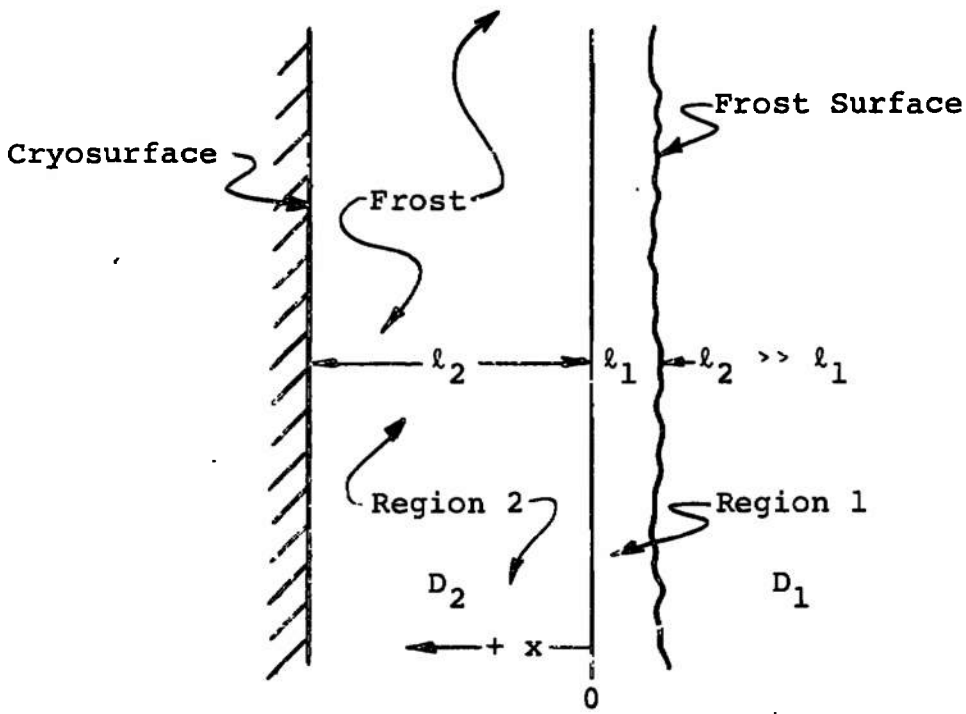

The thin surface layer (Region 1) is equivalent to a few monolayers thick (i.e., $\ell_1 \simeq 10^{-7}$ cm) and is assumed to have a diffusion constant D_1 which characterizes surface diffusion away from the adsorption surface. Region 2, the bulk of the frost layer, is assumed to possess a diffusion

constant, D_2, which describes the diffusion process in the porous sorbent. Region 1 is introduced to account for the possible existence of a penetration barrier at the frost surface, and that the rate at which molecules penetrate this barrier may govern the pumping. If there were no barrier at the surface one would simply let $\ell_1 = 0$.

It is necessary to solve the diffusion equation (Equation 2) for each region, which for the general case where D is a function of n may be written:

$$\frac{\partial n_1(x,t)}{\partial t} = \frac{\partial}{\partial x}\left[D_1 \frac{\partial n_1(x,t)}{\partial x}\right] \tag{36a}$$

$$\frac{\partial n_2(x,t)}{\partial t} = \frac{\partial}{\partial x}\left[D_2 \frac{\partial n_2(x,t)}{\partial x}\right] \tag{36b}$$

where n_1 and n_2 are the number densities of sorbed molecules in Regions 1 and 2, respectively. These two equations are coupled at the interface between the two regions, at $x = 0$, by the requirements that:

$$n_1(0,t) = n_2(0,t) \tag{37a}$$

and

$$D_1 \frac{\partial n_1(0,t)}{\partial x} = D_2 \frac{\partial n_2(0,t)}{\partial x} \tag{37b}$$

that is, the number of particles at the interface and their

flux rates across the interface are conserved. It is further assumed that initially there are no sorbed molecules in the frost, thus,

$$n(x,0) = 0 \tag{38}$$

and, that the sorbed molecules do not penetrate the metallic cryosurface, or

$$\frac{\partial n_2(\ell_2,t)}{\partial x} = 0 \tag{39}$$

The general boundary condition which exists at the frost surface may be specified by equating Equations 34 and 35[15], and expressing the number of molecules on the surface in terms of an equivalent number density,

$$\ell^* \frac{\partial n_1(-\ell_1,t)}{\partial t} + D_2 \frac{\partial n_2(0,t)}{\partial x} = \frac{c[n_1(-\ell_1,t)]\ P(t)}{\sqrt{2\pi mkT_g}} - \frac{n_1(-\ell_1,t)\,\ell^*}{\tau}\ e^{-E_d[n_1(-\ell_1,t)]/kT_f} \tag{40}$$

---

[15] $n_1(-\ell_1,t)$ denotes the number density of adsorbed molecules on the surface, while $n(0,t)$ denotes the number density just inside the frost (where $x = \ell_1$ and $x = 0$ correspond to ℓ and ℓ' in Equation 35). The latter is the potential that drives diffusion in Region 2. The difference between these two is proportional to a gradient which could exist at the surface if a large penetration potential barrier exists there.

Equation 40 illustrates that in the most general case the boundary condition at the frost surface is time dependent. The possibility that the sorption pumping dynamics may be governed by the rate at which molecules are adsorbed on the frost surface is introduced through this equation.

If Equations 36a and 36b could be solved subject to the conditions specified by Equations 37 through 40, the solution would provide the distribution of sorbed molecules in the cryodeposit at any time. The flux of molecules being pumped could then be obtained from,

$$J_p = \ell^* \frac{\partial n_1(-\ell_1,t)}{\partial t} + D_2 \frac{\partial n_2(0,t)}{\partial x} \tag{41}$$

In addition, the number of molecules sorbed by the frost as a function of time could be obtained by

$$n^* = \frac{1}{\ell_1} \int_0^{\ell_1} n_1(x,t)dx + \frac{1}{\ell_2} \int_0^{\ell_2} n_2(x,t)dx \tag{42}$$

while the total number of molecules pumped is given by,

$$N_T = \int_0^t A_f J_p(t)dt \tag{43}$$

Because the dependence of: (1) the diffusion constant $D(n)$, (2) the sticking probability $c(n)$ and to some

extent, (3) the desorption energy $E_d(n)$ on n is not known, a priori, it is not possible to solve the Equations 36 through 40. Moreover, even if one knew how D, c and E_d varied with n the nonlinear nature of the boundary condition given by Equation 40 would still, in all probability prevent a solution to these equations in closed form. However, these equations may be solved in closed form for a number of simpler special cases which may be used to indicate the relative importance of adsorption, surface penetration and diffusion for various kinds of frost cryosorbents.

III. SORPTION LIMITED BY THE PENETRATION AND DIFFUSION RATE ONLY

Because the nonlinear boundary condition at the frost surface (Equation 40) prevents a closed form solution to the problem, obviously some simplification must be made here. We will first consider the case where the adsorption rate is not the limiting one. Thus, it is assumed that adsorption, desorption equilibrium is established very rapidly and after a very short time $\frac{\partial n_1(-\ell_1,t)}{\partial t}$ approaches zero. This implies that the number density of molecules on the frost surface $n_1(-\ell_1,t)$ approaches a constant, n_o, after a short time[16]. As molecules diffuse

[16] n_o is often called the surface concentration in the literature

into the cryodeposit, n_o is assumed to be maintained constant by additional molecules being adsorbed onto the surface from the gas phase. This process is sketched in part b of Figure 46, page 150. In effect, these special solutions neglect the adsorption "starting transient" shown in this figure. Since adsorption, desorption equilibrium is assumed, knowledge of $c(n)$ and $E_d(n)$ (at the surface) is no longer needed. Also, it is assumed that the diffusion constant is independent of n.

With these assumptions, solutions have been obtained where the sorption pumping is governed by;

(1) Diffusion only.

(2) Surface penetration resistance only.

(3) A combination of surface resistance and diffusion.

1. Diffusion Only

Dawbarn [13] was the first to propose that diffusion alone may govern the sorption characteristics of frosts. His ideas are quoted in Chapter II. The sorption pumping model considered here is consistent with Dawbarn's proposal. Since the possibility of a surface barrier is not considered, only Region 2 need be considered and with the above assumptions, Equation 36 simplifies to,

$$\frac{\partial n(x,t)}{\partial t} = D \frac{\partial^2 n(x,t)}{\partial x^2} \tag{44}$$

Equation 37 is not applicable and the initial condition (Equation 38) is

$$n(x,0) = 0 \tag{45}$$

For a frost of thickness, ℓ, the boundary conditions at the cryosurface ($x = \ell$) and at the surface of the frost ($x = 0$) are:

$$\frac{\partial n(\ell,t)}{\partial x} = 0 \tag{46}$$

and

$$n(0,t) = n_o \tag{47}$$

Assuming a product solution of the form $n(x,t) = X(x)T(t)$, Equation 44 is easily solved by separation of variables. The solution with these boundary conditions is already available in the diffusion literature [31] and heat conduction literature [33, page 275] and takes the form:

$$n(x,t) = n_o \left\{ 1 - \frac{4}{\pi} \sum_{n=0}^{\infty} \left[\frac{(-1)^n}{2n+1} \right] \cos\left[\frac{(2n+1)\pi(\ell-x)}{2\ell} \right] \right.$$

$$\left. \times \exp\left[- \frac{(2n+1)^2 \pi^2 Dt}{4\ell^2} \right] \right\} \tag{48}$$

The flux of molecules diffusing into the frost may be determined from Equation 41, which for this case

simplifies to:

$$J_p = D \left.\frac{\partial n(x,t)}{\partial x}\right]_{x=0}$$

Because the flux of molecules diffusing into the frost must equal the flux of molecules being removed from the gas phase, the rate at which molecules are removed from the gas phase in terms of the pumping speed is given by,

$$S = J_p \frac{kT_g}{P}$$

assuming that the gas phase obeys the perfect gas law. Thus, for diffusion limited pumping the pumping speed is given by:

$$S = \frac{2Dn_o\, kT_g}{P\ell} \sum_{n=0}^{\infty} e^{-(2n+1)^2 \pi^2 Dt/4\ell^2} \qquad (49)$$

Equation 48 together with Equation 42 may also be used to obtain an expression for mean number of molecules that may be sorbed per unit volume of sorbent. Equation 42 simplifies to:

$$n^* = \frac{1}{\ell} \int_0^{\ell} n(x,t)dx$$

Carrying out this integration results in:

$$n^* = n_o\left[1 - \frac{8}{\pi^2}\sum_{n=0}^{\infty}\frac{e^{-(2n+1)^2\pi^2 Dt/4\ell^2}}{(2n+1)^2}\right] \qquad (50)$$

The limit of Equation 50 as $t \to \infty$ shows that

$$n^*\Big]_{max} = n_o \quad \text{molecules/unit volume of frost} \qquad (51)$$

Thus, molecules will diffuse into the frost until their number density throughout the frost is uniform and equal to the number density which can be adsorbed in equilibrium on the surface. Values of n_o may be estimated from experimental equilibrium isotherm data (Chapters V and VI); hence, Equation 51 illustrates: (1) the role and importance of the isotherm data, and (2) that the dynamic pumping process will approach the equilibrium condition given by an isotherm as $t \to \infty$.

Equations 49 and 50 specify the dynamic characteristics of sorption when diffusion alone limits the process. However, they involve a factor which is not known, the diffusion constant of H_2 in various solidified gases. As was summarized at the end of Chapter II, the diffusion constant (for H_2 in frosts at temperatures below 20°K) could have values anywhere from 10^{-8} to 10^{-18} cm^2/sec. Consequently, a series of calculations of the pumping

speed and sorption capacity have been made for a wide range of values of D. They are presented in Figure 47. It is evident that the shapes of the computed theoretical curves are not consistent with the observed experimental trends shown, for example, in Figure 1, page 10, and the data given in Chapter VII. The theoretical predictions would only appear to match the experimental trends in the range where the frost is nearly saturated with the sorbate gas, that is for the longer times. This suggests that during the initial stages of pumping, molecules can diffuse into the cryodeposit at a much faster rate than they can be adsorbed, and initially the pumping is limited by some other mechanism. But, as more and more molecules are sorbed there is a decreasing concentration gradient in the frost (which is the potential that drives the diffusion process) and the process becomes diffusion-rate limited during the latter stages of pumping. Thus, it is believed that although the diffusion process suggested by Dawbarn plays a role in frost cryosorption pumping, the overall process is much more complicated and involves other mechanisms.

2. Surface Resistance Only

This case corresponds to the situation where the adsorbed molecules would not readily migrate from their adsorption site and pass into the interior of the frost. However, once the molecules reach the interior, they diffuse

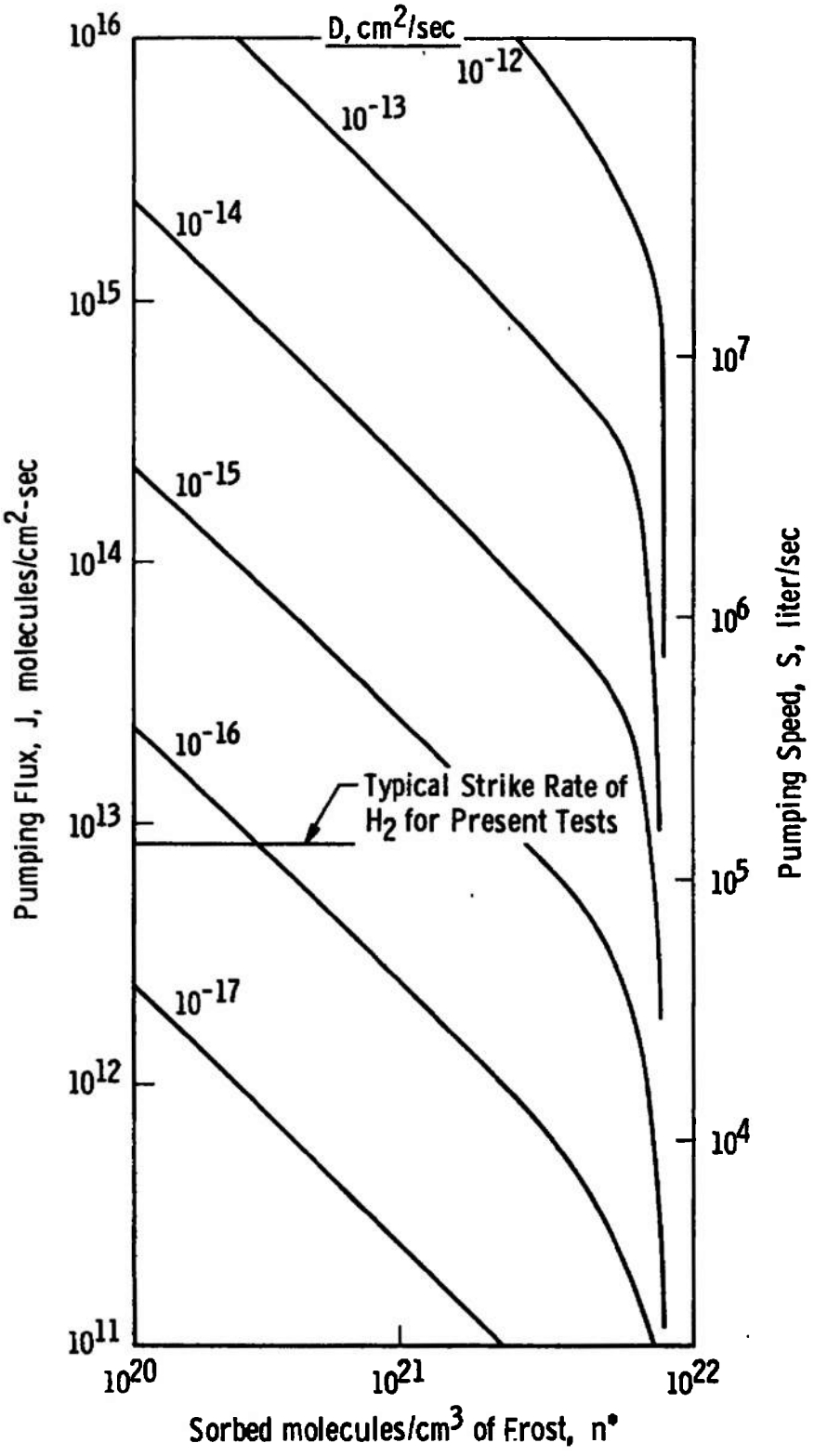

Figure 47. Theoretical Sorption Characteristics with Internal Resistance Only (Diffusion-Limited).

throughout the frost almost instantaneously. Because diffusion is not considered as significant to the pumping process no useful information is obtained from Equation 36.

The number density of sorbed molecules is independent of x and only depends on time, $n = n(t)$. In this case, Equation 41 is all that is needed, and since $\partial n/\partial x = 0$, it may be written,

$$J_p = \ell \frac{dn(t)}{dt} = G[n_o - n(t)] \tag{52}$$

with the initial condition,

$$n(0) = 0 \tag{53}$$

The term G is a mass transfer coefficient which describes how effectively adsorbed molecules are able to enter the frost. Equation 52 states that the flux of molecules across the surface is proportional to the difference in the sorbed particle number densities on the frost surface (n_o) and just inside the frost. This case corresponds to that of Newtonian heating or cooling in an analogous heat transfer problem (see [33] for details).

The solution of Equations 52 and 53 is straightforward and results in,

$$n(t) = n_o(1 - e^{-Gt/\ell}) \tag{54}$$

The flux of molecules pumped may be obtained from Equation 52 and Equation 54 as,

$$J_p = n_o G e^{-Gt/\ell} \tag{55}$$

and the number density of sorbed molecules may be obtained from Equations 43 and 55 as,

$$n_T = n_o(1 - e^{-Gt/\ell}) \tag{56}$$

Equations 55 and 56 may be combined to show that,

$$\frac{n_T}{n_o} = 1 - \frac{J_p}{n_o G} \tag{57}$$

Equation 57 then illustrates the variation of the pumping flux with the amount of gas sorbed for the case where the rate at which molecules can enter the frost is the limiting mechanism. It is shown graphically in Figure 48. Although this case exhibits trends that have been observed for some frost sorbents (compare Figure 48 to Figure 1, page 10), it cannot produce the variety of pumping speed curve shapes that have been experimentally observed. Consequently, the sorption process must be governed by more than surface resistance alone.

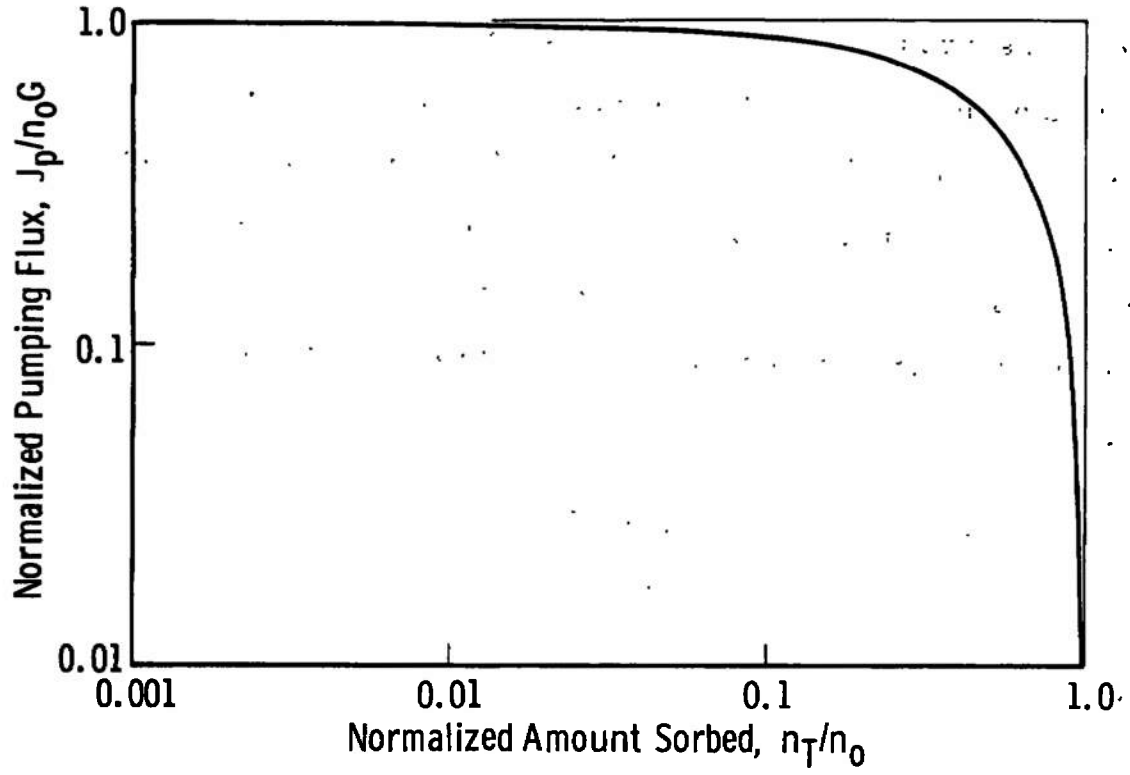

Figure 48. Theoretical Sorption Characteristics with Surface Resistance Only (Penetration-Limited).

3. Combined Surface Resistance and Diffusion

Basic derivation. A solution can also be obtained which accounts for the penetration of adsorbed molecules into the frost as well as for the subsequent diffusion through the frost. The two-layer model outlined above was originally established for this purpose. With the assumptions of the diffusion constant being independent of the amount of gas sorbed and a constant number of adsorbed molecules on the frost surface, the equations of Section II become;

$$\frac{\partial n_1(x,t)}{\partial t} = D_1 \frac{\partial^2 n_1(x,t)}{\partial x^2} \tag{58a}$$

and

$$\frac{\partial n_2(x,t)}{\partial t} = D_2 \frac{\partial^2 n_2(x,t)}{\partial x^2} \tag{58b}$$

where at the interface between the regions,

$$n_1(0,t) = n_2(0,t) \tag{59a}$$

$$D_1 \frac{\partial n_1(0,t)}{\partial x} = D_2 \frac{\partial n_2(0,t)}{\partial x} \tag{59b}$$

and the initial condition and boundary conditions are,

$$n_1(x,0) = n_2(x,0) = 0 \tag{60}$$

$$\frac{\partial n_2(\ell_2,t)}{\partial x} = 0 \tag{61}$$

$$n_1(-\ell_1,t) = n_o \tag{62}$$

Equations 58 through 62 may be solved by separation of variables and the solution which could not be found elsewhere is contained in the Appendix. It takes the form

$$n_1(x,t) - n_o = \sum_{n=1}^{\infty} A_1^{(n)} \left[\frac{\sin\lambda_1^{(n)}\ (x+\ell_1)}{\sin\lambda_1^{(n)}\ \ell_1}\right] e^{-\lambda_1^{(n)2} D_1 t} \tag{63a}$$

$$n_2(x,t) - n_o = \sum_{n=1}^{\infty} A_1^{(n)} \left[\frac{\cos\lambda_2^{(n)}\ (x-\ell_2)}{\cos\lambda_2^{(n)}\ \ell_2}\right] e^{-\lambda_2^{(n)2} D_2 t} \tag{63b}$$

where the Fourier coefficients $A_1^{(n)}$ are given by:

$$A_1^{(n)} = \frac{\left(\frac{n_o(\cos\lambda_1^{(n)}\ \ell_1 - 1)}{\lambda_1^{(n)}\ \sin\lambda_1^{(n)}\ \ell_1}\right) - \left(\frac{n_o\ \sin\lambda_2^{(n)}\ \ell_2}{\lambda_2^{(n)}\ \cos\lambda_2^{(n)}\ \ell_2}\right)}{\left(\frac{2\lambda_1^{(n)}\ \ell_1 - \sin 2\lambda_1^{(n)}\ \ell_1}{4\lambda_1^{(n)}\ \sin^2\lambda_1^{(n)}\ \ell_1}\right) + \left(\frac{2\lambda_2^{(n)}\ \ell_2 + \sin 2\lambda_2^{(n)}\ \ell_2}{4\lambda_2^{(n)}\ \cos^2\lambda_2^{(n)}\ \ell_2}\right)} \tag{64}$$

and the eigenvalues $\lambda_1^{(n)}$ and/or $\lambda_2^{(n)}$ are obtained from

$$\cot(\lambda_1^{(n)}\ \ell_1) = \frac{D_2\lambda_2^{(n)}}{D_1\lambda_1^{(n)}} \tan(\lambda_2^{(n)}\ \ell_2) \tag{65}$$

and

$$[\lambda_1^{(n)}]^2 D_1 = [\lambda_2^{(n)}]^2 D_2 \tag{66}$$

Approximation for small ℓ_1. Because $\ell_1 << \ell_2$, the number of sorbed molecules ultimately stored in Region 1 is quite small compared to the number which may be stored in the rest of the frost. Without great loss in generality, one may simplify the preceding solution for the case of an infinitesimal surface layer ℓ_1.

From Equations 65 and 66, one obtains,

$$\sqrt{\frac{D_2}{D_1}} \tan\left[\sqrt{\frac{D_2}{D_1}}\ \lambda_2^{(n)}\ \ell_1\right] = \cot(\lambda_2^{(n)}\ \ell_2) \tag{67}$$

Then, for small values of

$$\sqrt{\frac{D_2}{D_1}}\ \lambda_2^{(n)}\ \ell_1$$

which will occur for infinitesimal values of ℓ_1, the tangent of the angle is approximated by the angle, so,

$$\tan\left[\sqrt{\frac{D_2}{D_1}}\ \lambda_2^{(n)}\ \ell_1\right] \simeq \sqrt{\frac{D_2}{D_1}}\ \lambda_2^{(n)}\ \ell_1$$

and the characteristic equation becomes,

$$\ell_2\ \lambda_2^{(n)} = N_D \cot(\lambda_2^{(n)}\ \ell_2) \tag{68}$$

in which

$$N_D = \frac{(D_1/\ell_1)\,\ell_2}{D_2}$$

This parameter may be physically interpreted as the ratio of internal to surface resistance to diffusion and is analogous to the Biot modulus which is frequently encountered in heat transfer. It will be referred to here as the diffusion Biot number.

The limit of $A_1^{(n)}$ for small values of ℓ_1 may be obtained by successive application of L'Hospital's rule, and results in,

$$A_1^{(n)} = \frac{-n_o \sin[2\lambda_2^{(n)}\,\ell_2]}{\lambda_2^{(n)}\,\ell_2 + \dfrac{\sin[2\lambda_2^{(n)}\,\ell_2]}{2}} \tag{69}$$

The final approximate expression for $n_2(x,t)$ becomes,

$$\frac{n_2(x,t)}{n_o} = 1 - \sum_{n=1}^{\infty} \frac{2e^{-[\lambda_2^{(n)}\ell_2]^2\, Dt/\ell_2^2} \sin^2[\lambda_2^{(n)}\ell_2]\cos[\lambda_2^{(n)}\ell_2(1 - \frac{x}{\ell_2})]}{N_D \cos[\lambda_2^{(n)}\ell_2] + \sin^2[\lambda_2^{(n)}\,\ell_2]\cos[\lambda_2^{(n)}\ell_2]} \tag{70}$$

where the characteristic values of $\lambda_2^{(n)}$ are obtained from the roots of Equation 68. These roots have been tabulated by Carslaw and Jaeger [78]. The existence of the surface layer has not disappeared in the solution inasmuch as the ratio (D_1/ℓ_1) is still contained in Equation 68. With this simplification two quantities must be provided, D_2 and (D_1/ℓ_1). The latter ratio still represents the notion that the diffusion barrier near the surface is different from the interior of the sorbent.

Another viewpoint. Smits and Miller [79] have solved Ficks 2nd law for conditions which correspond to the diffusion of impurities in semiconductors. They considered a semi-infinite medium with a boundary condition that specified the existence of a mass transfer coefficient G, at the surface. Smith [80] and Boltaks [81] have examined this solution further and found that it agreed with experimental results. A sorption pumping model may be formulated in a similar way.

A single diffusion equation,

$$\frac{\partial n(x,t)}{\partial t} = D \frac{\partial^2 n(x,t)}{\partial x^2}$$

is solved for the conditions that,

$$n(x,0) = 0, \quad \frac{\partial n(\ell,t)}{\partial x} = 0, \quad D \frac{\partial n(0,t)}{\partial x} = G[n_o - n(0,t)]$$

The solution with this set of boundary conditions is already available ([82], page 250) and takes the form,

$$n(x,t) = n_o - n_o \sum_{n=1}^{\infty} \frac{2e^{-\lambda^{(n)2}Dt} \sin[\lambda^{(n)} \ell] \cos[\lambda^{(n)} (\ell-x)]}{\lambda^{(n)} \ell + \frac{\sin(2\lambda^{(n)} \ell)}{2}} \qquad (71)$$

where $\lambda^{(n)}$ values are obtained from the characteristic equation,

$$\lambda^{(n)} \ell = \frac{G\ell}{D} \cot[\lambda^{(n)} \ell] \qquad (72)$$

It is evident by comparing Equations 71 and 72 to Equations 70 and 68 that the "small ℓ_1" approximation of the two-layer diffusion model is equivalent to a mass transfer coefficient model, where the surface mass transfer coefficient is defined by,

$$G \equiv \frac{D_1}{\ell_1} \qquad (73)$$

Thus, the two-layer formulation and solution illustrates the physical significance of the mass-transfer coefficient, G.

From the simplified forms of Equations 41 and 42 (with $\ell_1 = 0$) expressions for the pumping flux and quantity of gas sorbed can be obtained as,

$$\frac{J_p}{n_o(D_1/\ell_1)} = 2 \sum_{n=1}^{\infty} \frac{\sin^2[\lambda_2^{(n)}\ \ell_2]\ e^{-[\lambda_2^{(n)}\ \ell_2]^2 \frac{D_2 t}{\ell_2^2}}}{N_D + \sin^2[\lambda_2^{(n)}\ \ell_2]} \tag{74}$$

$$\frac{n^*}{n_o} = 1 - 2 \sum_{n=1}^{\infty} \frac{\sin^2[\lambda_2^{(n)}\ \ell_2]\ \tan^2[\lambda_2^{(n)}\ \ell_2]\ e^{-[\lambda_2^{(n)}\ \ell_2]^2 \frac{D_2 t}{\ell_2^2}}}{N_D\left(N_D + \sin^2[\lambda_2^{(n)}\ \ell_2]\right)} \tag{75}$$

It might also be noted that the Fourier modulus

$$N_F = \frac{Dt}{\ell^2}$$

may also be employed to nondimensionalize the time.

Analytical calculations. The results of a systematic series of calculations of the sorbed particle flux (Equation 74) and the sorption capacity (Equation 75) are summarized in Figure 49. The diffusion Biot number is employed as a parameter in this presentation. Values of the diffusion Biot number less than unity correspond to the case where the forces resisting diffusion away from the sorbent surface would be greater than those resisting diffusion within the sorbent. With increasing Biot number internal diffusion dominates and the calculated dynamic

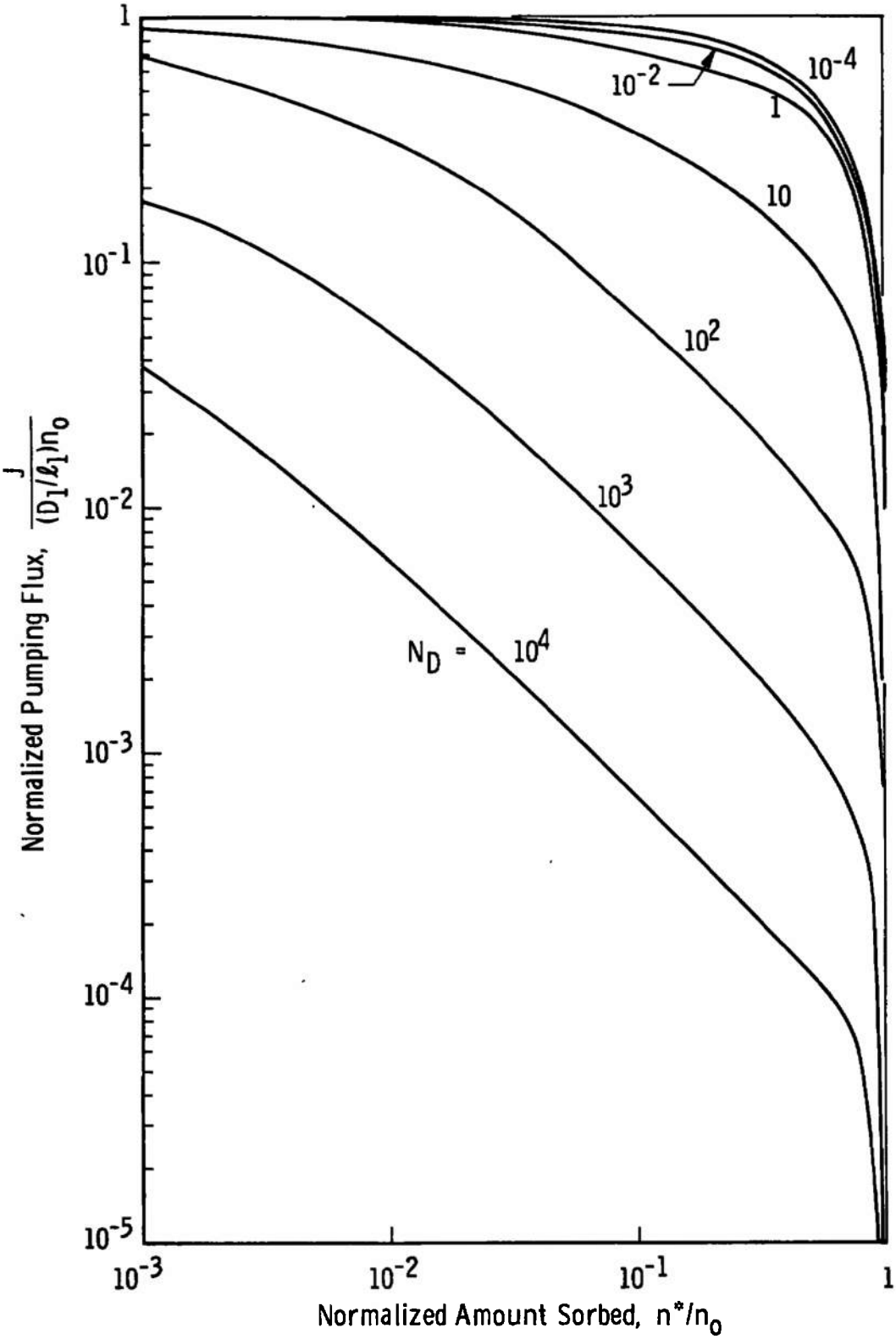

Figure 49. Theoretical Sorption Characteristics with a Combination of Surface and Internal Resistance.

pumping curves are similar to those obtained from the diffusion-limited model derived in the preceding. Also, it is observed that for $N_D << 1$, the calculated curves have the same general trend as the measured dynamic pumping curves, and approach the limit given by Equation 57 for the surface resistance limiting case. Thus, as $N_D \to \infty$ and $N_D \to 0$ this model contains as limiting cases the two simpler models obtained previously.

4. Comparison of Diffusion- and Penetration-Limited Solution with Experiment

Because the combined surface resistance and diffusion-limited approximation (Equations 74 and 75) is capable of producing a variety of theoretical sorption curve shapes, it has been compared to some of the experimental data. Measured values of the initial pumping speed and equilibrium sorption capacity may be used to determine n_o and (D_1/ℓ_1), since for short times the limit of Equation 74 is,

$$J_p = n_o (D_1/\ell_1)$$

which in terms of the initial pumping speed may be written

$$S_o = J_o \frac{kT_g}{P} = n_o \left(\frac{D_1}{\ell_1}\right) \frac{kT_g}{P}$$

While for long times, as saturation is approached, the limit of Equation 75 is,

$$n^* \Big]_{sat} = n_o$$

or, in terms of the measured equilibrium capacity,

$$n_o = \frac{C_{sat} \cdot Q_{sorbent}}{V_f \, kT_g}$$

Values of n_o and (D_1/ℓ_1) for the dynamic sorption pumping test results presented here and by Hunt, et al. [10] are summarized in Table IV. Frost densities given in Chapter IV were employed to estimate the frost thickness and volume.

The only remaining unspecified factor is the diffusion constant of the bulk solid, D_2. Because there are no known measurements for the diffusion of H_2 in cryodeposited frost (see Chapter II), Equations 74 and 75 must be solved with D_2 as an adjustable parameter. The results of such calculations should provide values of the diffusion constant which are consistent with other characteristics of the frost.

Theoretical predictions from Equations 74 and 75 are compared to experimental results for various sorbents [10] in Figure 50. The theoretical curves shown correspond to values of D_2 which appear to best fit the experimental data and to values of n_o and D_1/ℓ_1 given in Table IV. This comparison illustrates that the combined surface penetration, diffusion model is capable of reproducing the

TABLE IV

VALUES OF n_o AND D_1/ℓ_1 FOR H_2 SORBED BY VARIOUS FROSTS

Frost	P_{form} torr	T_f, °K	ℓ_f, cm	C_{sat}	n_o molecules/cm^3	J_o molecules/sec-cm^2	(D_1/ℓ_1) cm/sec
CO_2	10^{-9} to 10^{-8}	11°	2.7×10^{-6}	0.050	9.5×10^{20}	7.6×10^{13}	8.0×10^{-8}
Ar			2.5×10^{-6}	0.015	6.5×10^{20}	1.6×10^{13}	2.5×10^{-8}
N_2			5.7×10^{-6}	0.013	2.5×10^{20}	1.1×10^{13}	4.4×10^{-8}
O_2			2.8×10^{-6}	0.014	5.0×10^{20}	2.5×10^{13}	5.0×10^{-8}
H_2O			2.7×10^{-6}	0.040	8.0×10^{20}	15.2×10^{13}	1.9×10^{-8}
CO_2	2×10^{-6}	12.4°	1×10^{-4}	0.260	5.6×10^{21}	9.3×10^{13}	1.6×10^{-8}
	2×10^{-5}			0.350	7.5×10^{21}	9.3×10^{13}	1.2×10^{-8}
	2×10^{-4}			0.450	9.6×10^{21}	8.7×10^{13}	0.9×10^{-8}
	1×10^{-5}			0.480	1.0×10^{22}	8.1×10^{13}	0.8×10^{-8}
CO_2	2×10^{-5}	12.4°	1×10^{-4}	0.350	7.5×10^{21}	9.3×10^{13}	1.2×10^{-8}
		16.5°		0.180	3.8×10^{21}	7.2×10^{13}	1.9×10^{-8}
		21.5°		0.040	0.8×10^{21}	6.0×10^{13}	7.5×10^{-8}

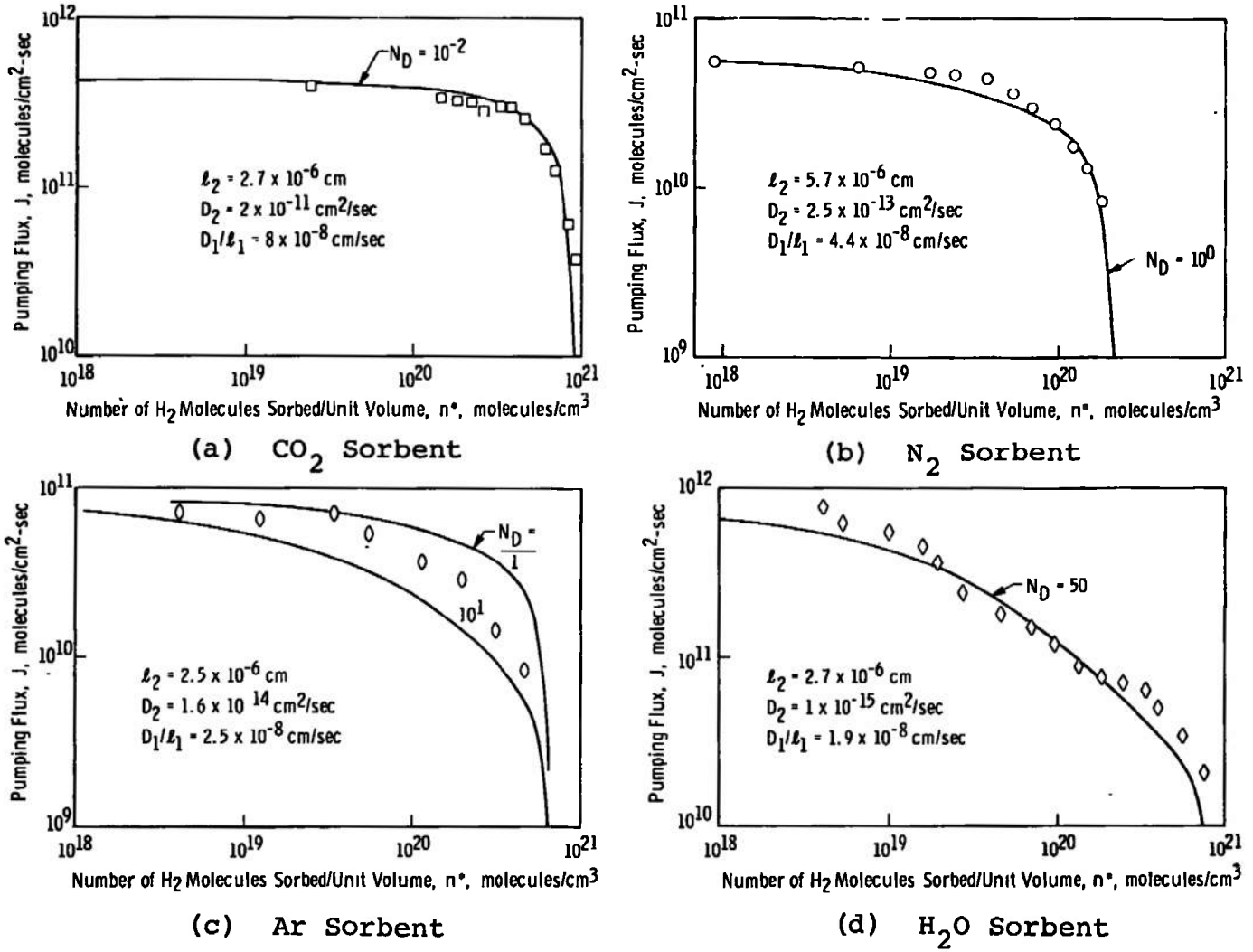

Figure 50. Comparison of the Theoretical Dynamic Sorption Pumping Curves with the Measurements of Hunt, Taylor, Omohundro.

variety of dynamic pumping speed curve shapes which have been experimentally observed by Hunt, et al. Some of the dynamic pumping speed curves for CO_2 frost from this investigation and from [10] are compared to theoretical calculations in Figure 51.

The simplified solution obtained in this section basically accounts only for diffusional processes after an adsorbed layer is formed on the frost surface. Further, the sorption characteristics of the more ordered and compact frosts are more likely to be dominated by diffusion. Consequently, this approximate solution should compare best with the experimental results obtained with the more compact or less porous frosts. The comparisons given in Figure 50, page 177 and Figure 51 indicate that this is the case. The dynamic pumping characteristics of all of the frosts investigated by Hunt, et al. [10], which were formed very slowly and were probably the most ordered or compact frost cryosorbents investigated to date, could be duplicated by the two-layer, diffusion-limited simplified model (Figure 50). Similarly, the more ordered and compact CO_2 frosts formed at low strike rates have dynamic pumping curves which can be duplicated by the simplified two-layer, diffusion-limited solution (parts a and b of Figure 51). However, CO_2 frosts formed at higher strike rates and, hence, made more porous, exhibited pumping

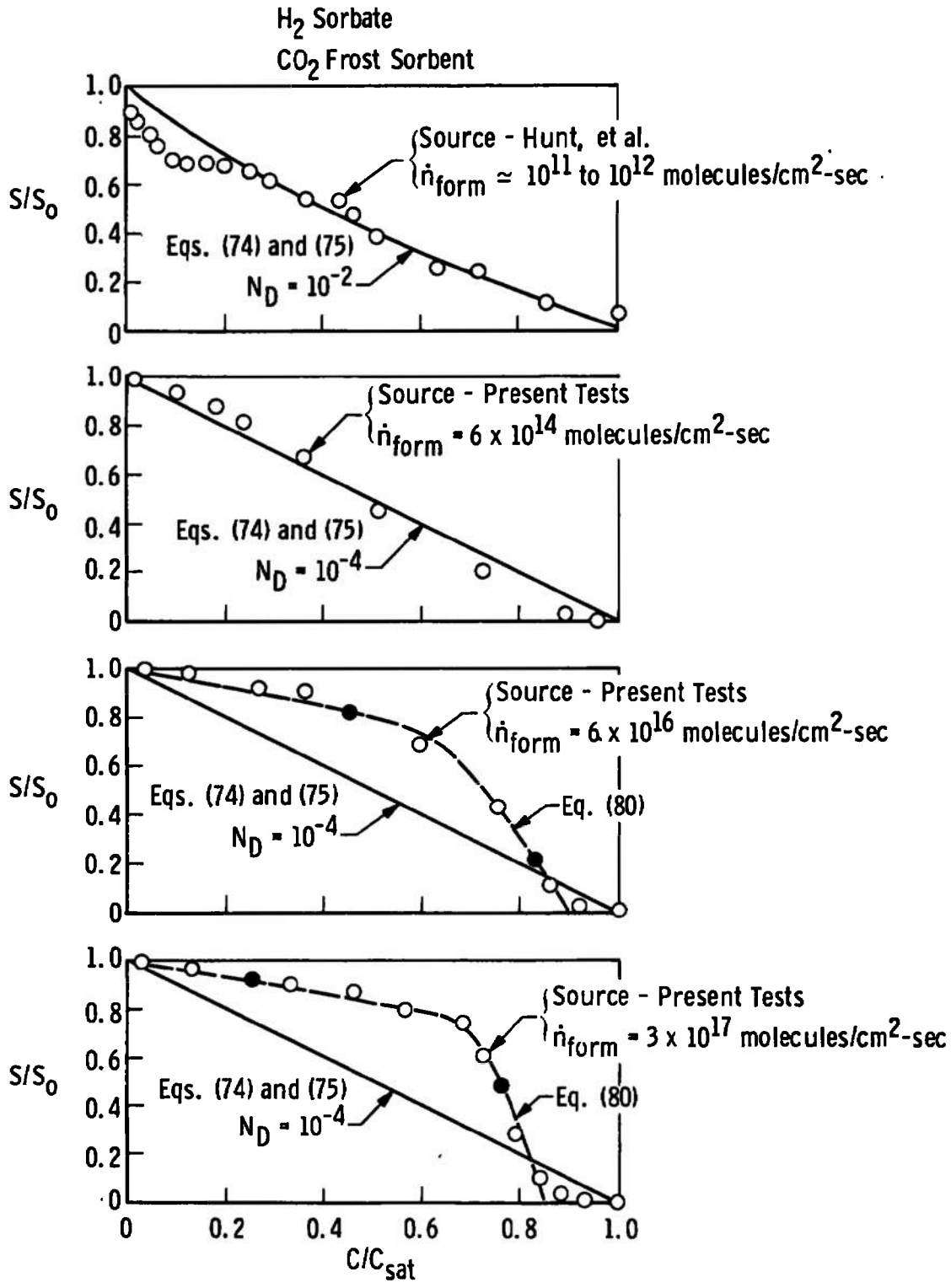

Figure 51. Comparison of Theoretical Dynamic Sorption Pumping Curves with Experimental Results for CO_2 Sorbents of Different Porosities.

speeds which decreased much more abruptly than this model could predict (parts c and d of Figure 51).

From the shape of the dynamic pumping curves (Figure 50, page 177) one would conclude that H_2O frost appears to be the most compact and has the lowest diffusion constant of the sorbents investigated to date. This is in agreement with the estimates of the frost porosity which were obtained from the refractive index measurements described in Chapter V. Estimates of the apparent diffusion constant needed to match theoretical predictions with the experiment data for the slowly formed frost sorbents are summarized in Table V. It should be emphasized that these apparent diffusion constants may only be indicative of the diffusion process in sorbent frosts formed at the conditions indicated. Also, these values should only be regarded as tentative inasmuch as they depend upon the simplifying assumptions made to solve the sorption equations.

The Lennard-Jones well-depth position distance, σ (see Figure 45, page 143) may be grossly interpreted as an index of the structural compactness of a crystalline-like frost. More compact frosts would be characterized by lower values of σ, and hence would also be expected to have lower diffusion constants. Values of σ (taken from [83]) are also given in Table V and appear to correlate with the inferred values of the diffusion constant.

TABLE V

APPARENT DIFFUSION CONSTANTS FOR H_2 IN VARIOUS FROST SPECIES

Frost Specie	Frost Formation Rate molecules/cm^2-sec	T_f °K	D_2 cm^2/sec	σ Å
H_2O	10^{11} to 10^{12}	11°	1.0×10^{-15}	2.650
Ar			1.6×10^{-14}	3.465
O_2			1.6×10^{-14}	3.541
N_2			2.5×10^{-13}	3.749
CO_2			2.0×10^{-11}	3.897
CO_2	6×10^{14}	12.4°	1.0×10^{-8}	3.897

This correlation may lend some support to at least the relative values of D for the various frost species and lead to the conjecture that the slowly formed frosts of [10] were probably polycrystalline.

One can only surmise that CO_2 frosts formed at strike rates above about 10^{15} molecules/cm^2-sec are characterized by diffusion constants for H_2 which are well above 10^{-8} cm^2/sec. It is believed that the more porous frosts have such high values of the diffusion constant that neither surface penetration or internal diffusion is the rate-limiting process. The two-layer, diffusion-limited equations would not be expected to be applicable to these very porous frosts.

IV. SORPTION LIMITED BY THE ADSORPTION RATE ONLY

Some of the frosts formed at high strike rates during this investigation sorbed at equilibrium almost one H_2 molecule for every two CO_2 molecules predeposited as the sorbent. It is reasonable to assume that such frosts would be so porous that surface penetration and internal diffusion would provide a "second-order" effect on the sorption dynamics; and, that the sorption process could be governed by the rate at which molecules are adsorbed on the frost surface. If diffusion is completely neglected, then Equations 36 through 40 reduce to only

$$\ell^* \frac{dn(t)}{dt} = \frac{c[n(t)]P(t)}{\sqrt{2\pi mkT_g}} - \frac{n(t)\ell^*}{\tau} e^{-E_d[n(t)]/kT_f} \quad (76)$$

and

$$n(0) = 0 \quad (77)$$

The solution of Equation 76 is hampered by the fact that the equation is nonlinear and that the functional forms of the sticking probability c(n) and desorption energy $E_d(n)$ are not known completely. Moreover, numerical solutions are not possible unless these functions are known. Inasmuch as dn(t)/dt and n(t) are proportional to the pumping speed and sorption capacity, respectively, Equation 76 already expresses a relationship between S and C.

Several attempts were made to simplify this equation such that it could be solved in closed form. However, none of the simplified solutions resulted in predicted pumping curves which were similar to those exhibited by very porous CO_2 frosts. These attempts illustrated that c(n) and $E_d(n)$ would have to be approximated in a realistic way, if the solutions to Equation 76 were to be meaningful.

As H_2 is being sorbed by a frost the sticking probability will decrease for the reasons noted on page 147. It appears reasonable to assume that the decrease will be linear with, n, or

$$c(n) \simeq c_o - c_1 n \tag{78}$$

This assumption is consistent with at least the initial portion of the observed dynamic pumping curves (see Figure 42, page 135, for example). With this approximation, Equation 76 may be expressed,

$$\ell^* \frac{dn(t)}{dt} = \frac{[c_o - c_1 n(t)]P}{\sqrt{2\pi mkT_g}} - \frac{n(t)\ell^*}{\tau} e^{-E_d[n(t)]/kT_f} \tag{79}$$

A sketch of the particle flow rates with the assumption of Equation 78 is given in part c of Figure 46, page 150. The initial slow decrease of the pumping speed is attributed to the decreasing sticking probability and the rapid decrease in S as saturation is approached would be due to increased desorption.

Since,

$$\frac{dn}{dt} \propto S \qquad \text{and} \qquad n \propto C$$

Equation 79 may be rewritten as

$$S \simeq S_o - A_1 C - A_2 C\, e^{-E_d(C)/kT_f} \tag{80}$$

The factor S_o represents the initial pumping speed; A_1 is proportional to the initial slope of the pumping speed capacity curve; A_2 is related to the rate at which molecules are desorbed when the sorption reaches saturation.

Although the basic form of Equation 80 resulted from an analysis of the pumping process, the values of S_o, A_1 and A_2 must be empirically determined from the test data as does $E_d(C)$.

Values of the desorption energy, E_d, were determined over a range of capacities from the equilibrium isotherms and given in Table III, page 127. They are plotted in Figure 52. The dash-line extrapolations are somewhat arbitrary but were guided by the previously published variations of the desorption energy of H_2 from cold charcoal and cold zeolites given in [29]. In any case the desorption energy would not decrease into the cross-hatched region since this would require the desorption rate to be greater than the rate at which molecules strike the surface[16] (i.e., $\dot{N}_i < \dot{N}_d$).

Using values of E_d given in Figure 52, some of the experimental data given in Figure 42, page 135, are employed to evaluate the constants S_o, A_1 and A_2. This involved determination of;

(1) The initial pumping speed (S_o).

(2) The initial slope of the pumping speed curve, A_1.

(3) Use of one additional data point on the steep portion of the curve to evaluate A_2.

---

[16] $\dot{N}_d > \dot{N}_i$ would imply the occurrence of spontaneous desorption of the previously sorbed H_2.

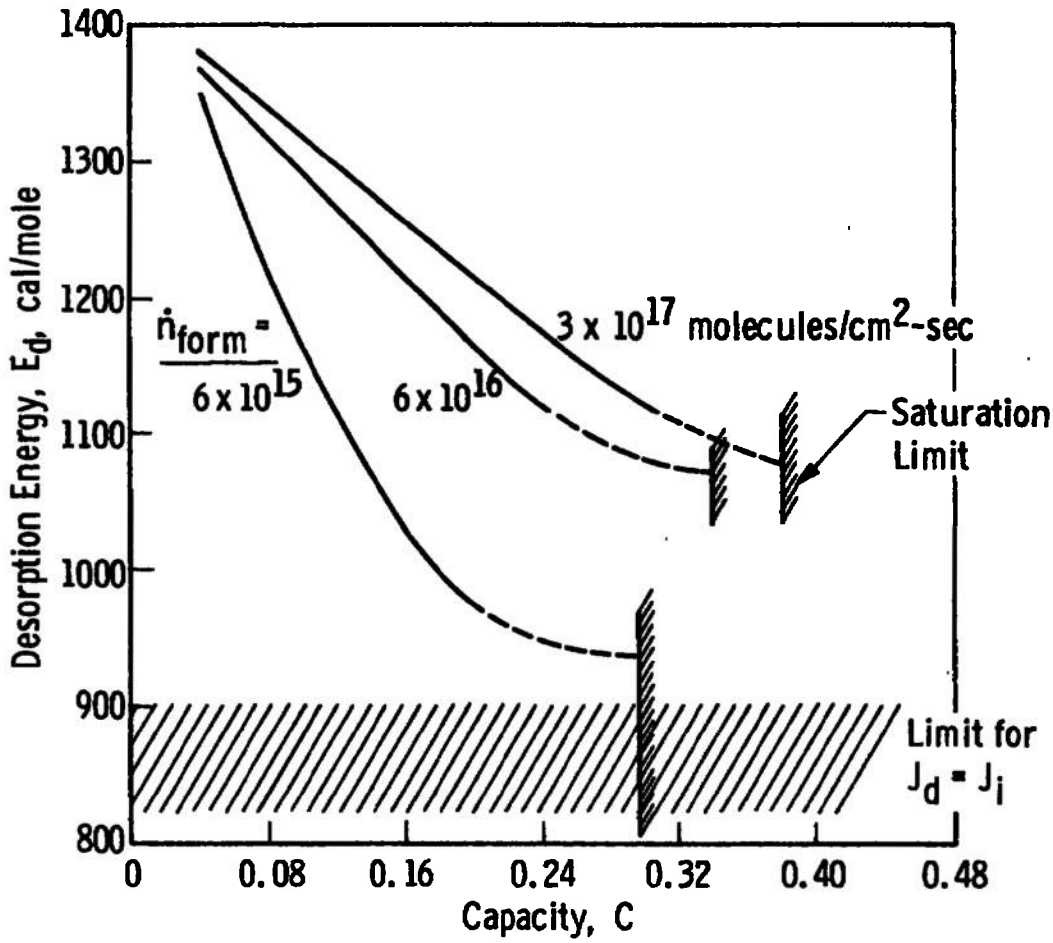

Figure 52. Estimates of Desorption Energy from the Equilibrium Isotherm Measurements.

Values of the resulting empirical constants are given in Table VI.

TABLE VI

CONSTANTS FOR EQUATION 80 FOR H_2 SORBED BY 12.4°K CO_2 FROST

$\dot{n}_{form}$ $\frac{molecules}{cm^2\text{-}sec}$	S_o $\frac{liter}{cm^2\text{-}sec}$	A_1 $\frac{liter}{cm^2\text{-}sec}$	A_2 $\frac{liter}{cm^2\text{-}sec}$
6×10^{15}	30.25	40	1.8×10^{18}
6×10^{16}	29.0	23	5.4×10^{20}
3×10^{13}	26.5	20	8.5×10^{20}

Equation 80 with values of E_d taken from Figure 52 and values of the empirical constants from Table VI is also plotted in Figure 51, page 179, for the more porous frosts. It compares quite well with the complete experimental curves, although the manner in which the constants were evaluated force it to pass through only two of the data points (shown by the solid symbols). The form of Equation 80 was suggested by the analysis; it is far from being an arbitrary polynomial fit to the data. Inasmuch as Equation 80 agrees with the form of the measured curves

reasonably well, one may have more confidence in the formulation of the general sorption theory.

V. SUMMARY

Although the complex boundary condition at the frost surface prevents a general closed-form solution to the proposed sorption theory (Equations 36 through 40), comparison of experimental results with the solutions for several special cases indicated that frost cryosorption may be controlled by the adsorption, surface penetration and diffusion. The structural characteristics of the frost determines which mechanisms are dominant.

If the frost is formed at a low rate, or at near its condensation temperature, it is less porous and diffusion appears to govern its sorption behavior. An approximate solution obtained for the special case of surface-penetration and diffusion dominated sorption (Equations 74 and 75) produced results that agreed with the experimental sorption characteristics of the more compact frosts which would be expected to be diffusion limited.

On the other hand, if the frost sorbent is formed at a rapid rate and at temperatures well below that needed to cryopump it, it is quite porous and its sorption characteristics are dominated by the rate at which molecules can be adsorbed on the surface. Another approximate, but in this case semi-empirical, solution (Equation 80) was

developed for the adsorption-limited case. This solution also agreed with the observed pumping characteristics of frosts which were believed to be very porous.

The favorable comparison between these limiting cases and the experimental data provides some confidence in the formulation of the general sorption theory. However, lack of knowledge about the reflection and desorption properties of the sorbate molecules for a wide variety of frost species and frost structures will limit even a numerical analysis of the general theory.

CHAPTER IX

CONCLUSIONS

Sorption pumping is basically a dynamical process during which the pumping speed decreases from some initial value, and approaches zero as the frost is saturated by the sorbate at some equilibrium condition. As a result of this experimental and analytical investigation of frost cryosorption pumping, it is now possible to put the various facets of this pumping process into much clearer perspective.

I. INITIAL PUMPING SPEED

It appears that the initial pumping speed (s_o) is primarily governed by the nature of the sorbent surface and the gas-surface interaction between the sorbate and the frost sorbent. An accurate prediction of s_o requires a much better understanding of the capture probability and re-evaporation characteristics of the sorbate-sorbent system than is currently available.

Although only limited data are available, a sorbent which interacts strongly with the sorbate molecules will exhibit greater initial pumping speeds. The initial pumping speed of a CO_2 sorbent for H_2 can be somewhat increased by forming the frost in a manner to give it a

smoother surface. This may be achieved by lowering the strike rate and/or increasing the temperature at which the sorbent is deposited, which apparently changes the sorbent surface, sorbate interaction phenomena.

Carbon dioxide frost sorbents which have been investigated the most extensively, have an initial pumping speed of about 30 liter/cm^2-sec; this corresponds to an effective capture probability of about 0.7. Other sorbents exhibit pumping speeds from a few liters/cm^2-sec to about 40 liter/cm^2-sec for H_2O frost. Inasmuch as the initial values of the pumping speed are relatively high, it is believed that further study of some of the other aspects of frost sorption pumping would be more beneficial avenues of any future research on frost cryosorption pumping.

II. SORPTION DYNAMICS

The dynamic sorption characteristics of frost cryosorbents are governed by one or some combination of the following factors: (1) the rate at which molecules are adsorbed on the surface, (2) the rate at which they are able to enter the interior of the frost, and (3) their diffusion rate into the frost structure.

A sorption theory has been formulated which takes these three rate-limiting mechanisms into account.

Although it was not possible to solve the equations in their most general form, special solutions were

obtained in closed form for the cases where: (1) the sorption is governed by the penetration and diffusion rates and is independent of the adsorption rate, and (2) where the sorption is governed by the adsorption rate and is independent of diffusional processes.

The penetration and diffusion limiting solution (Equations 74 and 75) agreed with the measured dynamic sorption curves for the more compact frost formed at slow rates. The adsorption rate limiting solution (Equation 80) on the other hand agreed with the experimental results obtained with the very porous frosts. Inasmuch as the solutions for these special cases agreed with the experimental results in the ranges where they should, it is believed that the more general sorption theory has been properly formulated.

Because frost sorbents (even of the same specie) have been formed at rates which span many orders of magnitude, they can have greatly different structures. As a result it is believed that the three previously mentioned rate-limiting processes influence sorption pumping but to different degrees depending upon the porosity of the frost.

The diffusion constant for the sorbate in the sorbent is an adjustable parameter in the penetration and diffusion limiting solution. Values needed to fit the experimental results for the sorption of H_2 by CO_2 frost were consistent with the rough estimates based on similar systems. Moreover

the diffusion constants varied with frost structure in the expected manner. Since diffusion constants for H_2 in solidified gases are not available elsewhere, it is suggested that the values given herein may be useful until more definitive and direct measurements can be made.

The form of the adsorption-rate limited equation (Equation 80) which is applicable to very porous frosts was inferred from analysis. However, in order to carry out numerical calculations with it, it was necessary to determine three empirical constants from the available data. This procedure provided an expression with far more physical significance than if a high-order polynomial equation was arbitrarily fit to the existing data.

III. SORPTION EQUILIBRIUM

The amount of gas which may be sorbed at equilibrium by a cryodeposited frost depends upon:

(1) The temperature at which the sorbent frost was deposited.

(2) The strike rate at which the sorbent frost was deposited.

(3) The temperature history of the frost.

These factors determine the structural characteristics of the frost and the sorption capacity of a frost is rather sensitive to its structural characteristics. This investigation has clearly illustrated that measured sorption

capacity or isotherm data are only meaningful and useful to others, if they are documented with the conditions under which the frost was formed and a description of its temperature history.

Carbon dioxide cryodeposits which were formed at temperatures much lower than their condensation temperatures and/or at higher strike rates are much more porous and disordered, and have a much greater capacity to sorb gases. In some cases CO_2 frost sorbents were produced which had sorption capacities two to three times greater than had been measured by previous investigators and a maximum of 43 H_2 molecules could be sorbed for each 100 CO_2 predeposited in the frost.

Equilibrium sorption isotherms of CO_2 frost sorbents at low pressures were found to follow the semi-empirical Dubinin-Radushkevich (D-R) isotherm equation (Equation 27). The D-R isotherm equation can be used to estimate the sorption capacity of frost sorbents formed over a wide range of conditions, if an isotherm at one temperature is known. This method was used to provide a set of isotherm design charts which summarize the H_2 sorption capacity of CO_2 frosts, and may be used to quickly estimate the H_2 sorption capacity expectations of cryodeposited CO_2.

Frost sorbents may also be re-used if the means is available to desorb them once they have been saturated. This may be accomplished by: (1) lowering the chamber

pressure by some auxiliary pump or by (2) increasing the frost temperature and then again lowering it. The latter means is by far the most effective; but, it results in a reorientation of the frost to a more ordered structure, and an attendant loss in the subsequent sorption capacity. Warming CO_2 sorbents to about 25°K and then recooling them offers about the best compromise in achieving maximum re-use capacity. When CO_2 frosts were warmed to over about 30°K an as yet unreported large-scale structural transition or phase change occurred, after which the re-use sorption capacity of the frost is drastically reduced.

BIBLIOGRAPHY

BIBLIOGRAPHY

1. Dawson, J. P., and J. D. Haygood. "Cryopumping," Cryogenics, 5:57-67, April, 1965.

2. Heald, J. H., Jr., and R. F. Brown. "Measurements of Condensation and Evaporation of Carbon Dioxide, Nitrogen and Argon at Cryogenic Temperatures Using a Molecular Beam," Arnold Engineering Development Center TR-68-110, Arnold Air Force Station, Tennessee, September, 1968.

3. Wayte, M. J., J. A. Dsida, and W. J. Sheeran. "A Study of Rocket Exhaust Plumes at High Altitudes," American Institute of Aeronautics and Astronautics Paper No. 69-575, presented at AIAA 5th Propulsion Joint Specialist Conference, US Air Force Academy, Colorado, June, 1969.

4. Haygood, J. D., D. M. Trayer, and R. F. Brown. "Review on the Vacuum Pumping of Hydrogen," Arnold Engineering Development Center TR-69-109, Arnold Air Force Station, Tennessee, December, 1969.

5. Clausing, R. E. "Large-Scale Getter Pumping Experiment Using Vapor Deposited Titanium Films," 1961 Transactions of the Eighth Vacuum Symposium. Section IX. New York: Pergamon Press, 1962. Pp. 345-356.

6. Tempelmeyer, K. E. "Sorption Pumping of Hydrogen by Cryodeposits -- Sorption Capacity Measurement," Arnold Engineering Development Center TR-69-266, Arnold Air Force Station, Tennessee, February, 1970.

7. Tempelmeyer, K. E. "Sorption Pumping of Hydrogen by Cryodeposits -- Prediction of Sorption Capacity," Arnold Engineering Development Center TR-69-270, Arnold Air Force Station, Tennessee, February, 1970.

8. Tempelmeyer, K. E. "Sorption Pumping of Hydrogen by Cryodeposits -- Dynamic Pumping Characteristics," Arnold Engineering Development Center TR-70-102, Arnold Air Force Station, Tennessee, 1970.

9. Hunt, A. L., C. E. Taylor, and J. E. Omohundro. "Rates of Hydrogen Adsorption on Solidified Gas Films," Lawrence Radiation Laboratory Report No. 6679, University of California, Berkeley; November, 1961.

10. Hunt, A. L., C. E. Taylor, and J. E. Omohundro. "Adsorption of Hydrogen on Solidified-Gas Films," Advances in Cryogenic Engineering. Vol. 8. New York: Plenum Press, 1963. Pp. 100-109.

11. Southerlan, R. E. "10 - 22°K Cryosorption of Helium on Molecular Sieve 5A and Hydrogen on Condensed Vapors," Arnold Engineering Development Center TR-65-18, Arnold Air Force Station, May, 1965.

12. Busol, F. E., and V. B. Yuferov. "New Method of Pumping Hydrogen," Soviet Physics - Technical Physics, 11:125-127, July, 1966.

13. Dawbarn, Ronald. "Cryosorption of Hydrogen by 12 - 20°K Carbon Dioxide Cryodeposits," Arnold Engineering Development Center TR-67-125, Arnold Air Force Station, Tennessee, July, 1967.

14. Yuferov, V. B., and F. E. Busol. "Sorption of Hydrogen and Neon by Layers of Solids Formed by Vapor Condensation," Soviet Physics - Technical Physics, 11:1518-1524, May, 1967.

15. Müller, E. "Adsorption Isotherms on Solid Carbon Dioxide," Cryogenics, 6:242-243, August, 1966.

16. Haygood, J. D., and Ronald Dawbarn. "Helium Pumping by 4.2°K Cryodeposits," Arnold Engineering Development Center TR-66-204, Arnold Air Force Station, Tennessee, January, 1967.

17. Dawbarn, Ronald, and J. D. Haygood. "Development and Evaluation of a Cryodeposit Sorption Pump Capable of Pumping Helium," Arnold Engineering Development Center TR-68-90, Arnold Air Force Station, Tennessee, September, 1968.

18. Yuferov, V. B., V. A. Kovalenko, and P. M. Kobzev. "Helium Sorption by Layers of Condensed Gases," Soviet Physics - Technical Physics, 12:1265-1266, March, 1968.

19. Keesom, W. H., and G. Schmitt. "Measurements on the Adsorption of Helium on Glass at Liquid Helium Temperatures," K. Akademie van Wetwschappen, 36:832-835, Leiden, Holland, 1933.

20. Brackmann, R. T., and W. L. Fite. "Condensation of Atomic and Molecular Hydrogen at Low Temperatures," Journal of Chemical Physics, 34:1572-1579, May, 1961.

21. Gareis, P. J., and J. R. Pitler. "Development and Application of Cryosorption Pumping of Hydrogen at 20°K by Molecular Sieve Adsorbent Panels," Arnold Engineering Development Center TR-65-18, Arnold Air Force Station, Tennessee, January, 1965.

22. Lunev, V. M., and A. A. Romanov. "Adsorption Properties of Type A Zeolites at Liquid-Nitrogen Temperatures," Soviet Physics - Technical Physics, 10:1287-1291, March, 1966.

23. Southerlan, R. E. "Developmental Evaluation of Near 17°K Molecular Sieve 5A for Hydrogen Cryosorption," Arnold Engineering Development Center TR-65-48, Arnold Air Force Station, Tennessee, April, 1965.

24. Stern, S. A., et al. "Cryosorption Pumping of Hydrogen and Helium at 20°K," Journal of the American Vacuum Society, 2:165-177, January/February, 1965.

25. Hengevoss, J., and E. A. Trendelenberg. "Continuous Cryotrapping of Hydrogen and Helium by Argon at 4.2°K," Transactions of the Tenth National Vacuum Symposium. Section III, New York: The MacMillan Co., 1963. Pp. 101-104.

26. Hemstreet, R. A., et al. "Research Study of the Cryotrapping of Helium and Hydrogen During 20°K Condensation of Gases Phases I and II," Arnold Engineering Development Center TDR-63-127, Arnold Air Force Station, Tennessee, May, 1963.

27. Dushman, Saul, and J. M. Lafferty. (editors). Scientific Foundations of Vacuum Technique. Second Edition. New York: John Wiley and Sons, Inc., 1962.

28. Adamson, Arthur W. Physical Chemistry of Surfaces. Second Edition. New York: Interscience Publishers, 1967.

29. Brunauer, Stephen. The Adsorption of Gases and Vapors. Vol. I. - Physical Adsorption. New Jersey: Princeton University Press, 1963.

30. McBain, James W. "Der Mechanisms der Adsorption ('Sorption') von Wasserstoff durch Kohlenstoff," Zeitschrift f. Physik. Chemie, 68:471, September, 1909.

31. Barrer, R. M. Diffusion in and through Solids. Cambridge, England: Cambridge University Press, 1941.

32. Jost, W. Diffusion in Solids, Liquids, Gases. New York: Academic Press, Inc., Publishers, 1952.

33. Arpaci, Vedat S. Conduction Heat Transfer. Reading, Massachusetts, Addison-Wesley Co., 1966.

34. Ash, R., R. M. Barrer, and C. G. Pope. "Flow of Adsorbable Gases and Vapors in a Microporous Medium" I - Single Sorbates, Proceedings of the Royal Society of London, 271(Series A):1-18, January, 1963.

35. Boato, G. "The Solidified Inert Gases," Cryogenics, 4:65-75, April, 1964.

36. Onsager, Lars, and L. K. Runnels. "Diffusion and Relaxation Phenomena in Ice," The Journal of Chemical Physics, 50:1089-1103, February, 1969.

37. Cremer, E. "Bestimmung der Selbstdiffusion in festem Wasserstoft aus dem Reaktionsverlauf der Ortho-Para-Umwandlung," Zeit. J. Physik Chem, 39B-445-464, September, 1938.

38. Müller, Peter Roland. "Measurements of Refractive Index, Density and Reflected Light Distributions for Carbon Dioxide and Water Cryodeposits and Also Roughened Glass Surfaces." Ph.D. dissertation, The University of Tennessee, Knoxville, June, 1969.

39. Rogers, K. W. "Experimental Investigation of Solid Nitrogen Formed by Cryopumping," NASA Report CR-553, Washington, D. C., August, 1966.

40. Stewart, J. W. "The Properties of Solidified Gases at High Pressure," Physics of High Pressures and the Condensed Phase, A. van Itterbeck, editor. New York: John Wiley and Sons, Inc., 1965. Chapter 5.

41. Hodgman, Charles D., Robert C. Weast, and Samuel M. Selby. Handbook of Chemistry and Physics. 39th Edition, Chemical Rubber Publishing Co., Cleveland, Ohio, 1958.

42. Young, D. M., and A. D. Crowell. Physical Adsorption of Gases. London: Butterworth, 1962.

43. Wyckoff, Ralph W. G. Crystal Structures. Vol. I. New York: Interscience Publishers, 1963.

44. Coucoulos, A., and E. Gregory. "Some Observations on the Microstructure and Fragmentation of Solid Carbon Dioxide," Transactions of the Metallurgical Society of AIME, 227:1134, October, 1963.

45. Graf, Rene, and Jacques Paulon. "Etude Radiocristallographique de la Structure d'un Cryodepôt de CO_2," Office National d'Etudes et de Recherches Aerospatiales TP No. 589, Chatillon, France, 1968.

46. Yuferov, V. B., R. F. Bulatova, P. M. Kobzev, and V. S. Kosan. "Study of the Mechanism for Hydrogen Sorption by Condensed Layers of CO_2," Soviet Physics - Technical Physics, 13:238-241, August, 1969.

47. Hengevoss, J. "Influence of the Temperature History of Condensed Argon on its Hydrogen Adsorptivity at Low Temperatures," The Journal of Vacuum Science and Technology, 6:58-61, January, 1969.

48. Colwell, J. H., E. K. Gill, and J. A. Morrison. Thermodynamic Properties of CH_4 and CD_4. Interpretation of the Properties of the Solids," The Journal of Chemical Physics, 39:635-653, August, 1965.

49. Stewart, J. W. "Phase Transitions and Compressions of Solid CH_4, CD_4 and O_2," Journal of Physics and Chemistry of Solids, 12:122-129, January, 1960.

50. Müller, P. R., B. A. Seiber, A. M. Smith, and B. E. Wood. "Refractive Indices and Density of CO_2 and H_2O Cryodeposits," To be published in the Journal of Applied Optics.

51. Kruger, J., and W. J. Ambs. "Optical Measurements on Thin Films of Condensed Gases at Low Temperature," Journal of the Optical Society of America, 49:1195-1198, December, 1959.

52. de Boer, J. H. The Dynamical Character of Adsorption. Second Edition. Oxford at the Clarendon Press, 1968.

53. Dubinin, M. M., B. P. Bering, and V. V. Serpenski. "Physical Adsorption at the Gas-Solid Interface," Recent Progress in Surface Science, J. F. Danielle, et al., editors. Vol. 2. New York: Academic Press, 1964.

54. Deitz, Victor R. "Gas Adsorption - The Extreme Limits of Surface Coverage," Interface Symposium-9, 57:49-66, May, 1965.

55. Hobson, J. P. "Physical Adsorption at Extremely Low Pressure," The Solid-Gas Interface, E. A. Flood, editor. New York: Marcel Dekker, Inc., Chapter 14.

56. Canjor, Lawrence N., and John A. Kostecke. (editor). Physical Adsorption Processes and Principles. Vol. 63. Chemical Engineering Progress Series, American Institute of Chemical Engineers, 1967.

57. Shupe, Dean S. "Theoretical Analysis of the Effect of Surface Processes on the Permeation of Gases through Metals." Ph.D. dissertation, Massachusetts Institute of Technology, Cambridge, 1969.

58. Danner, Ronald Paul. "The Adsorption of Binary Gas Mixtures on Molecular Sieves," Ph.D. dissertation, Lehigh University, Bethlehem, Pennsylvania, 1966.

59. Schmidlin, F. W., L. O. Heflinger, and E. L. Gorwin. "Some Investigations of Cryotrapping," Transactions of the Ninth National Vacuum Symposium of the American Vacuum Society. New York: The MacMillan Co., 1962. Pp. 197-211.

60. Haygood, J. D. "Steady-State Sorption of Gases during Vapor Deposition," Journal of Physical Chemistry, 67:2061-2064, October, 1963.

61. Barrer, R. M. "Surface and Volume Flow in Porous Media," The Gas-Surface Interaction. Vol. 2. New York: Marcel Dekker, Inc., 1967. Chapter 19.

62. Linson, B. G., and A. van den Heuvel. "Pore Structures," The Gas-Surface Interaction. Vol. 2. New York: Marcel Dekker, Inc., 1967. Chapter 35.

63. de Boer, J. H. "The Shape of Capillaries," Structure and Properties of Porous Materials. New York: Academic Press, Inc., Pp. 68-94.

64. Dubinin, M. M. "The Potential Theory of Adsorption of Gases and Vapors for Adsorbents with Energetically Nonuniform Surfaces," Chemical Reviews, 60:235-241, 1960.

65. Veguilla-Berdecia, L. A. "Some Theoretical Aspects of Cryosorption," NASA TMX-55168, Washington, D. C., 1964. Pp. B7-B20.

66. Hobson, J. P. "A New Method for Finding Heterogeneous Energy Distributions from Physical Adsorption Isotherms," Canadian Journal of Physics, 43:1934-1940, November, 1965.

67. Ross, Sydney, and James P. Olivier. On Physical Adsorption. New York: Interscience Publishers, 1964.

68. Hobson, J. P. "Analysis of Physical Adsorption Isotherms on Heterogeneous Surfaces at Very Low Pressures," Canadian Journal of Physics, 43:1941-1950, November, 1965.

69. Hobson, J. P. "Theoretical Isotherms for Physical Adsorption at Pressures Below 10^{-10} Torr," The Journal of Vacuum Science and Technology, 3:281-284, September/October, 1966.

70. Stickney, R. E. "A Discussion of Energy and Momentum Transfer in Gas-Surface Interactions," Arnold Engineering Development Center TR-66-13, Arnold Air Force Station, Tennessee, February, 1966.

71. Hurlbut, F. C. "Current Developments in the Study of Gas-Surface Interactions," Proceedings of the Fifth International Symposium on Rarefied Gas Dynamics, C. L. Brundin, editor. Vol. 1. New York: Academic Press, 1967. Pp. 1-34.

72. Stickney, Robert E. "Atomic and Molecular Scattering from Solid Surfaces," Advances in Atomic and Molecular Physics, D. R. Bates and Immanuel Estermann, editors. Vol. 3. New York: Academic Press, 1967. Pp. 143-201.

73. Goodman, F. O. "Preliminary Results of a Three-Dimensional Hard-Spheres Theory of Scattering of Gas Atoms from a Solid Surface," Proceedings of the Fifth International Symposium on Rarefied Gas Dynamics, C. L. Brundin, editor. Vol. 1. New York: Academic Press, 1967. Pp. 35-48.

74. Ricca, F. "Potential-Energy Profiles in Physisorption on f.c.c. Crystals," Supplemento al Nuovo Cimento, 5:339-353, February, 1967.

75. Hengevoss, J. "Gas Sorption by Surfaces Cooled to Low Temperatures," 1965 Transactions of the Third International Vacuum Congress, H. Adam, editor. Vol. 1. New York: Pergamon Press, 1966. Pp. 51-63.

76. Hobson, J. P., and P. A. Redhead. "Physical Processes in Vacuum," Proceedings of the Fourth International Vacuum Congress, Part One. London: Adlard and Son, Ltd., 1968. Pp. 3-20.

77. Frenkel, J. "Adsorption," Z. Physik, 26:117-138, 1924.

78. Carslaw, H. W., and J. C. Jaeger. Conduction of Heat in Solids. Second Edition. Oxford at the Clarendon Press, 1959.

79. Smits, F. M., and R. C. Miller. "Rate Limitation at the Surface for Impurity Diffusion in Semiconductors," Physical Review, 104:1242-1245, December, 1956.

80. Smith, A. M. "Diffusion," Fundamentals of Silicon Integrated Device Technology. Section II. Vol. 1. London: Prentice-Hall International, 1967.

81. Boltaks, B. I. Diffusion in Semiconductors. (Translation), New York: Academic Press, 1963. Chapter VI.

82. Schneider, P. J. Conduction Heat Transfer. Reading, Massachusetts: Addison-Wesley Publishing Co., Inc., 1957.

83. Herschfelder, Joseph O., Charles F. Curtiss, and R. Byron Bird. Molecular Theory of Gases and Liquids. New York: John Wiley and Sons, Inc., 1954.

APPENDIX

APPENDIX

DERIVATION FOR THE TWO-LAYER MODEL

In the solution of Equations 58 through 62, it is convenient to let

$$n' = n - n_o$$

in order to make the boundary conditions homogeneous. The form of Equations 58a and 58b is unchanged by this transformation; n is just replaced by n', while Equations 59 through 62 become

$$n_1'(0,t) = n_2'(0,t) \tag{A-1}$$

$$D_1 \frac{\partial n_1'(0,t)}{\partial x} = D_2 \frac{\partial n_2'(0,t)}{\partial x} \tag{A-2}$$

$$n_1'(-\ell_1,t) = 0 \tag{A-3}$$

$$\frac{\partial n_2'(\ell_2,t)}{\partial x} = 0 \tag{A-4}$$

$$n_1'(x,0) = n_2'(x,0) = - n_o \tag{A-5}$$

Equation 58 may be solved by separation of variables assuming a product solution of the form,

$$n' = T(t)X(x) \tag{A-6}$$

which has the well-known general solutions,

$$n_1'(x,t) = e^{-\lambda_1^2 D_1 t} (A_1 \cos\lambda_1 x + B_1 \sin\lambda_1 x) \tag{A-7}$$

$$n_2'(x,t) = e^{-\lambda_2^2 D_2 t} (A_2 \cos\lambda_2 x + B_2 \sin\lambda_2 x) \tag{A-8}$$

Substituting Equations A-7 and A-8 into the boundary conditions (Equations A-1 through A-4) leads to the following relationship between the constants of Equations A-7 and A-8,

$$B_1 = A_1 \cot\lambda_1 \ell_1 \tag{A-9}$$

$$B_2 = A_2 \tan\lambda_2 \ell_2 \tag{A-10}$$

$$A_1 = A_2 \frac{e^{-\lambda_2^2 D_2 t}}{e^{-\lambda_1^2 D_1 t}} \tag{A-11}$$

$$B_1 = B_2 \frac{(D_2\lambda_2) e^{-\lambda_2^2 D_2 t}}{(D_1\lambda_1) e^{-\lambda_1^2 D_1 t}} \tag{A-12}$$

which may be combined to obtain the characteristic equation,

$$\cot(\lambda_1^{(n)} \ell_1) = \frac{D_2 \lambda_2^{(n)}}{D_1 \lambda_1^{(n)}} \tan(\lambda_2^{(n)} \ell_2) \tag{A-13}$$

Because the equations are coupled at x = 0, the characteristic values, $\lambda_1^{(n)}$, are not independent of the values $\lambda_2^{(n)}$. This may be seen from Equations A-11 and A-12 which require that either,

$$A_1 = A_2 = B_1 = B_2 = 0 \tag{A-14}$$

or

$$\frac{d}{dt}\left[e^{-(\lambda_2^2 D_2 - \lambda_1^2 D_1)t}\right] = 0 \tag{A-15}$$

The physical significance of Equation A-14 corresponds to the frost being saturated ($n = n_o$ = constant) which is the almost trivial equilibrium case. Thus, in general, the second condition (Equation A-15) must hold which leads to the fact that

$$\lambda_1^2 D_1 = \lambda_2^2 D_2 \tag{A-16}$$

Then combining Equations A-13 and A-16 results in the characteristic equation,

$$\cot\left[\sqrt{\frac{D_2}{D_1}}\,\lambda_2^{(n)}\ell_1\right] = \sqrt{\frac{D_2}{D_1}}\,\tan(\lambda_2^{(n)}\ell_2) \tag{A-17}$$

The roots of Equation A-17 yield one set of characteristic values, $\lambda_2^{(n)}$, although it could equivalently be written in terms of $\lambda_1^{(n)}$.

Inserting Equations A-9 and A-10 into Equations A-7 and A-8 and writing the result in terms of the characteristic values gives,

$$n_1'(x,t) = A_1^{(n)} \, e^{-\lambda_1^{(n)2} D_1 t} \, \{\cos[\lambda_1^{(n)} x] + \cot[\lambda_1^{(n)} \ell_1] \sin[\lambda_1^{(n)} x]\} \tag{A-18}$$

$$n_2'(x,t) = A_2^{(n)} \, e^{-\lambda_2^{(n)2} D_2 t} \, \{\cos[\lambda_2^{(n)} x] + \tan[\lambda_2^{(n)} \ell_2] \sin[\lambda_2^{(n)} x]\} \tag{A-19}$$

Since $[\lambda_1^{(n)}]^2 D_1 = [\lambda_2^{(n)}]^2 D_2$, it is seen from Equation A-11 that $A_1^{(n)} = A_2^{(n)}$. Using this fact and some simple trigonometric relationships allows Equations A-18 and A-19 to be rewritten as,

$$n_1'(x,t) = \sum_{n=1}^{\infty} A_1^{(n)} \left\{\frac{\sin\lambda_1^{(n)} (x+\ell_1)}{\sin[\lambda_1^{(n)} \ell_1]}\right\} e^{-\lambda_1^{(n)2} D_1 t} \tag{A-20}$$

$$n_2'(x,t) = \sum_{n=1}^{\infty} A_1^{(n)} \left\{\frac{\cos\lambda_2^{(n)} (x-\ell_2)}{\cos[\lambda_2^{(n)} \ell_2]}\right\} e^{-\lambda_2^{(n)2} D_2 t} \tag{A-21}$$

The values of $A_1^{(n)}$ which correspond to the characteristic values of $\lambda_1^{(n)}$ and $\lambda_2^{(n)}$ may be obtained as Fourier

coefficients by application of the initial condition (Equation A-5), if the bracketed functions in Equations A-20 and A-21 are orthognal.

I. PROOF OF ORTHOGONALITY

When the initial condition is applied to Equations A-20 and A-21, they become,

$$- n_o = \sum_{n=1}^{\infty} A_1^{(n)} \psi^{(n)}(x) \qquad \text{(A-22)}$$

where

$$\psi_1^{(n)}(x) = \frac{\sin\lambda_1^{(n)} (x+\ell_1)}{\sin\lambda_1^{(n)} \ell_1} \quad \text{for } -\ell_1 \leq x \leq 0 \qquad \text{(A-23)}$$

$$\psi_2^{(n)}(x) = \frac{\cos\lambda_2^{(n)} (x-\ell_2)}{\cos\lambda_2^{(n)} \ell_2} \quad \text{for } 0 \leq x \leq \ell_2 \qquad \text{(A-24)}$$

To determine the values of $A_1^{(n)}$ each region, Equation A-22 may be multiplied by a corresponding function $\psi^{(m)}(x)$ and integrated over the intervals $-\ell_1$ to 0 and 0 to ℓ_2 for each region. Performing these operations results in

$$- n_o \int_{-\ell_1}^{0} \psi_1^{(m)}(x)dx - n_o \int_{0}^{\ell_2} \psi_2^{(m)}(x)dx =$$

$$= \sum_{n=1}^{\infty} A_1^{(n)} \left[\int_{-\ell_1}^{0} \psi_1^{(m)}(x)\ \psi_1^{(n)}(x)dx + \int_{0}^{\ell_2} \psi_2^{(m)}(x)\cdot \psi_2^{(n)}(x)dx \right] \tag{A-25}$$

If the functions $\psi^{(m)}(x)$ and $\psi^{(n)}(x)$ are orthognal then, $\psi^{(m)}(x) = \psi^{(n)}(x)$ for m = n, and

$$\int \psi^{(m)}(x)\ \psi^{(n)}(x)dx = 0$$

for all values of $m \neq n$ and all of the integral terms in the summation on the right hand side of Equation A-25 vanish except the term for m = n. Thus, Equation A-25 simplifies to:

$$-n_o \int_{-\ell_1}^{0} \psi_1^{(n)}(x)dx - n_o \int_{0}^{\ell_2} \psi_2^{(n)}(x)dx$$

$$= A_1^{(n)} \left[\int_{-\ell_1}^{0} [\psi_1^{(n)}(x)]^2 dx + \int_{0}^{\ell_2} [\psi_2^{(n)}(x)]^2 dx \right] \tag{A-26}$$

Inserting Equations A-23 and A-24 into Equation A-26 and carrying out the integrations, results in an expression for $A_1^{(n)}$

$$A_1^{(n)} = \frac{\left\{\frac{n_o[\cos\lambda_1^{(n)}\ell_1 - 1]}{\lambda_1^{(n)}\sin\lambda_1^{(n)}\ell_1}\right\} - \left\{\frac{n_o[\sin\lambda_2^{(n)}\ell_2]}{\lambda_2^{(n)}\cos\lambda_2^{(n)}\ell_2}\right\}}{\left\{\frac{2\lambda_1^{(n)}\ell_1 - \sin 2\lambda_1^{(n)}\ell_1}{4\lambda_1^{(n)}\sin^2\lambda_1^{(n)}\ell_1}\right\} + \left\{\frac{2\lambda_2^{(n)}\ell_2 + \sin 2\lambda_2^{(n)}\ell_2}{4\lambda_2^{(n)}\cos^2\lambda_2^{(n)}\ell_2}\right\}} \tag{A-27}$$

It is yet necessary to prove that:

$$\int_{-\ell_1}^{\ell_2} \psi^{(n)}(x)\ \psi^{(m)}(x)dx = 0 \tag{A-28}$$

This may be rewritten for each region as,

$$\Psi(x) = \int_{-\ell_1}^{\ell_2} \psi^{(n)}(x)\ \psi^{(m)}(x)dx$$

$$= \int_{-\ell_1}^{0} \frac{\sin[\lambda_1^{(n)}(x+\ell_1)]\ \sin[\lambda_1^{(m)}(x+\ell_1)]}{\sin[\lambda_1^{(n)}\ell_1]\ \sin[\lambda_1^{(m)}\ell_1]}\,dx$$

$$+ \int_{0}^{\ell_2} \frac{\cos[\lambda_2^{(n)}(x-\ell_2)]\ \cos[\lambda_2^{(m)}(x-\ell_2)]}{\cos[\lambda_2^{(n)}\ell_2]\ \cos[\lambda_2^{(m)}\ell_2]}\,dx \tag{A-29}$$

Performing the integrations on the right hand side results in:

$$\Psi(x) = \frac{1}{\sin[\lambda_1^{(n)} \ell_1] \sin[\lambda_1^{(m)} \ell_1]} \left[\frac{\sin\{[\lambda_1^{(n)} - \lambda_1^{(m)}] \ell_1\}}{2[\lambda_1^{(n)} - \lambda_1^{(m)}]} - \frac{\sin\{[\lambda_1^{(n)} + \lambda_1^{(m)}] \ell_1\}}{2[\lambda_1^{(n)} + \lambda_1^{(m)}]} \right] + \frac{1}{\cos[\lambda_2^{(n)} \ell_2] \cos[\lambda_2^{(m)} \ell_2]}$$

$$\times \left[\frac{\sin\{[\lambda_2^{(n)} - \lambda_2^{(m)}] \ell_2\}}{2[\lambda_2^{(n)} - \lambda_2^{(m)}]} + \frac{\sin\{[\lambda_2^{(n)} + \lambda_2^{(m)}] \ell_2\}}{2[\lambda_2^{(n)} + \lambda_2^{(m)}]} \right] \quad \text{(A-30)}$$

Recalling Equations A-13 and A-16 which may be combined to give,

$$\tan(\lambda_2 \ell_2) = \frac{\lambda_2}{\lambda_1} \cot(\lambda_1 \ell_1) \quad \text{(A-31)}$$

and, using formulae for the trigonometric functions of the sums and differences of angles, allows Equation A-30 to be rewritten and simplified to

$$\Psi(x) = \left[\frac{1}{\lambda_1^{(n)} - \lambda_1^{(m)}} - \frac{\lambda_2^{(m)}/\lambda_1^{(m)}}{\lambda_2^{(n)} - \lambda_2^{(m)}} + \frac{\lambda_2^{(m)}/\lambda_1^{(m)}}{\lambda_2^{(n)} + \lambda_2^{(m)}} - \frac{1}{\lambda_1^{(n)} + \lambda_1^{(m)}} \right] \frac{\cot[\lambda_1^{(m)} \ell_1]}{2} + \left[\frac{\lambda_2^{(n)}/\lambda_1^{(n)}}{\lambda_2^{(n)} - \lambda_2^{(m)}} - \frac{1}{\lambda_1^{(n)} - \lambda_1^{(m)}} + \frac{\lambda_2^{(n)}/\lambda_1^{(n)}}{\lambda_2^{(n)} + \lambda_2^{(m)}} - \frac{1}{\lambda_1^{(n)} + \lambda_1^{(m)}} \right] \frac{\cot\lambda_1^{(n)} \ell_1}{2} \quad \text{(A-32)}$$

Now, if the bracketed terms of Equation A-32 are equal to zero, then $\Psi(x) = 0$. When the first of these (i.e., the coefficient of cot $\lambda_1^{(m)} \ell_1$) is rewritten with a common denominator, expanded and simplified, there results,

$$\left[\frac{[\lambda_1^{(m)}]^2 [\lambda_2^{(n)}]^2 - [\lambda_1^{(n)}]^2 [\lambda_2^{(m)}]^2}{[\lambda_1^{(n)} - \lambda_1^{(m)}] [\lambda_2^{(n)} - \lambda_2^{(m)}] [\lambda_2^{(n)} + \lambda_2^{(m)}] [\lambda_1^{(n)} + \lambda_2^{(m)}]} \right] \frac{2}{\lambda_1^{(m)}} \quad \text{(A-33)}$$

From Equation A-16, one may write,

$$[\lambda_1^{(n)}]^2 D_1 = [\lambda_2^{(n)}]^2 D_2$$

and (A-34)

$$[\lambda_1^{(m)}]^2 D_1 = [\lambda_2^{(m)}]^2 D_2$$

When Equations A-34 are inserted into Equation A-33, the numerator vanishes; consequently, the coefficient of $\cot[\lambda_1^{(m)} \ell_1]$ in Equation A-32 is zero. Similarly it may be shown that the second bracketed term of Equation A-32 vanishes. Hence, this means

$$\int_{-\ell_1}^{\ell_2} \psi^{(n)}(x)\ \psi^{(m)}(x)dx = 0$$

and $\psi^{(n)}(x)$ and $\psi^{(m)}(x)$ are orthognal.

Thus, Equations A-20 and A-21 specify the distribution of sorbed molecules in Regions 1 and 2 where $A_1^{(n)}$ is given by Equation A-27.

UNCLASSIFIED

Security Classification

DOCUMENT CONTROL DATA - R & D

(Security classification of title, body of abstract and indexing annotation must be entered when the overall report is classified)

1. ORIGINATING ACTIVITY (Corporate author)	2a. REPORT SECURITY CLASSIFICATION
Arnold Engineering Development Center ARO, Inc., Operating Contractor Arnold Air Force Station, Tennessee	UNCLASSIFIED
	2b. GROUP N/A

3. REPORT TITLE

A SUMMARY REPORT OF THE CRYOSORPTION PUMPING OF HYDROGEN BY CARBON DIOXIDE FROST

4. DESCRIPTIVE NOTES (Type of report and inclusive dates)

Final Report - April 1969 through September 1969

5. AUTHOR(S) (First name, middle initial, last name)

K. E. Tempelmeyer, ARO, Inc.

6. REPORT DATE	7a. TOTAL NO. OF PAGES	7b. NO. OF REFS
June 1970	235	83

8a. CONTRACT OR GRANT NO.	9a. ORIGINATOR'S REPORT NUMBER(S)
F40600-69-C-0001	AEDC-TR-70-123
b. PROJECT NO.	
c. Program Element 64719F	9b. OTHER REPORT NO(S) (Any other numbers that may be assigned this report) N/A
d.	

10. DISTRIBUTION STATEMENT

This document has been approved for public release and sale; its distribution is unlimited.

11. SUPPLEMENTARY NOTES	12. SPONSORING MILITARY ACTIVITY
Available in DDC	Arnold Engineering Development Center, Air Force Systems Command, Arnold Air Force Station, Tenn.

13. ABSTRACT

The sorption of hydrogen by cryodeposited frosts of CO_2, SO_2, and CH_3Cl at temperatures between 12 and 22°K has been investigated both analytically and experimentally. Equilibrium sorption isotherms and the dynamic pumping characteristics of the sorbent, sorbate combination were systematically measured for chamber pressures between 10^{-7} and 10^{-4} torr. Frost cryosorbents which were formed in a manner to make them more amorphous exhibited greater equilibrium sorption capacities for hydrogen. Carbon dioxide sorbents were formed which were able to sorb one hydrogen molecule for every two predeposited CO_2 molecules. It was found that equilibrium sorption isotherms of frost cryosorbents could be predicted by the semi-empirical Dubinin-Radushkevich Equation. A general model of the sorption dynamics was formulated and approximate closed-form solutions were obtained: (1) in the limit of rather compact frost whose sorption behavior would be limited by the ability of the molecules to penetrate and diffuse into the frost, and (2) in the limit of very porous frosts in which the adsorption rate on the frost surface governs the pumping. Theoretical calculations for these limiting cases agreed with the observed pumping characteristics of the more compact and more porous frosts.

DD FORM 1 NOV 65 1473

UNCLASSIFIED

Security Classification

UNCLASSIFIED

Security Classification

14. KEY WORDS	LINK A		LINK B		LINK C	
	ROLE	WT	ROLE	WT	ROLE	WT
1 cryopumping						
2 sorption						
3 carbon dioxide						
4 hydrogen -- Pumping.						
frost						
4. Carbon dioxide frost -						

AFSC
Arnold AFS Tenn

UNCLASSIFIED

Security Classification